NASA CR-135269

(NASA-CR-135269) MANUFACTURE AND ENGINE TEST OF ADVANCED OXIDE DISPERSION STRENGTHENED ALLOY TURBINE VANES Final Report (General Electric Co.) 158 p HC A08/MF A01 CSCL 11F G3/26
N78-11232
Unclas 52378

MANUFACTURE and ENGINE TEST of ADVANCED OXIDE DISPERSION STRENGTHENED ALLOY TURBINE VANES

CONTRACT NAS3-18915

FINAL REPORT

MATERIAL AND PROCESS TECHNOLOGY LABORATORIES
AIRCRAFT ENGINE GROUP
GENERAL ELECTRIC COMPANY
CINCINNATI, OHIO 45215

P. G. Bailey
October, 1977

Prepared for
NASA-Lewis Research Center
Cleveland, Ohio 44135

1. Report No.	2. Government Accession No.	3. Recipient's Catalog No.
NASA CR-135269		

4. Title and Subtitle	5. Report Date / 6. Performing Organization Code
MANUFACTURE AND ENGINE TEST OF ADVANCED OXIDE DISPERSION STRENGTHENED ALLOY TURBINE VANES	October 1977
7. Author(s): P. G. Bailey	8. Performing Organization Report No.: R77AEG569
	10. Work Unit No: G6740
9. Performing Organization Name and Address: General Electric Company, Aircraft Engine Group, 1 Jimson Road, Cincinnati, Ohio 45215	11. Contract or Grant No.: NAS3-18915
	13. Type of Report and Period Covered: Contractor Report
12. Sponsoring Agency Name and Address: National Aeronautics and Space Administration	14. Sponsoring Agency Code: 4433

15. Supplementary Notes

Project Manager, C. P. Blankenship, NASA-Lewis Research Center, Cleveland, Ohio

16. Abstract

The ODS-NiCrAl alloys, awaited with great expectations of being no-coat replacement materials for the ODS-Ni-20Cr vane alloys, have proven inadequate, both in mechanical strength in engine testing and environmental resistance in a variety of situations.

HDA 8077 from Cabot and YD NiCrAl from Special Metals, selected from offerings including other ODS-NiCrAl, NiFeCrAl and FeCrAl alloys, met established melting point, stress rupture and oxidation resistance criteria, but sustained more thermal cracking in engine testing than the current F101 vane alloy, MA 754 (ODS-NiCr).

High temperature environmental resistance is exceptional in simple non-corrosion oxidation for the selected HDA 8077 and YD NiCrAl alloys but apparently at the 4% aluminum level of these alloys, the formation of a protective alumina scale is too tenuous a process. The scale-forming process is apparently very susceptible to degradation by the presence of (for instance) iron oxide and fuel-rich conditions.

The ODS-NiCrAl alloys, despite their mechanical property and environmental shortcomings, proved to be easily fabricable by machining and brazing processes established for the MA 754 alloy.

The Huntington Alloys ODS-FeCrAl candidate MA 956 performed exceptionally in all forms of environmental testing but proved very inadequate in thermal fatigue resistance, thus removing it early in the program from consideration for engine testing.

Better laboratory or rig tests capable of more accurately predicting engine performance are needed to prevent the surprises encountered on the program.

The environmental resistance deficiencies of the ODS-NiCrAls can be explained in retrospect on the basis of lean levels of aluminum and chromium. Improving the deficiencies by readjusting those levels upward would be expected to reduce mechanical properties further. Explaining the poorer mechanical behavior of the alloys defies rigorous explanation. Suffice to say that all ODS producers who have attempted an ODS-NiCrAl have found mechanical properties inferior to the corresponding ODS-NiCr alloy.

17. Key Words (Suggested by Author(s))	18. Distribution Statement
Oxide Dispersion Strengthened, ODS, oxidation resistance, hot corrosion resistance, vane fabrication, engine testing	Unclassified - unlimited

19. Security Classif. (of this report)	20. Security Classif. (of this page)	21. No. of Pages	22. Price*
Unclassified	Unclassified	151	

* For sale by the National Technical Information Service, Springfield, Virginia 22151

NASA-C-168 (Rev. 6-71)

FOREWORD

The work described herein was conducted by the Aircraft Engine Group, General Electric Company, under NASA Contract NAS3-18915. The NASA Project Manager was C.P. Blankenship, NASA-Lewis Research Center. The General Electric Program Manager was E.J. Kerzicnik. The Technical Manager was P.G. Bailey.. Substantial contributions to the program were made by H.J. Bauer and J.A. Stahl. Technical assistance, relative to turbine vane requirements, was provided by C.A. Freck and G.P. Brandenburg. P.A. Bergman supplied technical consultation on oxidation and hot corrosion testing. R. Wilson assisted in the evaluation of engine-tested vanes.

TABLE OF CONTENTS

PRECEDING PAGE BLANK NOT FILMED

LIST OF ILLUSTRATIONS

LIST OF ILLUSTRATIONS (Cont'd)

LIST OF ILLUSTRATIONS (Cont'd)

LIST OF ILLUSTRATIONS (Concluded)

LIST OF TABLES

EXECUTIVE SUMMARY

The purpose of this program was to exploit, for turbine engine vanes, the Oxide-Dispersion-Strengthened (ODS) Ni-Cr-Al alloy system developed under NASA Contract NAS3-13490 for the Space Shuttle thermal protection system. That contract identified the Ni-16Cr (3 to 5) Al-ThO_2 system as having attractive high temperature oxidation resistance. Subsequent NASA work also indicated exceptional sulfidation resistance for these alloys.

The overall charter of the current program (NAS3-18915) was to evaluate available commercial and developmental advanced ODS alloys, select three based on established vane property goals and manufacturing criteria, and then evaluate the selected alloys in an engine test. Canvassing available ODS alloys produced the following candidate list:

Alloy	Alloy System	Dispersoid	Supplier
TD NiCrAl	Ni-Cr-Al	ThO_2	NASA (Fansteel)
HDA 8077	Ni-Cr-Al	Y_2O_3	Cabot
YD NiCrAl	Ni-Cr-Al	Y_2O_3	Special Metals
DS NiCrAl	Ni-Cr-Al	ThO_2	Sherritt-Gordon
MA 953	Ni-Fe-Cr-Al	La_2O_3	Huntington Alloys
MA 956	Fe-Cr-Al	Y_2O_3	Huntington Alloys

Screening the candidate alloys by strength, thermal fatigue resistance, oxidation and sulfidation resistance (Figure A), narrowed the field to HDA 8077 and YD NiCrAl. The MA 956 alloy appeared to satisfy all criteria except for the very important thermal fatigue resistance in which it performed very poorly. In hot corrosion testing, HDA 8077 performed well and YD NiCrAl not so well (Figure A). The latter was assumed to be atypical in light of successful HDA 8077 results which were confirmed by NASA testing.

The selected alloys HDA 8077 and YD NiCrAl were amenable to the vane fabrication techniques (machining and brazing) established for MA 754, the current vane material. Five F101 low pressure turbine (LPT) vane blanks, sent to the vane machining vendor, produced five acceptable parts; three are shown in Figure B.

Engine testing proved to be quite another story after the intermediate program successes achieved to that point. Originally planned F101 engine testing [including two high pressure turbine (HPT) and one low pressure (LPT) vane tests] had to be modified by substitution of one CF6-50 HPT test

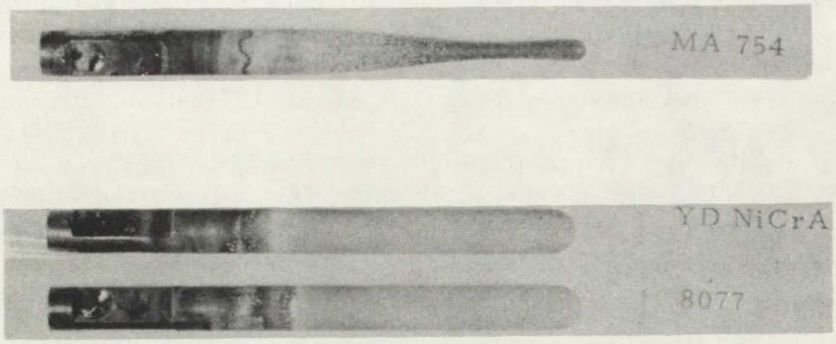

1.1X

MACH 1 OXIDATION
1204°C (2200°F)

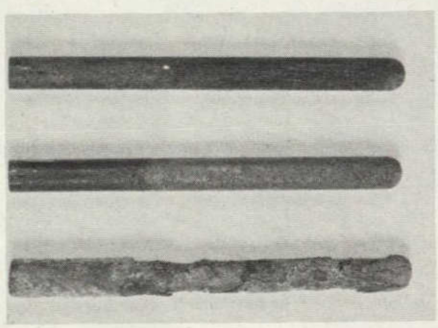

HDA8077 LPT

MA754

YDNiCrAl

1.3X

HOT CORROSION
927°C (1700°F)

Figure A Environmental Resistance of ODS-NiCrAl Allovs

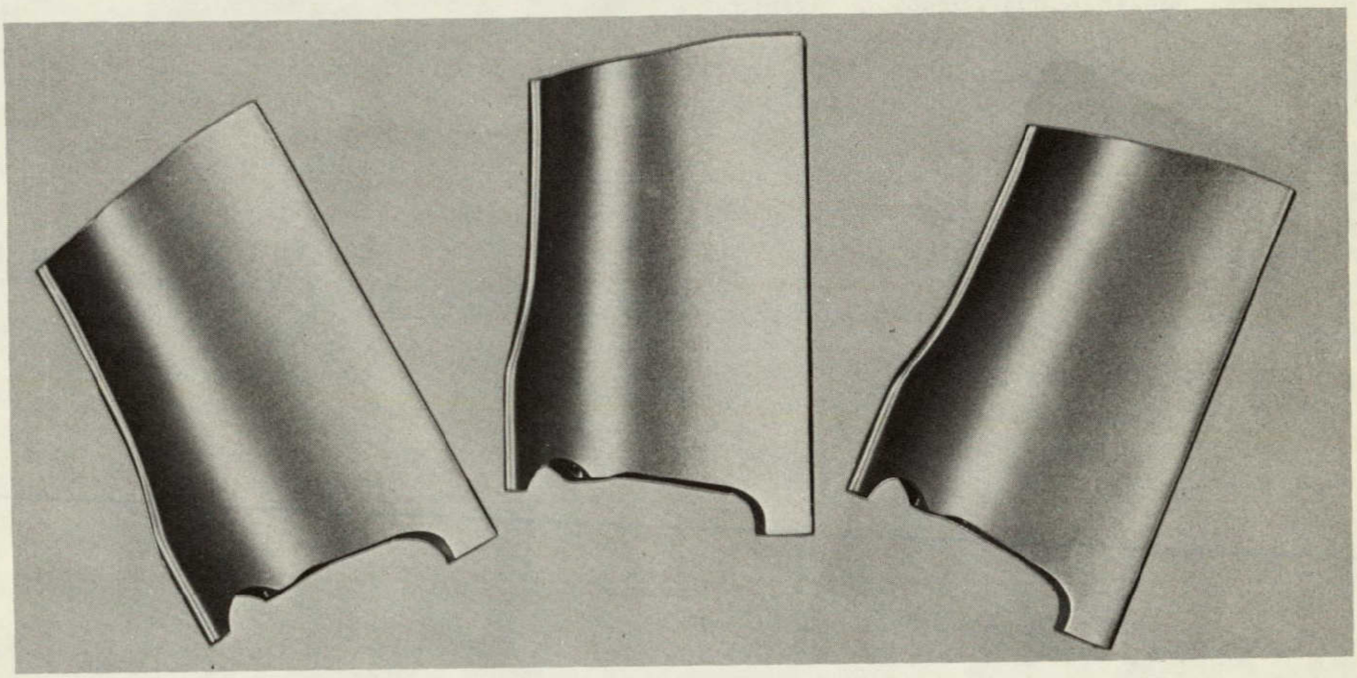

1X

Figure B Finished HDA8077 Vanes

because of material and machining delays and the unavailability of a suitable second HPT test engine. A representative HPT vane (CF6-50) is shown in Figure C. The engine testing showed the HDA 8077 and YD NiCrAl vanes to be inferior to the current ODS-NiCr vane alloy (MA 754) in crack resistance (Figure D). All engine tests were conducted with a maximum vane metal temperature above 1100° C (2000° F). Further, in other than simple, noncorrosive oxidizing conditions, the environmental resistance of these two materials was inadequate.

In summary, the ODS-NiCrAl (Ni-16Cr-4Al) alloys appear to have suffered in mechanical properties and overall environmental resistance compared to the ODS-NiCr alloys. The alloy system appears to be slightly below the critical amounts of both chromium and aluminum to have reliable surface stability in engine environments. The tenuous Al_2O_3 surface protection, once breached, leaves an alloy with too little chromium to protect itself from any one of several possible hot corrosion agents.

It would appear that better laboratory or rig tests, capable of accurately simulating engine environments, are needed in order to reduce the possibility of surprises such as were encountered in this program.

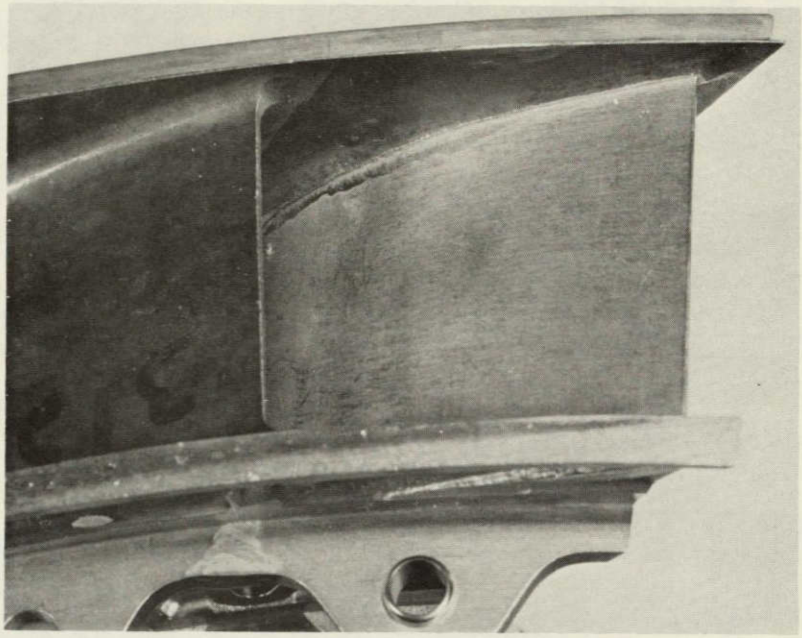

SUCTION SIDE

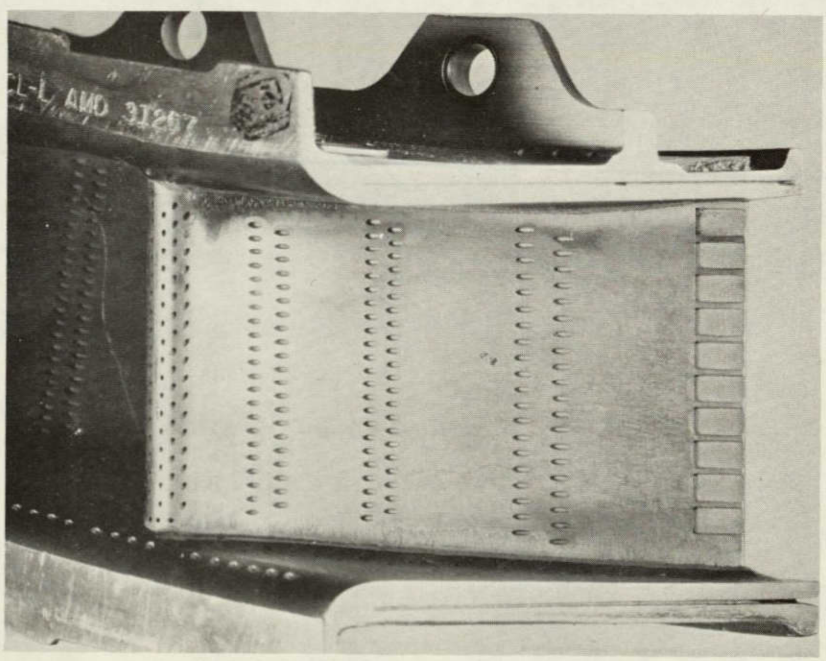

PRESSURE SIDE

Figure C YD NiCrAl CF6-50 HPT Vane

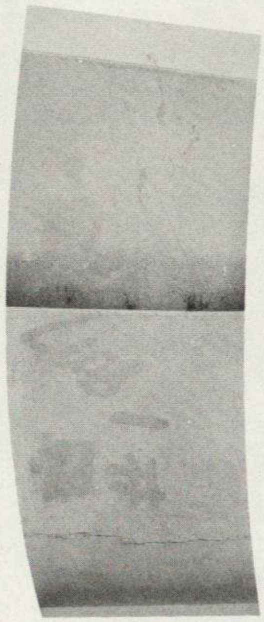

MA754
VANE

HDA8077
VANE

Figure D Engine Tested ODS-NiCrAl Vane

1.0 SUMMARY

The ODS-NiCrAl alloys, awaited with great expectations of being no-coat replacement materials for the ODS-Ni-20Cr vane alloys, have proven inadequate, both in mechanical strength in engine testing and in environmental resistance in a variety of situations.

HDA 8077 from Cabot and YD NiCrAl from Special Metals, selected from offerings including other ODS-NiCrAl, Ni-Fe-Cr-Al, and Fe-Cr-Al alloys, met established melting point, stress rupture, and oxidation resistance criteria, but sustained more thermal cracking in engine testing than the current F101 vane alloy, MA 754 (ODS-NiCr).

High temperature environmental resistance is exceptional in simple noncorrosion oxidation for the selected HDA 8077 and YD NiCrAl alloys; but, apparently at the 4% aluminum level of these alloys, the formation of a protective alumina scale is too tenuous a process. The scale-forming process apparently is very susceptible to degradation by the presence of (for instance) iron oxide and fuel-rich conditions.

The ODS-NiCrAl alloys, despite their mechanical property and environmental shortcomings, proved to be easily fabricable by machining and brazing processes established for the MA 754 alloy.

The Huntington alloys ODS-FeCrAl candidate MA 956 performed exceptionally in all forms of environmental testing but proved very inadequate in thermal fatigue resistance, thus removing it early in the program from consideration for engine testing.

Better laboratory or rig tests capable of more accurately predicting engine performance are needed to prevent the surprises encountered on the program.

The environmental resistance deficiencies of the ODS-NiCrAls can be explained in retrospect on the basis of lean levels of aluminum and chromium. Improving the deficiencies by readjusting those levels upward would be expected to reduce mechanical properties further. Explaining the poorer mechanical behavior of the alloys defies rigorous explanation. Suffice to say that all ODS producers who have attempted an ODS-NiCrAl have found mechanical properties inferior to the corresponding ODS-NiCr alloy.

2.0 INTRODUCTION

Commercial oxide-dispersion-strengthened (ODS) alloys are very attractive for use as vane materials in aircraft turbines because of their high temperature mechanical properties, thermal fatigue resistance, high melting point, and thermal stability. Despite all these favorable characteristics, application of the alloys has been rather limited. One of the factors limiting ODS alloy use (high cost) is responsible for development activity in the areas of power cost, larger billet sizes, lower cost recrystallization[1], and fabrication processes[2],[3]. Another factor limiting applications of ODS alloys lies in the need of oxidation protection. Coatings are required for all alloys commercialized to date, including the simple nickel-thoria and nickel-chrominum-thoria/yttria systems. In addition to cost, coatings have other deficiencies, such as the possible loss of oxidation protection by erosion or foreign object damage and the current lack of ability to coat internal vane surfaces.

The purpose of this program was to demonstrate the performance of advanced oxide-dispersion-strengthened (ODS) turbine vane alloys in an engine test. At least three advanced ODS-NiCrAl-type alloys were to be evaluated through appropriate screening tests to assess their potential for engine vane application without the need for a protective coating. Turbine vanes were manufactured from the advanced ODS alloys that met engine vane design requirements for engine testing. Testing of the vanes was accomplished in advanced gas turbine engines, the F101 and CF6-50, containing similar turbine vanes manufactured from a current, state-of-the-art, dispersion-strengthened vane alloy, MA 754. The advanced ODS vane alloys were tested without a protective coating. Bare and coated MA 754 vanes were included in the engine test. Engine test conditions provided a maximum vane metal temperature of at least 1100° C (2000° F). Minimum engine test time was to be 100 hours for each test component. A postengine test evaluation was made to assess the potential of the advanced ODS vane alloys for replacing the current ODS vane alloy in future engines and to assess the benefits that would result from the use of the advanced ODS vane alloys.

The program was conducted in three tasks:

- Task I - Material Selection and Characterization
- Task II - Manufacturing Technology Development and Fabrication of Advanced ODS Alloy Vanes
- Task III - Engine Test and Evaluation of Advanced ODS Alloy Vanes

Details of each of these tasks are described in this report.

3.0 TECHNICAL PROGRAM

3.1 TASK I-MATERIAL CHARACTERIZATION

3.1.1 Selection of Candidate Alloys

The alloys selected for screening in Task I were materials with a potential for substantial improvement in oxidation resistance over the ODS-Ni-20Cr alloys TD NiCr, DS NiCr, and MA 754. The majority were Ni-Cr-Al alloys, though a Ni-Fe-Cr-Al and an Fe-Cr-Al composition also were included. The oxide dispersions included ThO_2, Y_2O_3, and La_2O_3.

TD NiCrAl - TD Nickel Chromium Aluminum is an alloy of composition Ni-16Cr-5Al-$2ThO_2$ developed by Fansteel under Contract to NASA(4). Material was provided by Fansteel, both as extrusions and in billet form for later extrusion by NASA. The Fansteel work concluded that the 5% aluminum content afforded significant dynamic oxidation resistance over the Ni-20Cr-ThO_2 alloys TD NiCr and DS NiCr. It was shown that a hydrogen pretreatment to form an Al_2O_3 surface film enhanced the overall oxidation resistance of these materials. NASA and GE had conducted working and heat treatment studies with TD NiCrAl for the purpose of attaining coarse uniform recrystallized grain size of proper crystallographic orientation. Coarse grain <100> textures were obtained. The powder-making method employed for TD NiCrAl was wet attritor grinding of coprecipitation Ni-ThO_2 powder with a Cr-Al master alloy powder.

Haynes Development Alloy 8077 - This alloy of nominal composition Ni-16Cr-4Al-$1Y_2O_3$ is under development by the Stellite Division of the Cabot Corporation. A part of the effort was funded by NASA(5). Included in the NASA effort was the optimization of the aluminum content to maximize oxidation resistance, mechanical properties, and thermal fatigue resistance. Materials with yttria contents from 0.8 to 1.8% have been produced. Longitudinal stress rupture properties up to 75.8 MPa (11 ksi) for 20 hours at 1093° C (2000° F) have been attained. Extrusion parameters had been developed which produce the desired <100> longitudinal texture on recrystallization. Cabot reported the following oxidation data:

> Two tests, 982° C (1800° F) and 1093° C (2000° F), were run in Cabot's Mach 0.3 dynamic oxidation rig using No. 2 fuel oil at a 54 to 1 air/fuel mixture. The cycle time was 30 minutes. In the 982° C (1800° F) test of 100 hours duration, 8077 and DS NiCr had minimal surface recessions (0.004 mm in both cases), while HS 188 lost 0.04 mm. In testing at 1149° C (2100° F) for 100 hours, the 8077 surface recession remained minimal at 0.008 mm; while, for DS NiCr, it was 0.05 mm, and for HS 188, it was 0.063 mm. A preoxidized sample of 8077 was inserted after the test had run 40 hours. Surface recession data were not available; but, by visual inspection, the specimen oxidized less than the untreated sample.

HDA 8077 powder is manufactured by the Mechanical Alloying process(6), licensed from the International Nickel Co.

MA 953 - This alloy was under development by Huntington Alloys Inc. Its composition was Ni-19Cr-35Fe-5Al-0.9La_2O_3 and was made by the Mechanical Alloying powder process. Available data were limited at the start of the program, but stress rupture properties in excess of 100 hours at 82.7 (12 ksi) and 1093° C (2000° F) had been attained. Oxidation resistance, compared with TD NiCr in a cyclic 1093° C (2000° F) static air test, showed less than 1 mg/cm^2 weight loss when compared with TD NiCr at over 2 mg/cm^2, and with Haynes 188 at 8 mg/cm^2. In dynamic oxidation at 1093° C (2000° F), MA 953 gained 2 mg, compared with a loss in weight of over 100 mg for MAR M 509 and nearly 300 mg for WI 52. In hot corrosion/sulfidation testing for 100 hours at 927° C (1700° F), MA 953 corrosion penetration was 0.025 mm compared to Hastelloy X with a penetration of over 3.8 mm and sample destruction.

YD NiCrAl - This alloy is under development by Special Metals Corporation by a proprietary process claimed to be capable of excellent oxide dispersions at low cost. Nominal composition of the alloy is Ni-16Cr-4Al-1Y_2O_3. Electron micrographs of Ni-Cr-Y_2O_3 extrusions made by the same process had shown excellent dispersoid destruction.

DS NICrAl - Sherritt-Gordon, the manufacturer of DS NiCr powder and DS Ni sheet, had done limited development work in the Ni-Cr-Al alloy system. Two approaches were tried, Cr and Al diffusion of DS Ni sheet (which was not very successful and, at best, would be limited to thin sheet) and DS NiCrAl powder by processes similar to their DS NiCr process. Sample quantities of Ni-Cr-Al-ThO_2 powder, by the latter process, were supplied both to NASA and General Electric for evaluation. Extrusion of full-scale units of DS NiCrAl represented Sherritt-Gordon's first efforts at competing in the extruded product arena. Heretofore, except for DS Ni sheet, Sherritt had produced powder only and not mill product.

MA 956 - This candidate material of Fe-20Cr-4.5Al-0.5Y_2O_3 composition, offered by Huntington Alloys Inc. after the program had begun, indicated attractive potential properties for vane application; but, except for DS NiCrAl, it was the least developed of the candidate alloys. Because of excellent oxidation resistance, outstanding hot corrosion resistance, and a melting point advantage of ~110° C (200° F) over the Ni-Cr-Al alloys, it was considered worth the effort despite a higher risk of failure. Sheet stock of MA 956 has attained 1093° C (2000° F) 20-hour longitudinal and transverse properties of ~69 MPa (10 ksi), with some values even higher. Attainment of the desired <100> longitudinal texture in MA 956 was considered the most difficult task in development of this alloy.

3.1.2 Procurement of Material

The philosophy of material procurement for Task I was to allow maximum size/shape flexibility and "best effort" properties toward meeting the vane property goals shown in Table 1. Accordingly, all vendors except Cabot

Table 1. Vane Alloy Property Goals.

• Stress Rupture 1093° C (2000° F), 20 hours	
Longitudinal	75.8 MPa (11.9 ksi) (LPT) 48.3 MPa (7.0 ksi) (HPT)
Transverse	37.9 MPa (5.5 ksi) (LPT & HPT)
Short Transverse	34.5 MPa (5.0 ksi) (HPT) < 34.5 MPa (5.0 ksi) (LPT)
• Thermal Fatigue Resistance	≥ MA 754
• Stability	≤ 10% loss in stress rupture after 1 hour at 1315° C (2400° F)
• Machineability EDM ECM Conventional	≥ MA 754
• Brazeability	≥ MA 754
• Formability (Structural stability in twist & coining)	≥ MA 754
• Oxidation Resistance	≤ 0.063 mm (0.0025") surface loss in 500 hours Mach 1 1093° C (2000° F)
• Hot Corrosion Resistance	≤ 0.076 mm (0.003") surface loss in 500 hours 5 ppm salt 926° C (1700° F)
• Melting Point	≥ 1371° C (2500° F)

supplied a single candidate material for both vanes, while Cabot offered a "tailored" material for each vane, high pressure turbine (HPT) and low pressure turbine (LPT).

TD NiCrAl - Two heats of TD NiCrAl were supplied: 3935 in the as-extruded condition, and 3936 which had been extruded and hot rolled. Heat 3935 was nominally 3.2 cm × 10.8 cm (1 1/4" × 4 1/4") in cross section. Heat 3936 had been rolled from a similar size to approximately 2.54 cm × 11.7 cm (1" × 4 5/8").

YD NiCrAl - This alloy was produced for Task I of the program in 1.9 cm × 6.3 cm (3/4" × 2 1/2") rectangular section by extrusion and hot rolling. Two heats, X-40 and X-42 were supplied. The Special Metals data shown in Table 2 indicate conformance to property goals.

Haynes Development Alloy 8077 - Two heats of 8077 were supplied. One heat (202) with 1.8% Y_2O_3 was extruded to a rectangular shape for the LPT vane. The other heat, a kidney extrusion at 0.8% Y_2O_3, was sized for the HPT vane. Stress rupture data supplied by Cabot and reproduced in Table 2 show properties lower than the goals with a 1343° C (2450° F) heat treatment. Data obtained later after a 1315° C (2400° F) heat treatment at General Electric equaled or bettered the vane goals.

DS NiCrAl - Sherritt-Gordon produced four extrusions of DS NiCrAl, in LPT and HPT rectangular shapes. Two extrusion temperatures were used for each size. The material was found to be completely unsatisfactory, containing large amounts of macro-visible oxides. Sherritt-Gordon personnel determined the cause of the contamination to be in the powder-making step. This characteristic had not been observed in previous small-scale material supplied to NASA and General Electric.

MA 953 - This alloy was supplied by Huntington Alloys Inc. It was reported to have a melting point of ~1350° C (2460° F), somewhat below the goal of 1371° C (2500° F). Early full-scale bars with a 0.35% La_2O_3 level produced the desired <100> texture and a longitudinal modulus ~124 MPa (18 × 10^6 psi) but with 1093° C (2000° F) longitudinal 82.7 MPa (12 ksi) and transverse 37.9 MPa (5.5 ksi) stress rupture lives of the order of tenths of an hour, Table 2. Material for the program was produced with the La_3O_3 level increased to 0.9%.

MA 956 - The material for the program was the first scaled-up extruded material made by Huntington Alloys. Previous efforts had included small-scale extrusion and sheet development. Vendor rupture data indicated adequate longitudinal strength but low transverse values.

3.1.3 Recrystallization Studies

Recrystallization studies were carried out on each of the alloys as a precursor to the screening tests. The results are detailed by alloy. For each alloy, the heat treatments included slow and rapid heating rates to

Table 2. Vendor Stress Rupture Data - Task I.

Alloy	Heat No.	Vendor	Test Direction	Stress		1093° C (2000° F) Stress Rupture		
				MPa	(ksi)	Time (hrs)	Step Load (MPa)	Final Stress (ksi)
HDA 8077 (LPT)	202	Cabot	L	82.7	12.0	8.2	---	---
		Cabot	L	75.8	11.0	53.1	---	---
		Cabot	T	34.5	5.0	6.5	---	---
HDA 8077	203	Cabot	L	68.9	10.0	3.7	---	---
		Cabot	T	34.5	5.0	2.6	---	---
YD NiCrAl	X-40	Special Metals	L	48.3	7.0	20.0+	62.0	9.0
		Special Metals	T	37.9	5.5	20.0+	---	---
MA 953	A2A3	Huntington Alloys	L	82.7	12.0	0.5	---	---
		Huntington Alloys	T	37.9	5.5	0.5	---	---
MA 956	99A9	Huntington Alloys	L	62.0	9.0	4.7	---	---
		Huntington Alloys	L	55.1	8.0	1460+	---	---
		Huntington Alloys	T	17.2	2.5	470+		
	99A7	Huntington Alloys	L	58.6	8.5	24+	72.4	10.5
		Huntington Alloys	T	17.2	2.5	24+	27.6	4.0

1315° C (2400° F) and 1363° C (2485° F) and directional recrystallization[1] at 1343° C (2450° F) and 1363° C (2485° F) except for the MA 953 alloy; its 1349° C (2460° F) melting point precluded heat treatment at 1363° C (2485° F). For this alloy, conventional heat treatments and directional recrystallization were conducted at 1260° C (2300° F) and 1315° C (2400° F). The heat treatment for MA 956, 1371° C (2500° F), was selected with assistance from Huntington Alloys.

The objectives of the recrystallization studies were twofold: (1) development of medium-to-coarse grain size for high stress rupture strength, and (2) attainment of the low modulus <100> longitudinal texture for thermal fatigue resistance. Attainment of the desired <100> longitudinal orientation in face-centered-cubic ODS alloys produces what may be described as a "cube-on-edge" orientation of the transverse face (long transverse by short transverse). In this situation, the two transverse directions have <110> orientations. None of the alloys evaluated had a so-called wire texture (preferred orientation in longitudinal direction, random in transverse directions).

TD NiCrAl - The recrystallization response of the hot-rolled heat was most uniform, while the extruded material failed to recrystallize completely to coarse grain size regardless of heating cycle. In both heats, the tendency to coarse-grain recrystallization was enhanced by two factors: rapid heatup and high temperature. The most uniform structure was attained in the rolled material recrystallized by rapid heating by direct insertion in a $BaCl_2$ salt bath at 1363° C (2485° F). In no case was a full <100> longitudinal texture obtained in TD NiCrAl; though, with the slow heat-up cycles, there was a <100> component detected. The "slow" heat-up cycle employed was bath insertion at ~1100° C (2000° F) and a bath heat-up rate of ~3° C/min. (~5° F/min.).

The recrystallization results are listed in Table 3 and shown in transverse macrosection in Figures 1, 2, and 3.

YD NiCrAl - YD NiCrAl responded very uniformly to produce a coarse-grain longitudinal <100> recrystallized texture, except in fast heatup to a 1363° C (2485° F) recrystallization temperature, as shown in Figure 4. Minor areas of non <100> recrystallization at the edges of the cross section had been observed previously in DS NiCr extrusions made at the same extrusion source, RMI. An excessively steep extrusion die angle at this location was identified to be the source of that difficulty.

HDA 8077 - Cabot's preliminary heat treating studies showed that, for the 202 LPT material, a slow heatup produced the lowest modulus and a predominantly <100> texture; while, for the 203 HPT extrusion, fast heating produced the best properties with little effect on modulus (low) or texture, <100>. The General Electric heat treatment studies showed, for both extrusions, that a slow heat treatment was required to maximize the <100> texture; and, that rapid heatup by direct insertion into the salt bath at 1315° C (2400° F) or 1363° C (2485° F) produced a predominant high modulus longitudinal texture of <100>. The recrystallization responses of the 202 LPT extrusion are shown in Figure 5, and those for the 203 HPT material are shown in Figure 6.

Table 3. TD NiCrAl Recrystallization Response.

Heat No.	Heat Treat Cycle	Response
3935 (Extruded)	Slow to 1260° C (2300° F)	No Rx
	Slow to 1363° C (2485° F)	Fine Grain Rx
	Rapid to 1260° C (2300° F)	Surface Fine Grain Rx
	Rapid to 1315° C (2400° F)	Surface Medium Grain Rx
	Rapid to 1393° C (2450° F)	Surface Coarse Grain Rx
	Rapid to 1363° C (2485° F)	Surface Coarse Grain Rx
	ZAP at 1363° C (2485° F)	Fine Grain Rx
3936 (Rolled)	Slow to 1260° C (2300° F)	No Rx
	Slow to 1315° C (2400° F)	Surface Medium Grain Rx
	Slow to 1363° C (2485° F)	Nonuniform Fine and Coarse Grain
	Rapid to 1260° C (2300° F)	Corner Rx only
	Rapid to 1343° C (2400° F)	Uniform Medium/Coarse Grain
	Rapid to 1363° C (2485° F)	Uniform Coarse Grain
	ZAP at 1343° C (2450° F)	Nonuniform Fine and Coarse Grain
	ZAP at 1363° C (2485° F)	Nonuniform Fine and Coarse Grain

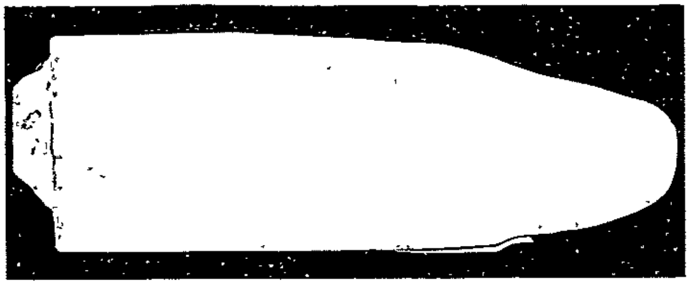

SLOW HEATUP
NIL RECRYSTALLIZATION
1260° C (2300° F)

SLOW HEATUP
OUTER ZONE RECRYSTALLIZATION
1315° (2400° F)

SLOW HEATUP
NEARLY COMPLETE RECRYSTALLIZATION
1363° C (2485° F)

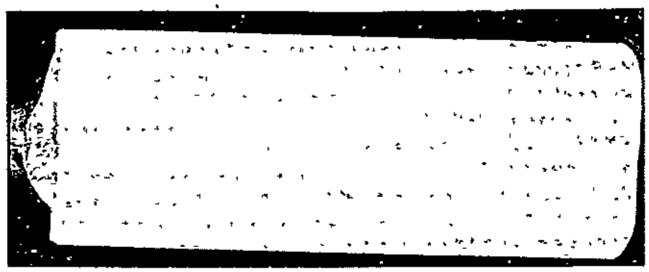

RAPID HEATUP
NIL RECRYSTALLIZATION
1260° C (2300° F)

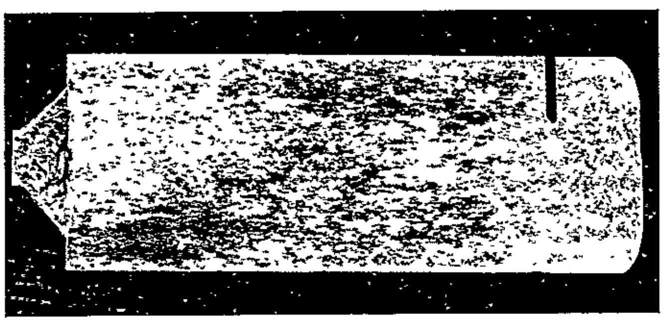

RAPID HEATUP
NEARLY COMPLETE RECRYSTALLIZATION
1315° C (2400° F)

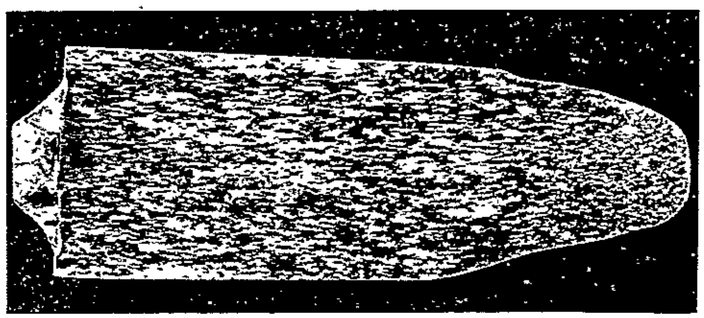

RAPID HEATUP
COMPLETE RECRYSTALLIZATION,
BUT HIGH MODULUS TEXTURE
1363° C (2485° F)

HEAT 3936-5

Figure 1 Rolled TDNiCrAl Furance Recrystallization Response

ORIGINAL PAGE IS
OF POOR QUALITY

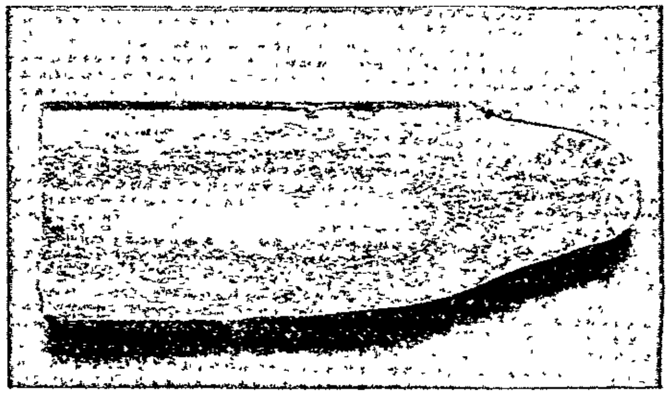

DIRECTIONAL RECRYSTALLIZATION
PARTIAL RECRYSTALLIZATION
1343° C (2450° F)

DIRECTIONAL RECRYSTALLIZATION
NEARLY COMPLETE RECRYSTALLIZATION
1363° C (2485° F)

HEAT 3936-5

Figure 2 Rolled TDNiCrAl Directional Recrystallization Response

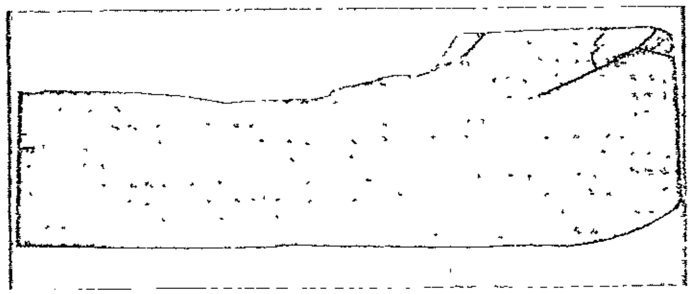

RAPID HEATUP - NO RECRYSTALLIZATION - 1260° C (2300° F)

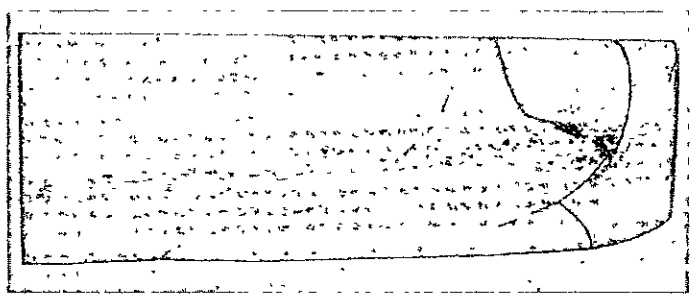

RAPID HEATUP - PARTIAL RECRYSTALLIZATION - 1315° C (2400° F)

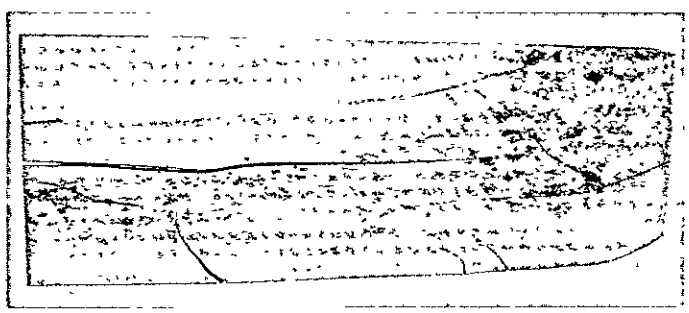

RAPID HEATUP - PARTIAL RECRYSTALLIZATION - 1363° C (2485° F)

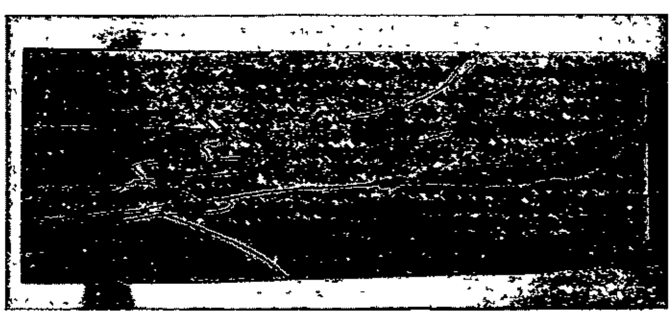

DIRECTIONAL RECRYSTALLIZATION - NO RECRYSTALLIZATION - 1363° C (2485° F)

HEAT 3535

(CRACKED BAR USED FOR EXPERIMENTS TO CONSERVE MATERIAL)

Figure 3 Extruded TDNiCrAl Recrystallization Response

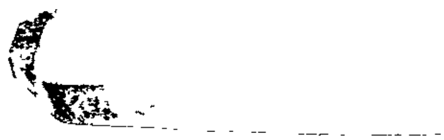

SLOW HEATUP
COMPLETE RECRYSTALLIZATION
LOW MODULUS TEXTURE
1315°C (2400°F)

SLOW HEATUP
COMPLETE RECRYSTALLIZATION
LOW MODULUS TEXTURE
1363°C (2485°F)

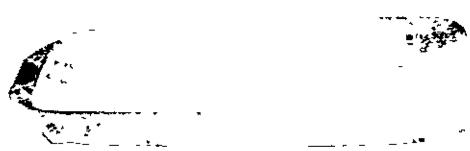

RAPID HEATUP
PATCH OF HIGH MODULUS TEXTURE
1315°C (2400°F)

RAPID HEATUP
MAJOR AMOUNT HIGH MODULUS TEXTURE
1363°C (2485°F)

DIRECTIONAL RECRYSTALLIZATION
COMPLETE RECRYSTALLIZATION
LOW MODULUS TEXTURE
1315°C (2400°F)

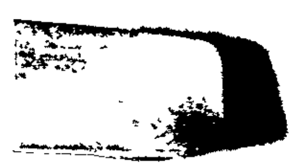

DIRECTIONAL RECRYSTALLIZATION
COMPLETE RECRYSTALLIZATION
LOW MODULUS TEXTURE
1363°C (2485°F)

HEAT X-40-4

Figure 4 YDNiCrAl Recrystallization Response

ORIGINAL PAGE IS
OF POOR QUALITY

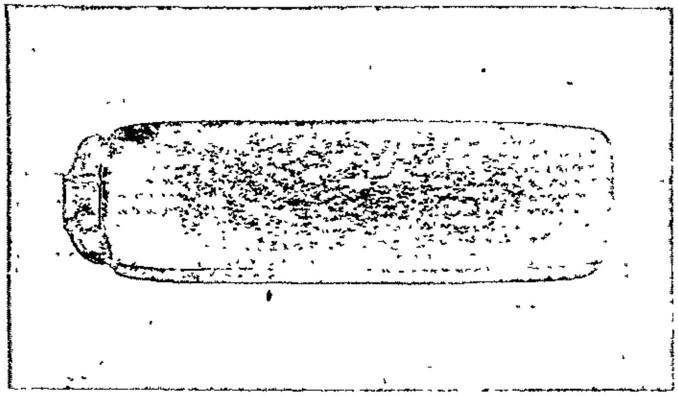

SLOW HEATUP
MOSTLY LOW MODULUS TEXTURE
1363° C (2485° F)

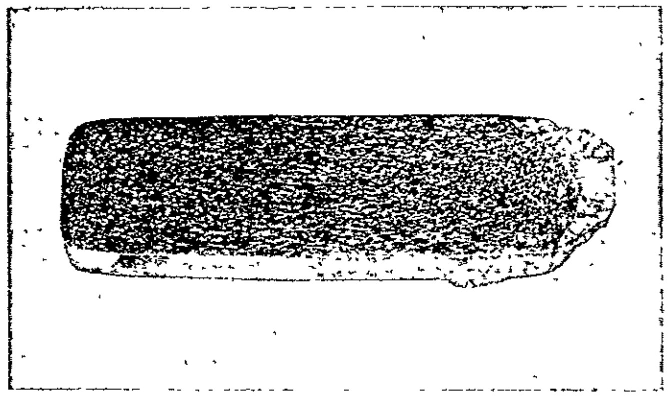

RAPID HEATUP
MOSTLY HIGH MODULUS TEXTURE
1363° C (2485° F)

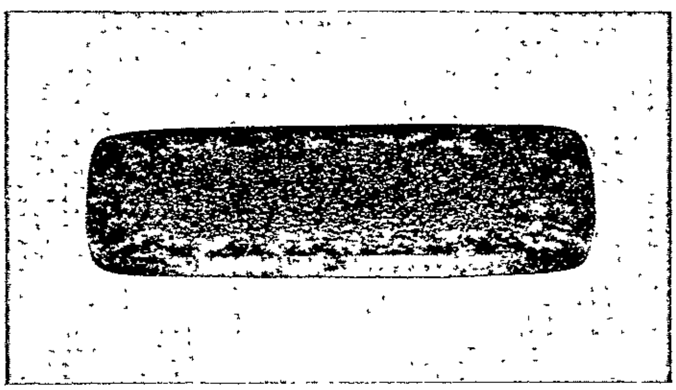

DIRECTIONAL RECRYSTALLIZATION
MOSTLY LOW MODULUS TEXTURE
1343° C (2450° F)

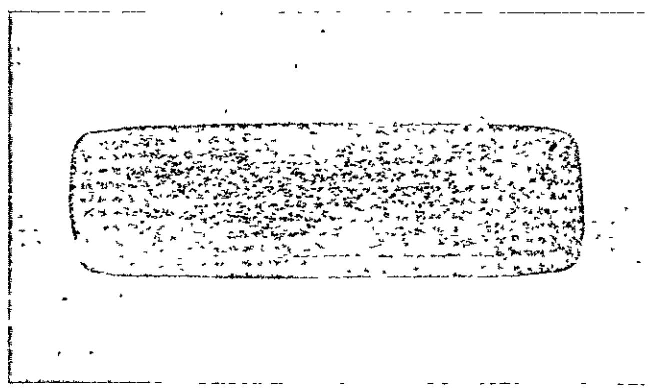

DIRECTIONAL RECRYSTALLIZATION
MOSTLY LOW MODULUS TEXTURE
1363° C (2485° F)

HEAT 202

Figure 5 HDA 8077 - LPT Recrystallization Response

SLOW HEATUP
COMPLETE RECRYSTALLIZATION
LOW MODULUS TEXTURE
1315° C (2400° F)

SLOW HEATUP
COMPLETE RECRYSTALLIZATION
LOW MODULUS TEXTURE
1363° C (2485° F)

RAPID HEATUP
HIGH MODULUS TEXTURE
1315° C (2400° F)

RAPID HEATUP
HIGH MODULUS TEXTURE
1363° C (2485° F)

DIRECTIONAL RECRYSTALLIZATION
COMPLETE RECRYSTALLIZATION
LOW MODULUS TEXTURE
1343° C (2450° F)
HEAT 203

Figure 6 HDA 8077 - HPT Recrystallization Response

MA 953 - In the recrystallization heat treatment studies spanning 1260° C (2300° F) to 1315° C (2400° F) using slow heating rates and directional recrystallization, little change in grain size or aspect ratios was noted. A uniform <100> texture was obtained in all slow heat treatments. The overall grain size was relatively fine. The rapid heat-up heat treatments produced some high modulus textures in the cross section centers. The macrostructures are shown in Figure 7.

MA 956 - Huntington Alloys reported attainment of coarse elongated grains but not the low modulus <100> longitudinal texture. Previous experimentation(7) in this body-centered-cubic ODS system also had failed to produce the <100> texture.

DS NiCrAl - As the heat-treated macrostructures shown in Figure 8 indicate, the material supplied proved to be contaminated, unlike previous small-scale material.

Selected Recrystallization Cycles

Since the recrystallization studies showed no improvement in grain elongation for the three nickel-base alloys by directional recrystallization, and either no texture effect or a promotion of the <100> texture by slow heatup, furnace recrystallization utilizing slow heatup was selected for all of these alloys bath insertion at ~1100° C (2000° F) and a heat-up rate of ~3° C (~5° F) per minute to a maximum of 1315° C (2400° F).

For MA 956, a 1-hour, 1371° C (2500° F) heat treatment, as recommended by Huntington Alloys, was used. Utilization of a single heat treatment method was considered satisfactory, since the Huntington Alloys materials have been relatively insensitive to heat treatment variations.

3.1.4 Preliminary Alloy Selection

Based on the promising stress rupture values and oxidation resistance information supplied by the material vendors and the recrystallization studies conducted at General Electric, the following alloys were selected for further evaluation:

HDA 8077-LPT	(1.8% Y_2O_3)	(Ni-Cr-Al)
HDA 8077-HPT	(0.8% Y_2O_3)	(Ni-Cr-Al)
YD NiCrAl		(Ni-Cr-Al)
MA 953		(Ni-Fe-Cr-Al)
MA 956		(Fe-Cr-Al)

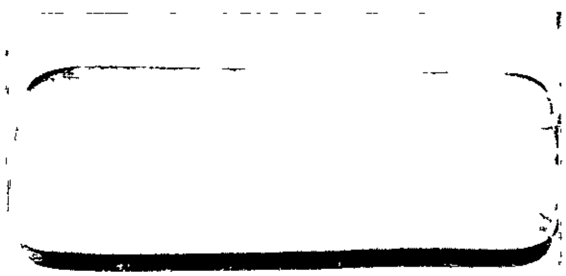

SLOW HEATUP
COMPLETE RECRYSTALLIZATION
LOW MODULUS TEXTURE
1260° C (2300° F)

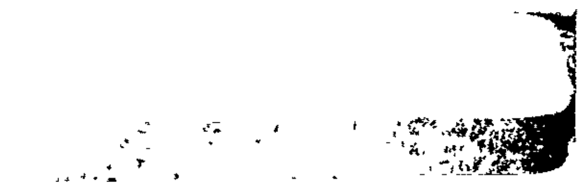

SLOW HEATUP
COMPLETE RECRYSTALLIZATION
LOW MODULUS TEXTURE
1315° C (2400° F)

RAPID HEATUP
MAJOR AMOUNT HIGH
MODULUS TEXTURE
1260° C (2300° F)

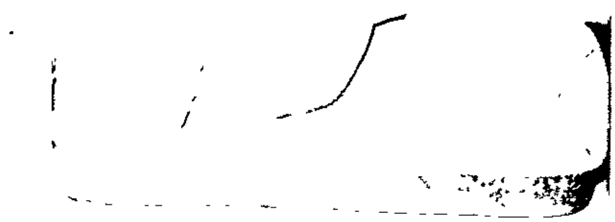

RAPID HEATUP
MAJOR AMOUNT HIGH
MODULUS TEXTURE
1315° C (2400° F)

DIRECTIONAL RECRYSTALLIZATION
NIL RECRYSTALLIZATION

Figure 7 MA953 Recrystallization Response

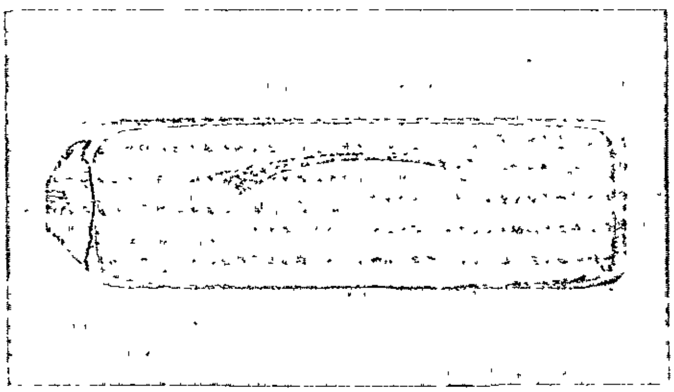

LPT EXTRUSION
1093° C (2000° F)

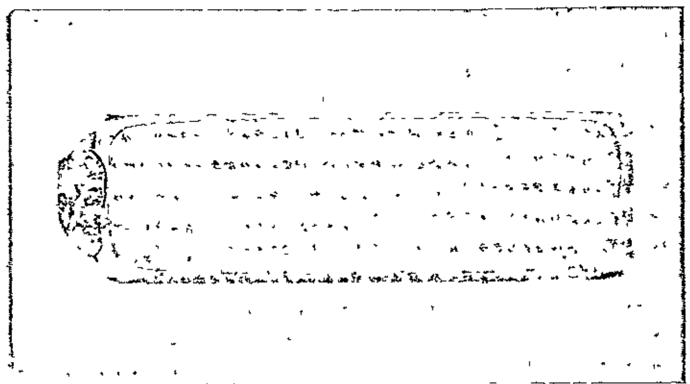

LPT EXTRUSION
1121° C (2050° F)

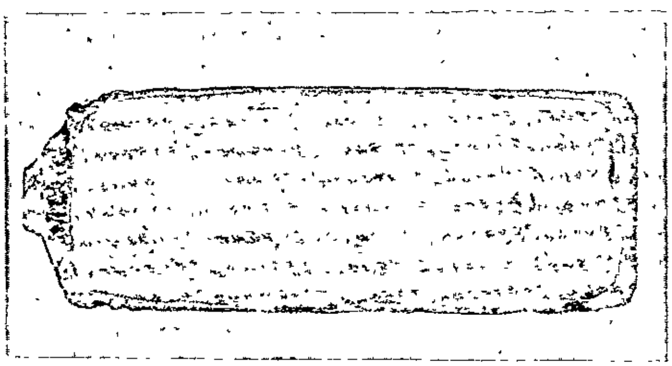

HPT EXTRUSION
1093° C (2000° F)

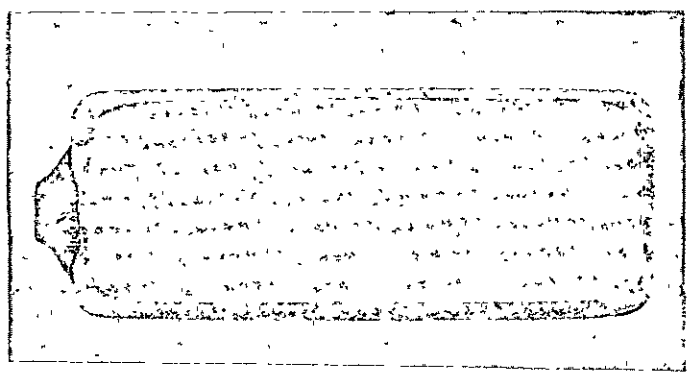

HPT EXTRUSION
1121° C (2050° F)

Figure 8 DSNiCrAl Recrystallization Response - Slow Heatup 1315°C (2400°F)

TD NiCrAl was dropped from consideration because of its inability to develop the low modulus texture. Gross oxide contamination of the scale-up heats of DS NiCrAl caused that alloy to be removed from consideration.

3.1.5 Property Test Plans

The generation of mechanical and physical property data was carried out in two campaigns, "Preliminary Screening" and "Material Characterization," as delineated in Tables 4 and 5. The test results of the two campaigns are reported in a combined format, however.

3.1.6 Tensile Testing

Tensile test data are recorded in Table 6, and ultimate tensile values are shown in Figures 9 through 12 including MA 754 for comparison. The comparison curves illustrate the greater low and medium temperature tensile strengths of the ODS-NiCrAl alloys compared with MA 754. At vane-use temperatures, however, MA 754 ultimate tensile strengths are approximately twice those of YD NiCrAl, 1.5 times those of HDA 8077 (HPT-type), and 1.25 times the LPT-type of HDA 8077. Comparison of high temperature ductility can be done only in an approximate manner because of the scattered data. Trial plots of tensile reduction of area in the three test directions (not incuded because there was not enough data to be statistically meaningful) did consistently show a trend of higher values for YD NiCrAl. Tensile ductility in the longitudinal direction in YD NiCrAl occasionally was manifest in substantially "necked-down" specimens. This phenomenon has not been observed in other ODS alloys by this experimenter.

3.1.7 Stress Rupture Testing

Stress rupture data are presented in Table 7 for HDA 8077 and YD NiCrAl, and in Figure 13 for the MA 754 values. The three principal test directions are shown. The longitudinal rupture strengths are roughly proportional to tensile values with MA 754 having twice the strength of YD NiCrAl and 1.5 and 1.25 times the HPT and LPT versions of HDA 8077. In the transverse directions, the proportionality to tensile values disappears with YD NiCrAl showing a slight edge over all the other alloys.

Stress rupture tests showed two alloys (HDA 8077 and YD NiCrAl) as viable HPT vane candidates. Only HDA 8077 met current LPT vane requirements. The longitudinal data show that HDT 8077, heat 202 (1.8% Y_2O_3) met the 75.8 MPa (11 ksi) 1093° C (2000° F)/20 hours which is the principal LPT vane requirement. HDA 8077, heat 203 (0.8% Y_2O_3) and YD NiCrAl both met the 48.3 MPa (7 ksi) longitudinal and 37.9 MPa (5.5 ksi) transverse requirements for the HPT vane. Though short transverse strengths were below the vane property aims, they did meet the current specification value for MA 754, 16.1 MPa (2.3 ksi)/1093° C (2000° F)/20 hours.

Table 4. Preliminary Screening Test Plan.

Test Description	Test Direction	Test Temperature ° C (° F)
Tensile	L	1093 (2000)
	T	1093 (2000)
	ST[1]	1093 (2000)
Stress Rupture	L	1093 (2000)
	T	1093 (2000)
	ST[1]	1093 (2000)
Dynamic Modulus	L	RT
	T	RT
Low Velocity Oxidation	L	1093 (2000)
	T	1093 (2000)
Brazeability	---	---
Chemistry	--- (including Gas Content) ---	

(1) Short Transverse (bar thickness direction).

Table 5. Material Characterization Test Plan.

Test Description	Test Directions	Test Temperature ° C (° F)
Tensile	L, T, ST	RT
	L, T, ST	760 (1400)
	L, T, ST	871 (1600)
	L, T, ST	982 (1800)
	L, T, ST	1093 (2000)
Creep	L, T, ST	871 (1600)
	L, T, ST	1093 (2000)
Low Cycle Fatigue	L, T	871 (1600)
	L, T	1093 (2000)
	L, T	1204 (2200)
Dynamic Modulus	L, T	RT
	L, T	1093 (2000)
Thermal Fatigue	L	1093 (2000)
Nil Strength	L, T	1260 (2300) to failure
Thermal Conductivity	---	RT to 1204 (2200)
Thermal Expansion	---	RT to 1204 (2200)
Density	---	RT
Dynamic Oxidation	L L	982 (1800) 1204 (2200)
Hot Corrosion	L	926 (1700)

Table 6. Tensile Test Data.

Alloy	Specimen Number	Test Direction	Temperature °C (°F)	Ultimate Strength MPa	Ultimate Strength ksi	Yield Strength (.2%) MPa	Yield Strength (.2%) ksi	Elong. (%)	R of A (%)
YD NiCrAl	21	Longitudinal	Room	1191	172.8	723.2	104.9	14.0	14.8
YD NiCrAl	26	Longitudinal	Room	1332	193.2	697.7	101.2	11.5	14.8
YD NiCrAl	51	Transverse	Room	940	136.3	681.1	98.8	18.3	20.0
YD NiCrAl	56	Transverse	Room	970	140.7	719.0	104.3	16.0	19.8
YD NiCrAl	8-2	Short Transverse	Room	903	131.0	732.8	106.3	10.8	7.6
YD NiCrAl	24	Longitudinal	760 (1400)	650	94.3	595.0	86.3	3.5	5.0
YD NiCrAl	52	Transverse	760 (1400)	584	84.7	561.9	81.5	3.3	6.2
YD NiCrAl	57	Transverse	760 (1400)	582	84.4	555.0	80.5	7.8	9.8
YD NiCrAl	1-3	Short Transverse	760 (1400)	588	85.3	560.5	81.3	4.5	1.3
YD NiCrAl	23	Longitudinal	871 (1600)	321	46.5	313.0	45.4	11.8	13.4
YD NiCrAl	28	Longitudinal	871 (1600)	305	44.2	292.3	42.4	16.5	18.1
YD NiCrAl	53	Transverse	871 (1600)	348	50.5	340.6	49.4	4.0	8.5
YD NiCrAl	8-6	Short Transverse	871 (1600)	364	52.8	357.8	51.9	3.0	2.5
YD NiCrAl	59	Transverse	982 (1800)	112	16.3	97.2	14.1	14.3	11.3
YD NiCrAl	1-4	Short Transverse	982 (1800)	96.5	14.0	94.4	13.7	14.8	8.6
YD NiCrAl	30	Longitudinal	1093 (2000)	84.8	12.3	76.5	11.1	20.3	27.8
YD NiCrAl	55	Transverse	1093 (2000)	86.2	12.5	82.7	12.0	8.8	6.3
YD NiCrAl	8-7	Short Transverse	1093 (2000)	81.3	11.8	77.9	11.3	7.0	3.8
YD NiCrAl	58	Transverse	1204 (2200)	73.1	10.6	70.3	10.2	7.5	4.9
8077 LPT	202-1	Longitudinal	Room	1286	186.6	874.2	126.8	7.0	8.5
8077 LPT	202-2	Longitudinal	Room	1237	179.5	839.0	121.7	7.5	9.6
8077 LPT	202-31	Transverse	Room	1134	164.5	797.6	115.7	8.0	9.6
8077 LPT	202-32	Transverse	Room	1118	162.2	807.3	117.1	7.3	7.3

Table 6. Tensile Test Data (Continued).

Alloy	Specimen Number	Test Direction	Temperature ° C (° F)	Ultimate Strength, MPa	Ultimate Strength, ksi	Yield Strength (.2%), MPa	Yield Strength (.2%), ksi	Elong. (%)	R of A (%)
8077 LPT	202-7-5	Short Transverse	Room	1172	170.0	844.5	122.5	7.5	1.3
8077 LPT	202-3	Longitudinal	760 (1400)	656	95.2	643.2	93.3	12.3	17.0
8077 LPT	202-4	Longitudinal	760 (1400)	679	98.5	663.9	96.3	14.5	12.3
8077 LPT	202-33	Transverse	760 (1400)	619	89.8	589.4	85.5	14.5	14.5
8077 LPT	202-34	Transverse	760 (1400)	605	87.8	579.8	84.1	4.3	8.5
8077 LPT	202-7-6	Short Transverse	760 (1400)	311	45.1	579.8	43.8	3.0	3.8
8077 LPT	202-5	Longitudinal	871 (1600)	300	43.5	284.0	41.2	17.0	28.0
8077 LPT	202-6	Longitudinal	871 (1600)	300	43.5	294.4	42.7	13.5	25.6
8077 LPT	202-35	Transverse	871 (1600)	305	44.3	302.6	43.9	6.0	11.0
8077 LPT	202-36	Transverse	871 (1600)	305	44.2	299.6	43.4	5.3	8.4
8077 LPT	202-7-7	Short Transverse	871 (1600)	319	46.2	315.1	45.7	4.5	2.5
8077 LPT	202-8	Longitudinal	982 (1800)	177	25.7	162.0	23.5	3.0	2.5
8077 LPT	202-7	Longitudinal	982 (1800)	174	25.2	151.7	22.0	14.8	10.1
8077 LPT	202-37	Transverse	982 (1800)	152	22.1	146.8	21.3	11.0	6.3
8077 LPT	202-38	Transverse	982 (1800)	152	22.0	143.4	20.8	8.0	3.8
8077 LPT	202-7-8	Short Transverse	982 (1800)	149	21.6	146.8	21.3	5.0	2.5
8077 LPT	202-9	Longitudinal	1093 (2000)	125	18.1	117.2	17.0	15.3	11.1
8077 LPT	202-10	Longitudinal	1093 (2000)	127	18.4	120.6	17.5	9.8	6.3
8077 LPT	202-39	Transverse	1093 (2000)	114	16.6	110.3	16.0	5.0	1.3
8077 LPT	202-40	Transverse	1093 (2000)	117	16.9	107.5	15.6	6.0	1.2
8077 LPT	202-7-9	Short Transverse	1093 (2000)	112	16.2	109.6	15.9	2.8	1.2
8077 HPT	203-11	Longitudinal	Room	1217	176.5	714.9	103.7	13.0	16.0
8077 HPT	203-12	Longitudinal	Room	1233	178.9	730.8	106.0	15.0	19.3
8077 HPT	203-41	Transverse	Room	1104	160.1	702.5	101.9	14.8	17.7
8077 HPT	203-42	Transverse	Room	1110	161.0	723.9	105.0	14.0	11.3
8077 HPT	203-2-5	Short Transverse	Room	1090	158.1	706.6	102.5	17.5	10.0

Table 6. Tensile Test Data (Concluded).

Alloy	Specimen Number	Test Direction	Temperature ° C (° F)	Ultimate Strength, MPa	Ultimate Strength, ksi	Yield Strength (.2%), MPa	Yield Strength (.2%), ksi	Elong. (%)	R of A (%)
8077 HPT	203-13	Longitudinal	760 (1400)	638	92.5	595.6	86.4	14.0	9.9
8077 HPT	203-14	Longitudinal	760 (1400)	647	93.8	587.4	85.2	2.8	7.4
8077 HPT	203-43	Transverse	760 (1400)	585	84.9	555.0	80.5	4.5	6.1
8077 HPT	203-44	Transverse	760 (1400)	581	84.3	527.4	76.5	5.0	6.6
8077 HPT	203-2-6	Short Transverse	760 (1400)	(Thread Failure)		(Thread Failure)			
8077 HPT	203-15	Longitudinal	871 (1600)	305	44.3	290.9	42.2	9.3	26.5
8077 HPT	203-16	Longitudinal	871 (1600)	315	45.7	294.4	42.7	17.3	28.0
8077 HPT	203-45	Transverse	871 (1600)	302	43.8	299.9	43.5	3.5	9.8
8077 HPT	203-46	Transverse	871 (1600)	292	42.3	286.1	41.5	7.8	8.5
8077 HPT	203-2-7	Short Transverse	871 (1600)	312	45.3	310.2	45.0	3.3	1.3
8077 HPT	203-17	Longitudinal	982 (1800)	140	20.3	128.2	18.6	20.8	20.0
8077 HPT	203-18	Longitudinal	982 (1800)	144	20.9	130.3	18.9	26.3	19.0
8077 HPT	203-47	Transverse	982 (1800)	129	18.7	122.0	17.7	9.3	10.0
8077 HPT	203-48	Transverse	982 (1800)	128	18.6	121.3	17.6	6.3	7.5
8077 HPT	203-2-8	Short Transverse	982 (1800)	128	18.5	123.4	17.9	13.3	4.9
8077 HPT	203-19	Longitudinal	1093 (2000)	102	14.8	93.1	13.5	---	10.0
8077 HPT	203-20	Longitudinal	1093 (2000)	99.3	14.4	95.8	13.9	14.0	13.8
8077 HPT	203-49	Transverse	1093 (2000)	99.3	14.4	97.2	14.1	4.5	2.5
8077 HPT	203-50	Transverse	1093 (2000)	97.2	14.1	93.1	13.5	6.3	1.3
8077 HPT	203-2-9	Short Transverse	1093 (2000)	93.8	13.6	93.1	13.5	6.0	1.3

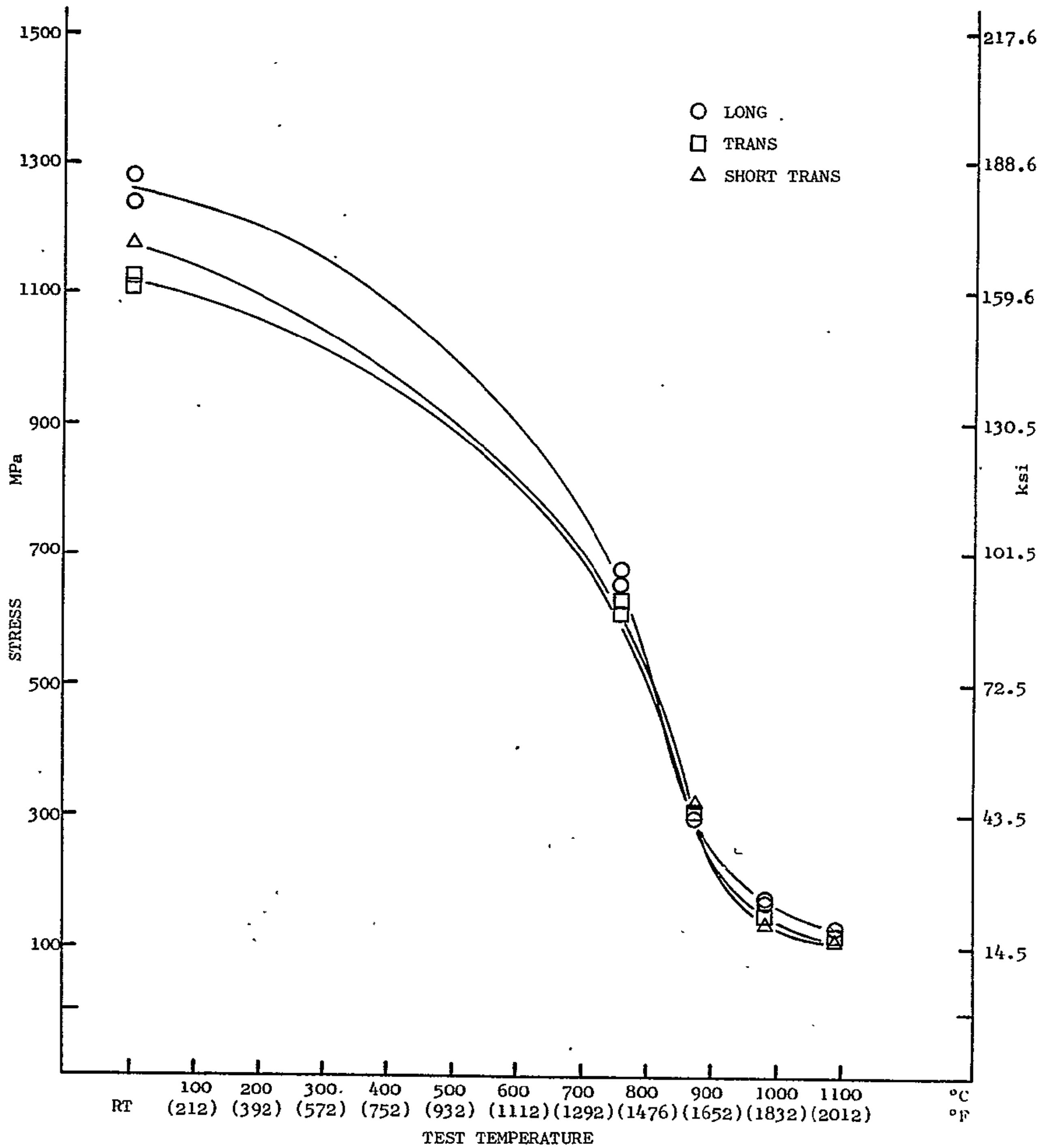

Figure 9 HDA 8077 LPT Ultimate Tensile Strength

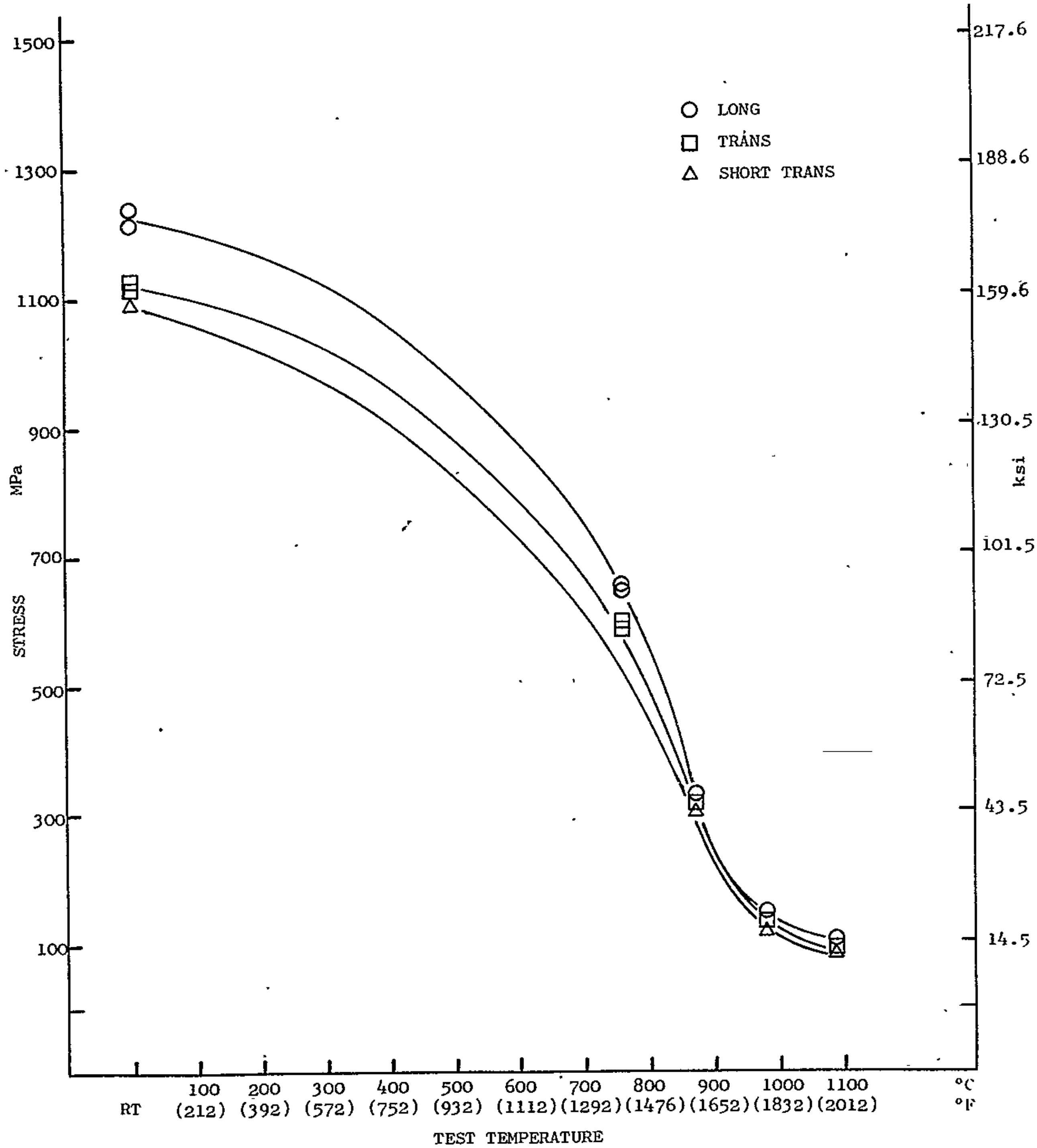

Figure 10 HDA 8077 Ultimate Tensile Strength

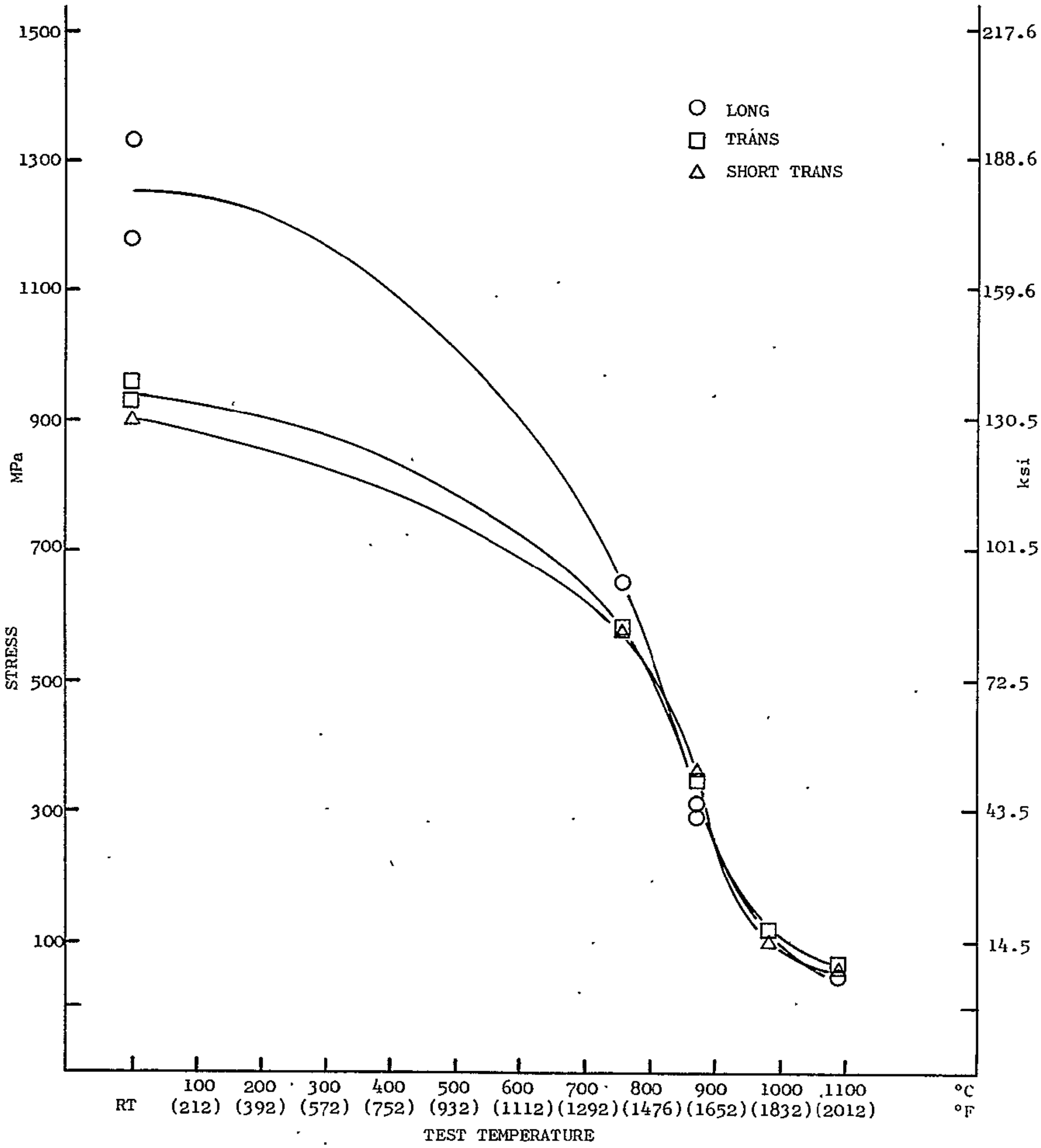

Figure 11 YDNiCrAl Ultimate Tensile Strength

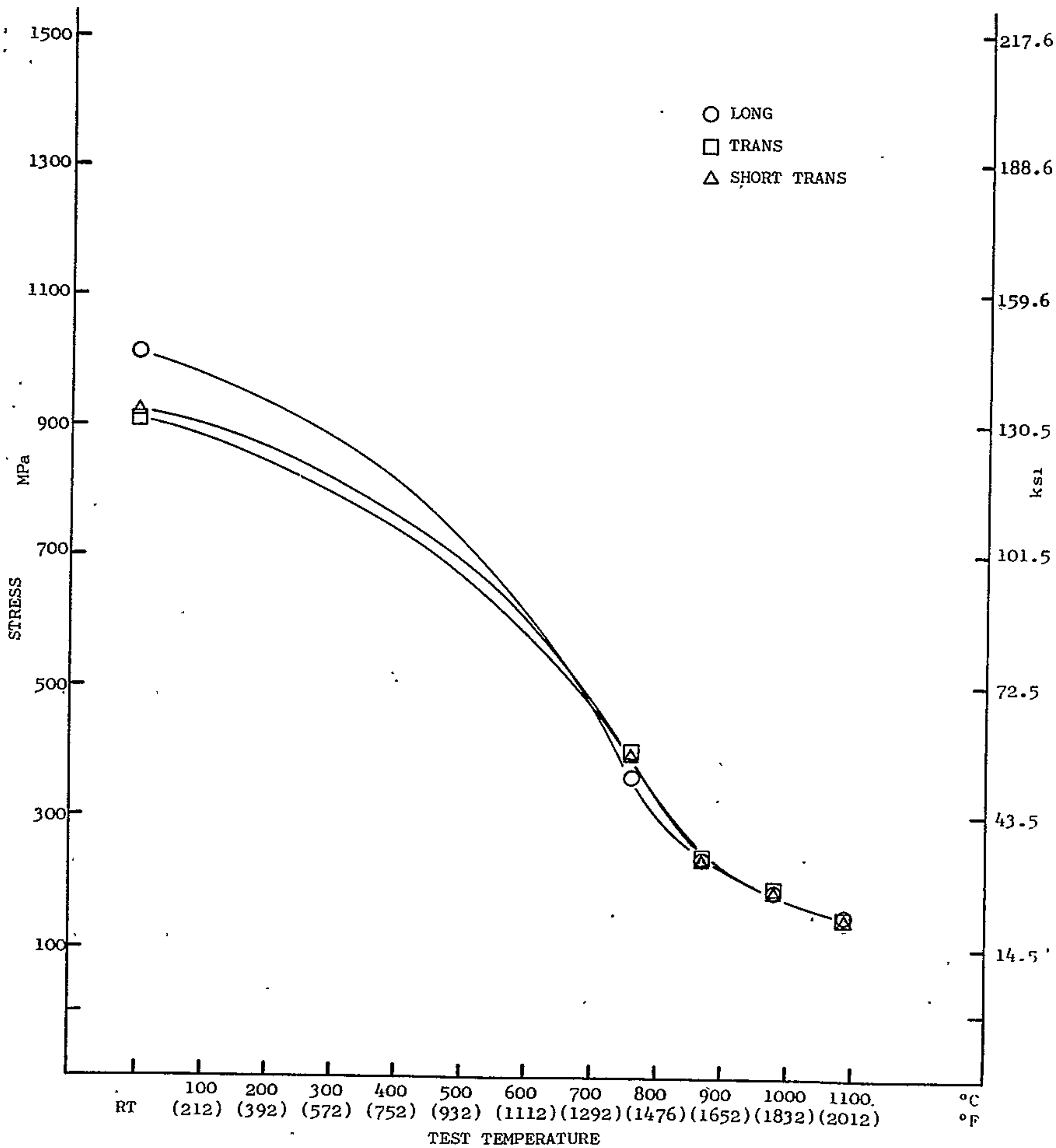

Figure 12 MA754 Ultimate Tensile Strength

Table 7. Stress Rupture Test Data.

Alloy	Specimen Number	Test Direction	Temperature ° C (° F)	Stress MPa	Stress Ksi	Life (Hrs)	Elong. (%)	R of A (%)
YD NiCrAl	77-6	Longitudinal	1093 (2000)	55.1	8.0	.7	6.8	11.0
YD NiCrAl	77-8	Longitudinal	1093 (2000)	55.1	8.0	3.1	10.3	37.0
YD NiCrAl	77-22	Longitudinal	1093 (2000)	51.7	7.5	2.1	9.3	3.9
YD NiCrAl	77-25	Longitudinal	1093 (2000)	51.7	7.5	61.4	7.8	2.6
YD NiCrAl	78-1	Longitudinal	1093 (2000)	51.7	7.5	53.3	---	3.4
YD NiCrAl	105-3	Longitudinal	1093 (2000)	51.7	7.5	36.6	---	53.0
YD NiCrAl	105-1	Longitudinal	1093 (2000)	51.7	7.5	83.5	(Thread Failure)	
YD NiCrAl	105-2	Longitudinal	1093 (2000)	51.7	7.5	89.4	4.4	59.0
YD NiCrAl	77-27	Longitudinal	1093 (2000)	51.7	7.5	8.9	7.5	3.8
YD NiCrAl	77-5	Longitudinal	871 (1600)	82.7	12.0	500.4		
				Step loaded to				
				110.3	16.0	580.8	6.6	5.0
YD NiCrAl	77-7	Longitudinal	871 (1600)	82.7	12.0	520.6		
				Step loaded to				
				131.0	19.0	704.6	10.3	22.4
YD NiCrAl	77-29	Longitudinal	871 (1600)	110.3	16.0	111.5	8.7	9.0
YD NiCrAl	77-14	Transverse	1093 (2000)	37.9	5.5	5.3	(Thread Failure)	
YD NiCrAl	77-60	Transverse	1093 (2000)	34.5	5.0	78.6	6.4	4.9
YD NiCrAl	105-4	Transverse	1093 (2000)	34.5	5.0	104.4	2.3	1.3
YD NiCrAl	105-5	Transverse	1093 (2000)	34.5	5.0	403	---	7.6
YD NiCrAl	78-7	Transverse	1093 (2000)	34.5	5.0	55.5	---	0
YD NiCrAl	78-8	Transverse	1093 (2000)	34.5	5.0	43.1	8.5	2.0
YD NiCrAl	77-16	Transverse	1093 (2000)	37.9	5.5	1.2	(Thread Failure)	
YD NiCrAl	77-54	Transverse	871 (1600)	89.6	13.0	144.1	5.9	2.9
YD NiCrAl	77-15	Transverse	871 (1600)	82.7	12.0	592.7	1.1	0
YD NiCrAl	77-13	Transverse	871 (1600)	68.9	10.0	336		
				Step loaded to				
				82.7	12.0	543.6	2.9	1.2

Table 7. Stress Rupture Test Data (Continued).

Alloy	Specimen Number	Test Direction	Temperature °C (°F)	Stress MPa	Stress Ksi	Life (Hrs)	Elong. (%)	R of A (%)
YD NiCrAl	77-8-4	Short Transverse	1093 (2000)	24.1	3.5	0.5	(Braze Failure)	
YD NiCrAl	77-8-5	Short Transverse	1093 (2000)	24.1	3.5	1.3	(Braze Failure)	
YD NiCrAl	77-1-1	Short Transverse	1093 (2000)	24.1	3.5	14.3	13.9	2.0
YD NiCrAl	77-8-3	Short Transverse	1093 (2000)	20.7	3.5	21.0	3.2	4.0
YD NiCrAl	77-8-1	Short Transverse	871 (1600)	68.9	10.0	10.6	5.8	1.9
YD NiCrAl	77-1-2	Short Transverse	871 (1600)	68.9	10.0	37.8	3.3	2.5
8077 LPT	202	Longitudinal	871 (1600)	144.8	21.0	11.7	5.7	8.7
8077 LPT	202-1	Longitudinal	871 (1600)	110.3	16.0	615.8+	---	---
					Step loaded to			
				158.6	23.0	748.9	3.2	6.8
8077 LPT	202	Transverse	871 (1600)	75.8	11.0	89.2	---	1.3
8077 LPT	202-9	Transverse	871 (1600)	62.0	9.0	504.4	---	---
					Step loaded to			
				75.8	11.0	520.7	5.1	0.7
8077 LPT	202	Longitudinal	1093 (2000)	82.7	12.0	162.2+	---	---
					Step loaded to			
				103.4	15.0	168	5.5	8.0
8077 LPT	202	Longitudinal	1093 (2000)	86.1	12.5	36.6	3.8	2.5
8077 LPT	202	Longitudinal	1093 (2000)	82.7	12.0	8.2	---	---
8077 LPT	202	Longitudinal	1093 (2000)	75.8	11.0	53.1	---	---
8077 LPT	202-2	Longitudinal	1093 (2000)	82.7	12.0	4.8	4.4	3.8
8077 LPT	202	Longitudinal	1093 (2000)	75.8	11.0	100+	---	---
					Step loaded to			
				82.7	12.0	105.3		
8077 LPT	202	Transverse	1093 (2000)	34.5	5.0	12.8	---	1.5
8077 LPT	202	Transverse	1093 (2000)	34.5	5.0	160.9+	---	---
					Step loaded to			
				41.4	6.0	160.9	---	---
8077 LPT	202	Transverse	1093 (2000)	34.5	5.0	6.5	---	---
8077 LPT	202-10	Transverse	1093 (2000)	34.5	5.0	8.0	7.4	0.6
8077 LPT	202	Transverse	1093 (2000)	31.0	4.5	100+	---	---
					Step loaded to			
				34.5	5.0	100.1	---	---

Table 7. Stress Rupture Test Data (Concluded).

Alloy	Specimen Number	Test Direction	Temperature °C (°F)	Stress MPa	Stress Ksi	Life (Hrs)	Elong. (%)	R of A (%)
8077 LPT	202-7-3	Short Transverse	871 (1600)	68.9	10.0	10.8	2.2	2.0
8077 LPT	202-7-4	Short Transverse	1093 (2000)	17.2	2.5	11.5	4.0	2.0
8077 LPT	202	Short Transverse	1093 (2000)	27.6	4.0	0.1	1.3	---
8077 LPT	202	Short Transverse	1093 (2000)	20.7	3.0	208.3	---	1.9
8077 HPT(269)	203-4	Longitudinal	1093 (2000)	72.4	10.5	1.0	7.6	10.9
8077 HPT	203-4	Longitudinal	871 (1600)	96.6	14.0	594.1+	---	---
					Step loaded to			
				124.1	18.0	671.6	7.3	3.7
8077 HPT	203-X3	Longitudinal	871 (1600)	124.1	18.0	109.3	7.1	7.1
8077 HPT	203-12	Transverse	1093 (2000)	34.5	5.0	159.2	---	0.7
8077 HPT	203-11	Transverse	871 (1600)	62.0	9.0	472+	---	---
					Step loaded to			
				82.7	12.0	641.4	9.7	0.7
8077 HPT	203-X4	Transverse	871 (1600)	82.7	12.0	96.7	4.3	1.9
8077 HPT	203-2-3	Short Transverse	871 (1600)	68.9	10.0	4.2	3.0	1.4
8077 HPT	203-2-1	Short Transverse	1093 (2000)	24.1	3.5	2.1	---	0
8077 HPT	203-2-2	Short Transverse	1093 (2000)	20.7	3.0	2.4	3.8	2.0
8077 HPT	203-2-4	Short Transverse	1093 (2000)	20.7	3.0	45.4	2.7	1.0

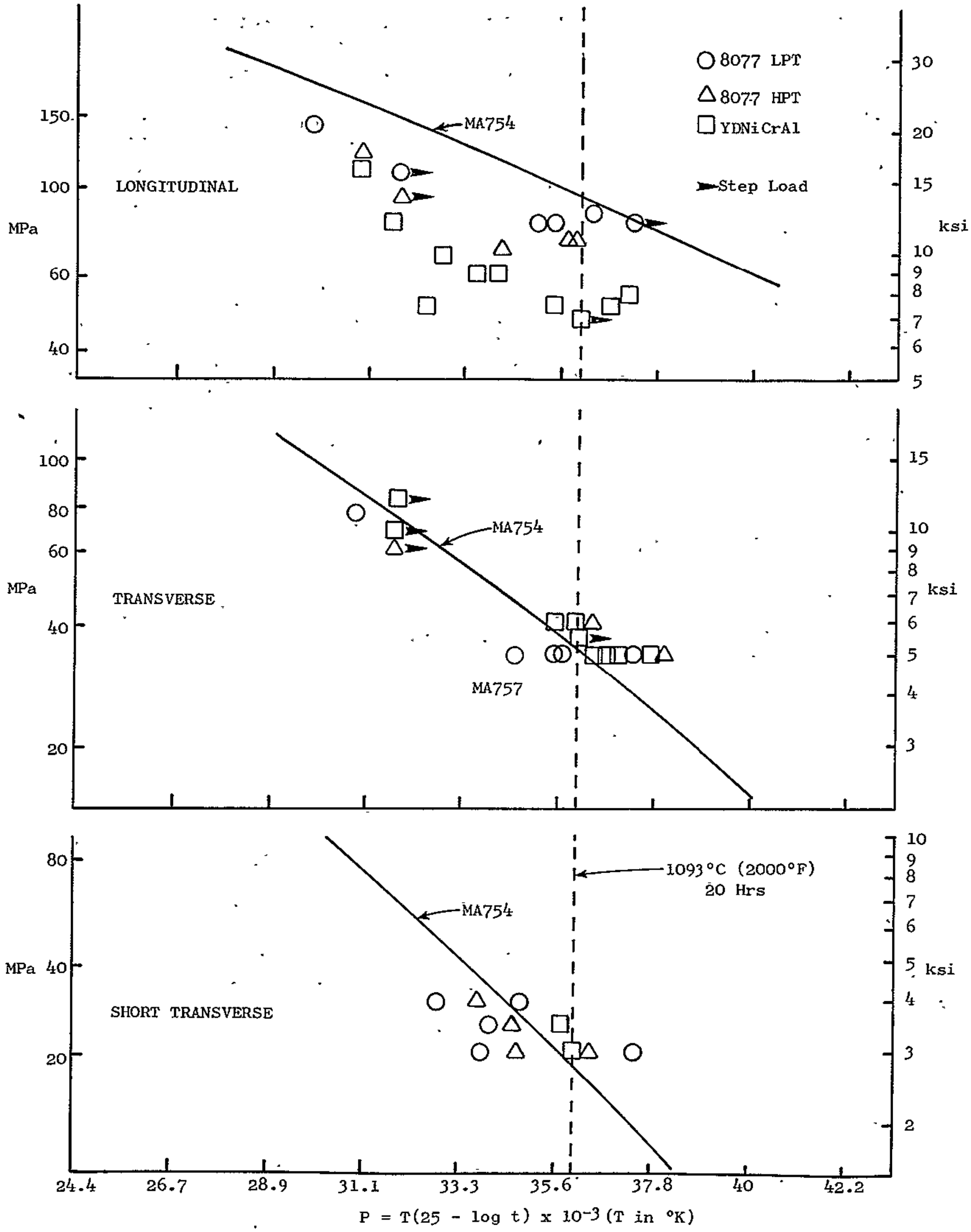

Figure 13 HDA 8077 and YDNiCrAl Stress Rupture Strength vs MA754

3.1.8 High Temperature Exposure Effect on Stress Rupture

Stress rupture testing of material exposed for 100-hour periods at temperatures of 1260° to 1315° C (2300° to 2400° F) indicates only a slight degradation of properties from the exposures. The testing included advanced alloys HDA 8077, YD NiCrAl, and the Ni-20Cr alloys DS NiCr and MA 754. Most testing was done in the transverse direction and all was done at 1093° C (2000° F); the data are listed in Table 8.

3.1.9 Creep Rupture Testing

Creep testing was done in both longitudinal and transverse directions at 1093° C (2000° F) on HDA 8077 (LPT-type) and YD NiCrAl. The planned testing at 871° C (1600° F) was not carried out because of the allocation of these specimens to additional stress rupture testing at 1093° C (2000° F).

Creep data are recorded in Table 9 and representative data are plotted in Figures 14 through 17. There is considerable data scatter, but a few comparative results stand out:

- HDA 8077 is resistant to higher creep stress in the longitudinal direction and less in the transverse than YD NiCrAl.
- The HDA 8077 samples show considerable elongation but minimal reduction of area. This usually is indicative of extensive internal cracking.
- The only sample showing significant reduction of area was the longitudinal YD NiCrAl.

3.1.10 Thermal Fatigue Testing

Thermal fatigue testing was conducted in a Simulated Engine Thermal Shock (SETS) rig which consists of a rotating specimen table and sequential gas burner heating and air jet cooling stations. The sample utilized was the wedge specimen depicted in Figure 18. The heating/cooling cycle of 50 seconds with a 1093° C (2000° F) maximum and a 427° C (800° F) minimum is shown also in Figure 18. The specimens are monitored periodically for cracks and rated per the indices described below:

THERMAL FATIGUE CRACK SEVERITY INDEX (CSI)

CODE

0 No cracking or surface deterioration

1 Pits at leading edge -- not discernible as cracks

Table 8. High Temperature Exposure Effect on Stress Rupture.

Alloy	Heat No.	Test Direction	Exposure			1093° C (2000° F) Rupture				
			hours	° C	(° F)	MPa	(ksi)	hrs	% Elong.	% R of A
HDA 8077-LPT	202	T	None	---	---	34.5	(5)	161+	---	---
		T	None	---	---	34.5	(5)	12.8	---	---
		T	100	1260	(2300)	34.5	(5)	54.6	12.0	0
		T	100	1260	(2300)	34.5	(5)	54.1	---	---
		T	100	1288	(2350)	34.5	(5)	81.3	15.7	1.2
		T	100	1288	(2350)	34.5	(5)	8.5	---	---
		T	100	1288	(2350)	34.5	(5)	0.2	2.7	1.2
		T	100	1315	(2400)	34.5	(5)	2.8	---	2.4
		T	100	1315	(2400)	34.5	(5)	6.1	2.3	1.2
		T	100	1315	(2400)	34.5	(5)	5.7	---	---
		T	100	1315	(2400)	34.5	(5)	28.5	---	---
HDA 8077-HPT	203	T	None	---	---	41.4	(6)	36.6	---	---
		T	None	---	---	34.5	(5)	95.1	---	---
		T	100	1315	(2400)	34.5	(5)	56.7	---	---
		T	100	1315	(2400)	34.5	(5)	96.2	0.8	1.2
YD NiCrAl	X-42	L	None	---	---	62.0	(9)	0.9	21.9	66.7
		L	None	---	---	55.1	(8)	16.1	12.2	37.9
		L	100	1315	(2400)	55.1	(8)	0.2	47.1	93.7
		L	100	1315	(2400)	48.3	(7)	3.6	41.1	89.7
		T	None	---	---	41.4	(6)	17.1	---	---
		T	100	1260	(2300)	41.4	(6)	9.4	---	1.2
		T	100	1288	(2350)	41.4	(6)	9.7	4.8	3.7
		T	100	1315	(2400)	41.4	(6)	1.3	6.8	2.5
MA 754	---	T	None	---	---	41.4	(6)	60.8	2.6	0
		T	100	1288	(2350)	34.5	(5)	8.5	---	---
		T	100	1315	(2400)	41.4	(6)	51.1	0.8	0
DS NiCr	---	T	None	---	---	55.1	(8)	27.3	1.9	1.2
		T	100	1315	(2400)	55.1	(8)	2.5	(Thread Failure)	

Table 9. Creep Rupture Testing - HDA 8077 and YD NiCrAl - 1093° C (2000° F).

Alloy	Specimen	Test Direction	Stress		Hours			Failure, % E	Ductility, % R of A	Steady-State Creep Rate cm/cm hr
			MPa	(ksi)	0.1% E	0.2% E	Failure			
YD NiCrAl	105-1	T	41.4	(6)	1	20	31	---	2.1	7.5×10^{-6}
	105-2	T	37.9	(5.5)	18	64	153	---	1.3	20×10^{-6}
	105-3	T	34.5	(5)	28	60	144	1.2	1.3	0.7×10^{-6}
	105-5	T	34.5	(5)	200	750	Disc. (768)	---	---	1.0×10^{-6}
	105-6	T	34.5	(5)	350	---	Disc. (645)	---	---	0.3×10^{-6}
	1-T	T	34.5	(5)	210	450	589	---	0.6	0.1×10^{-6}
	1-L	L	51.7	(7.5)	1	11	483	1.2	23.9	0.6×10^{-6}
8077	202T	T	27.6	(4)	44	80	648	14.5	0	1.0×10^{-6}
	202L	L	68.9	(10)	0.8	58	623	15.1	1.2	2.5×10^{-6}

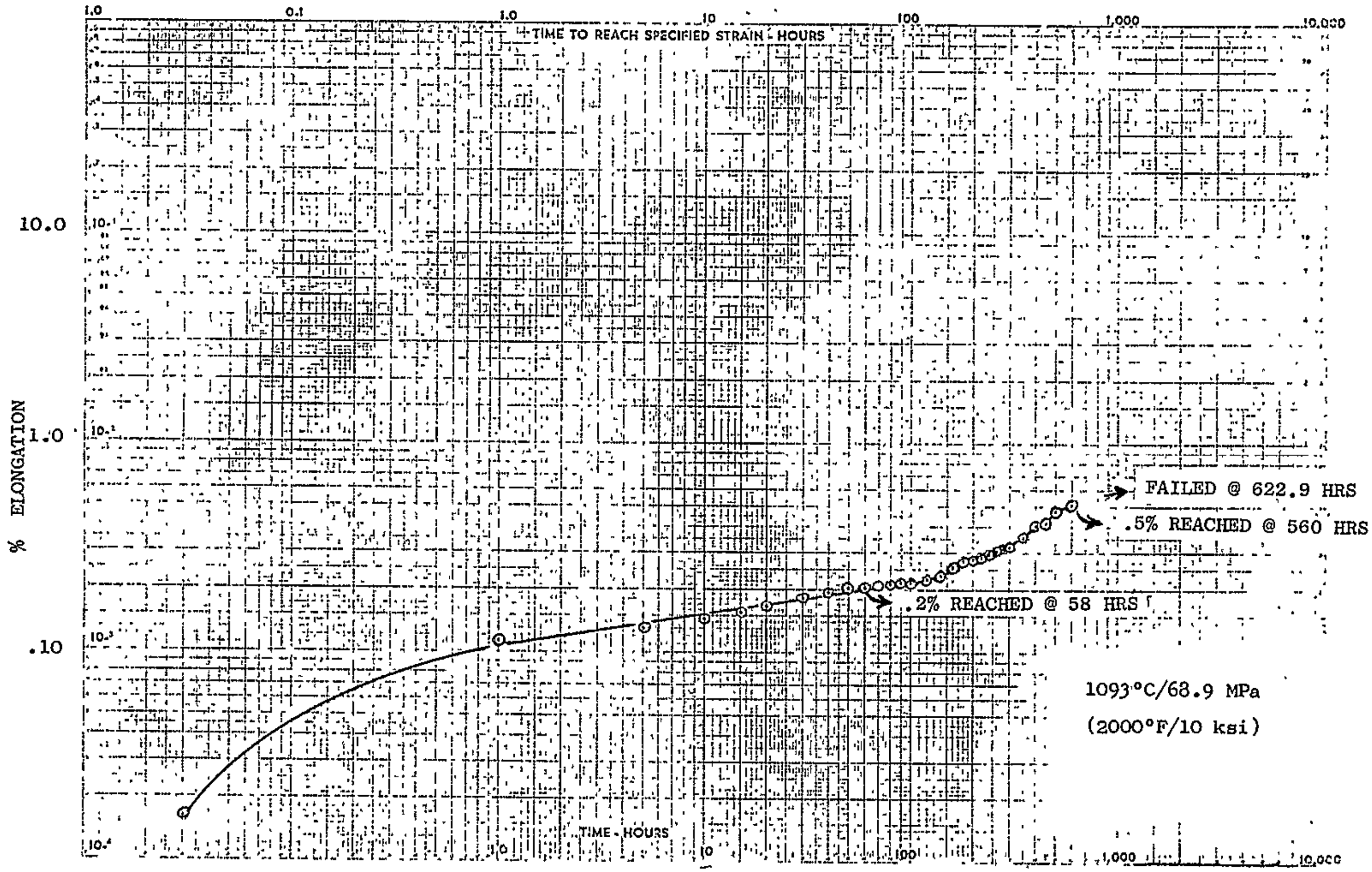

Figure 14 Creep Curve HDA 8077-202 Longitudinal

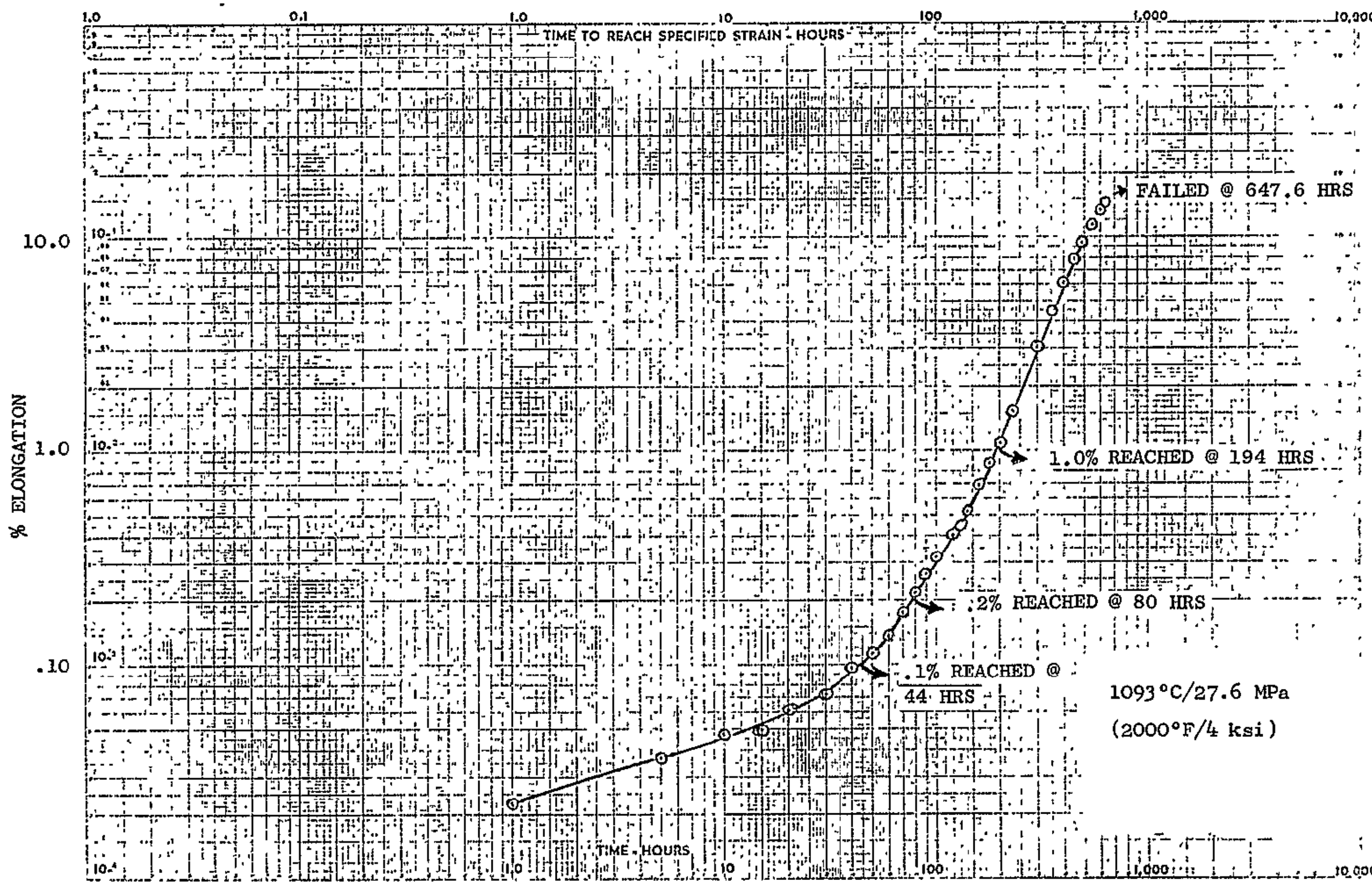

Figure 15 Creep Curve HDA 8077-202 Transverse

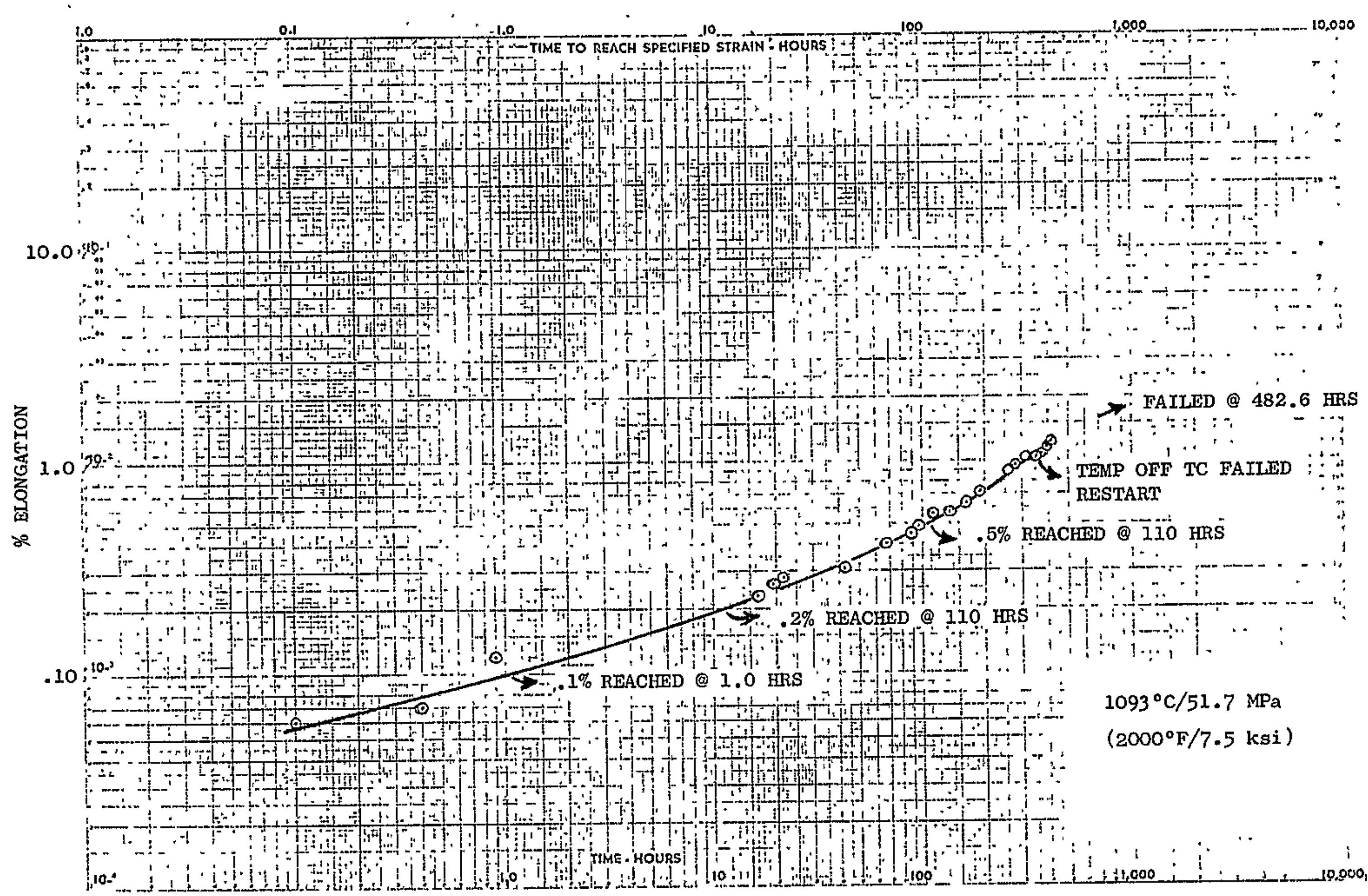

Figure 16 Creep Curve YDNiCrAl Longitudinal

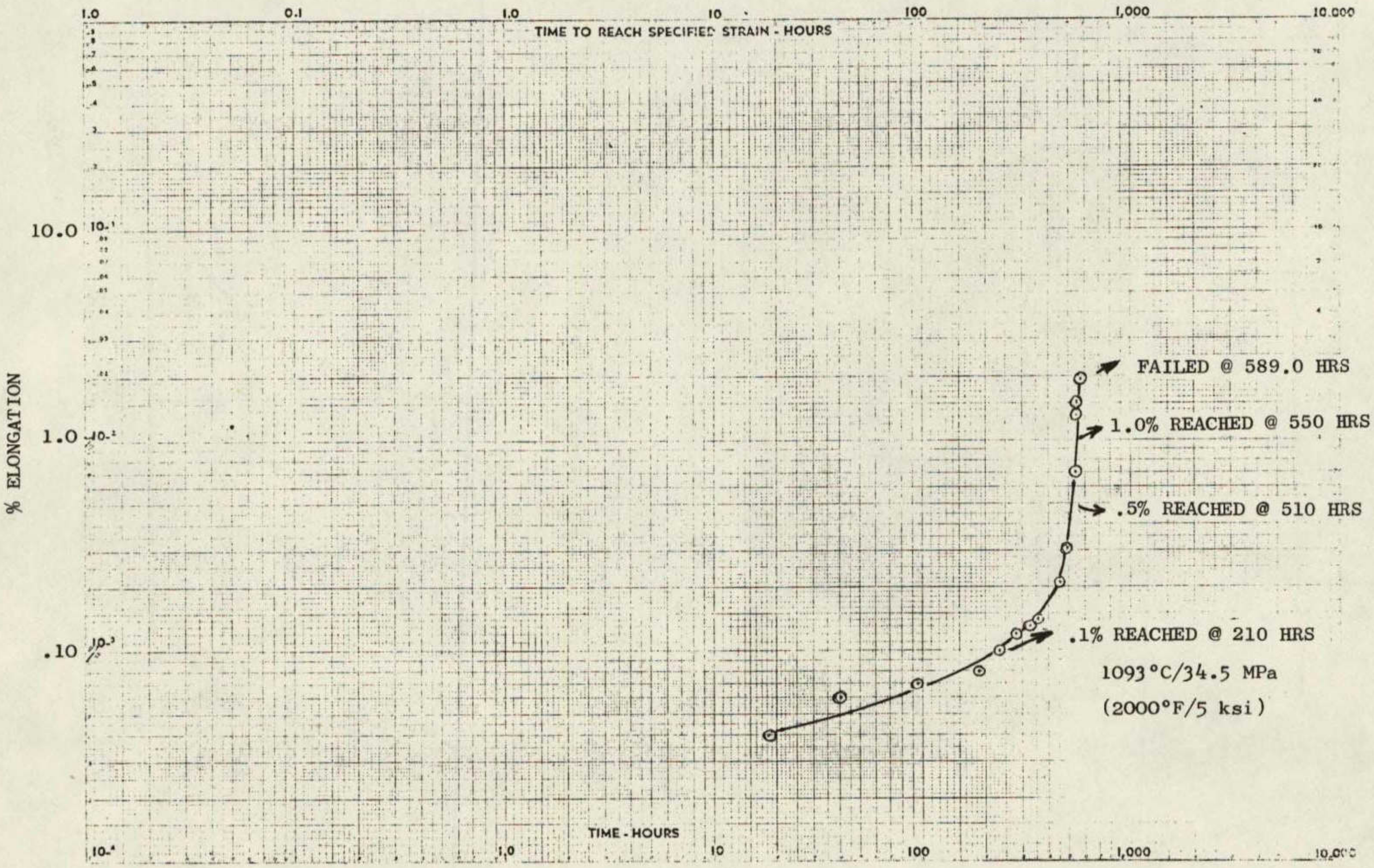

Figure 17 Creep Curve YDNiCrAl Transverse

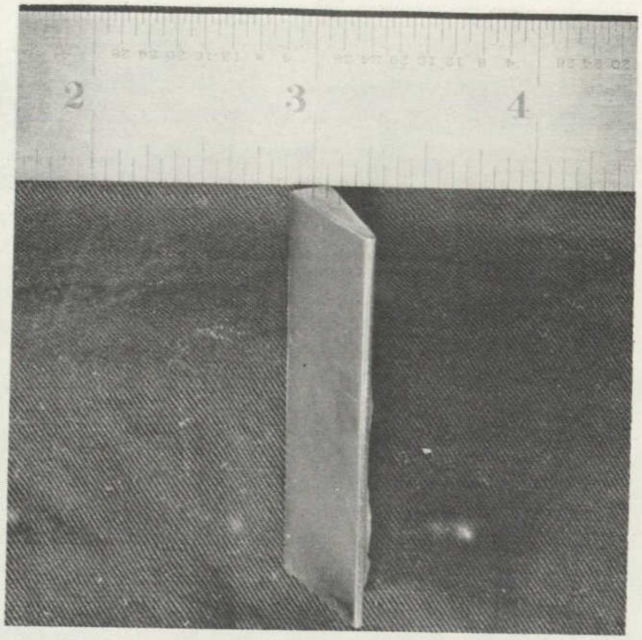

SETS WEDGE SPECIMEN

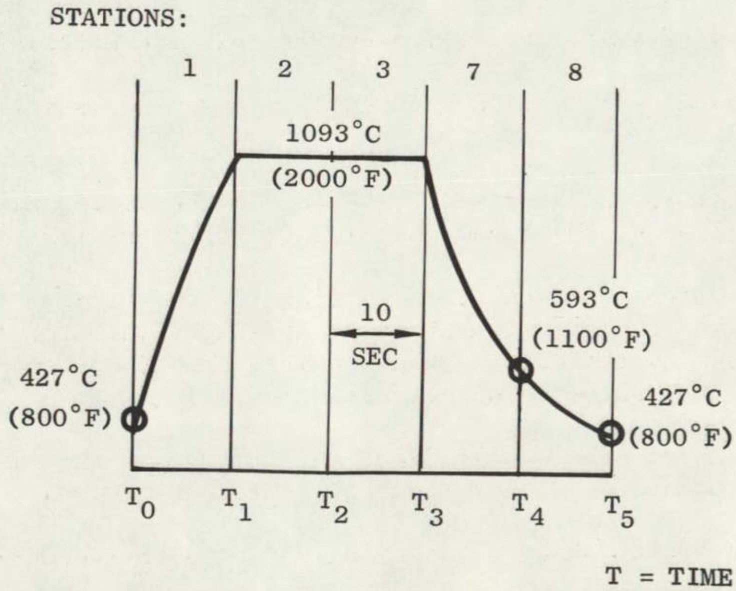

SETS CYCLE

Figure 18 Simulated Engine Thermal Shock (SETS) Specimen and Cycle

2. One to three cracks which do not traverse the leading edge arc
3. Four or more cracks which do not traverse the leading edge arc
4. One to three cracks which traverse the leading edge arc
5. Four or more cracks which traverse the leading edge arc
6. One to three cracks which extend past the leading edge arc
7. Four or more cracks which extend past the leading edge arc
8. One to three cracks which extend past the leading edge arc by at least 2.4 mm (3/32 inch)
9. Four or more cracks which extend past the leading edge arc by at least 2.4 mm (3/32 inch)
10. One or more cracks which extend past the leading edge arc by at least 4.8 mm (3/16 inch)

Thermal fatigue testing covered a number of facets:

- Comparison of program alloys with MA 754
- Comparison of program alloys with cast alloys
- Longitudinal and transverse testing
- Testing of properly and improperly textured material

The SETS results plotted in Figures 19 and 22 indicate the following:

- The selected program alloys (HDA 8077 and YD NiCrAl) and MA 754 are superior to the cast alloys tested in the longitudinal direction (vane leading edge) but inferior in the transverse direction.

- Longitudinal samples are significantly better than the transverse - a result of higher longitudinal strengths and, for the <100> material, lower moduli in the longitudinal directions as compared with the transverse directions.

- All samples both longitudinal and transverse show improved performance of the <100> longitudinal textured material.

- The YD NiCrAl shows a larger differential between <100> and non-<100> samples.

- The YD NiCrAl exhibits the best transverse thermal fatigue properties.

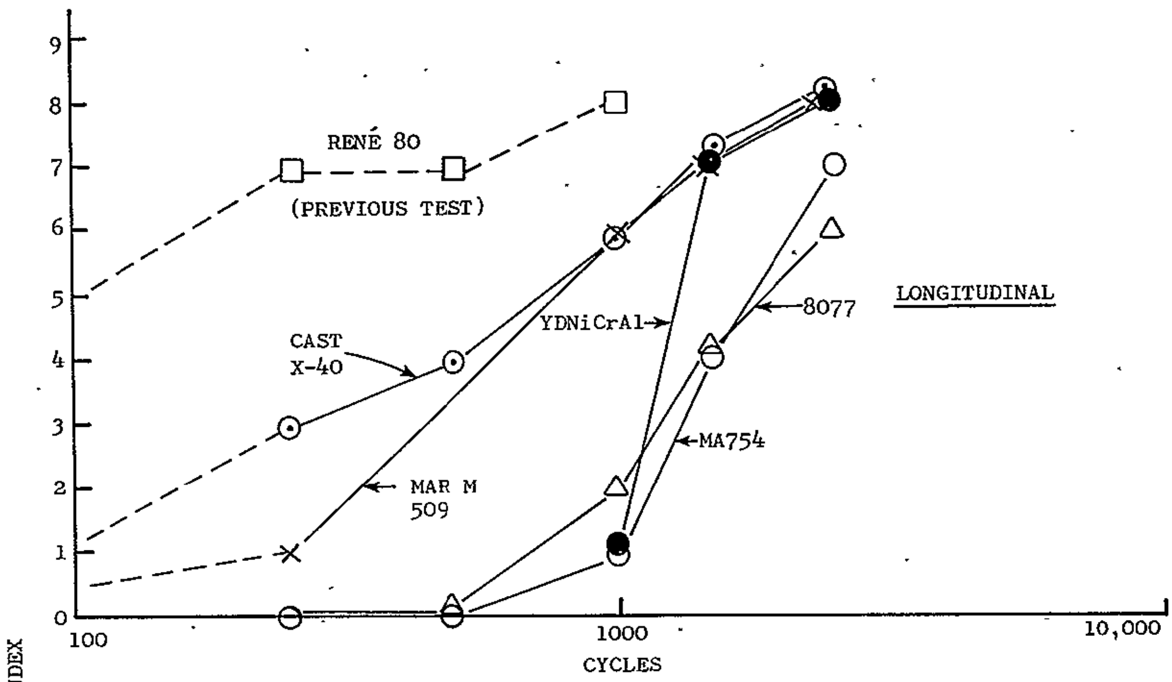

Figure 19 Thermal Fatigue of HDA 8077, YD NiCrAl, MA 754 and Cast Alloys

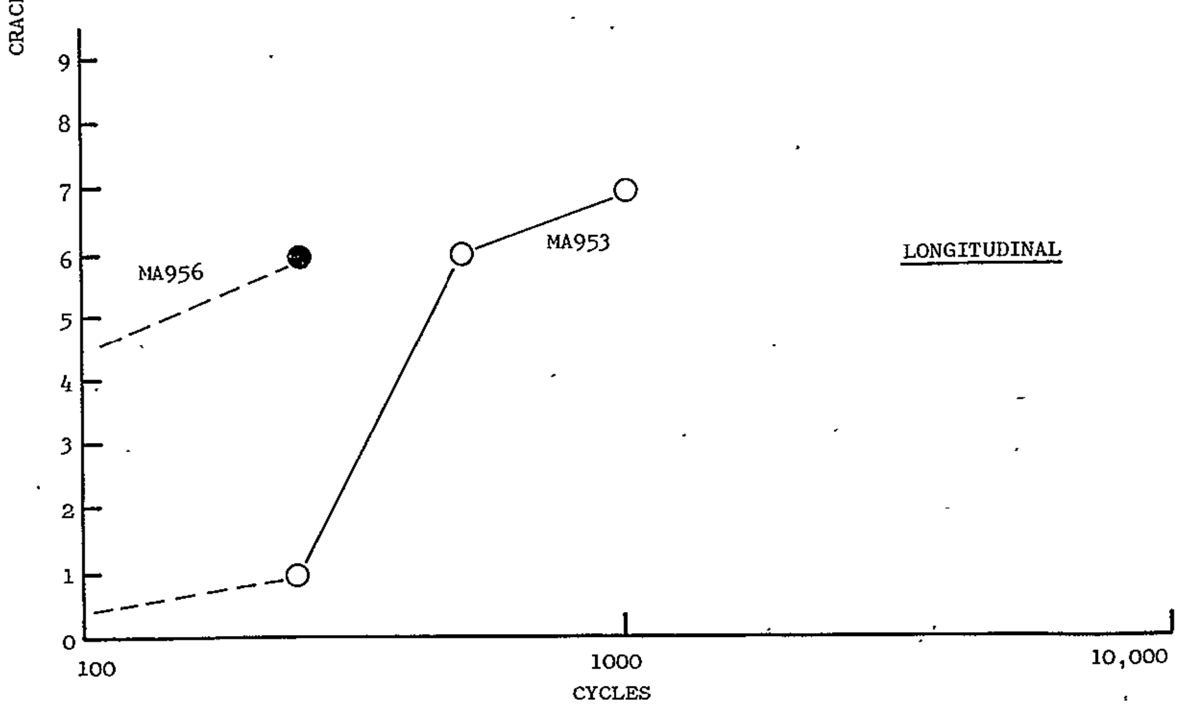

Figure 20 Thermal Fatigue of MA 953, MA 956

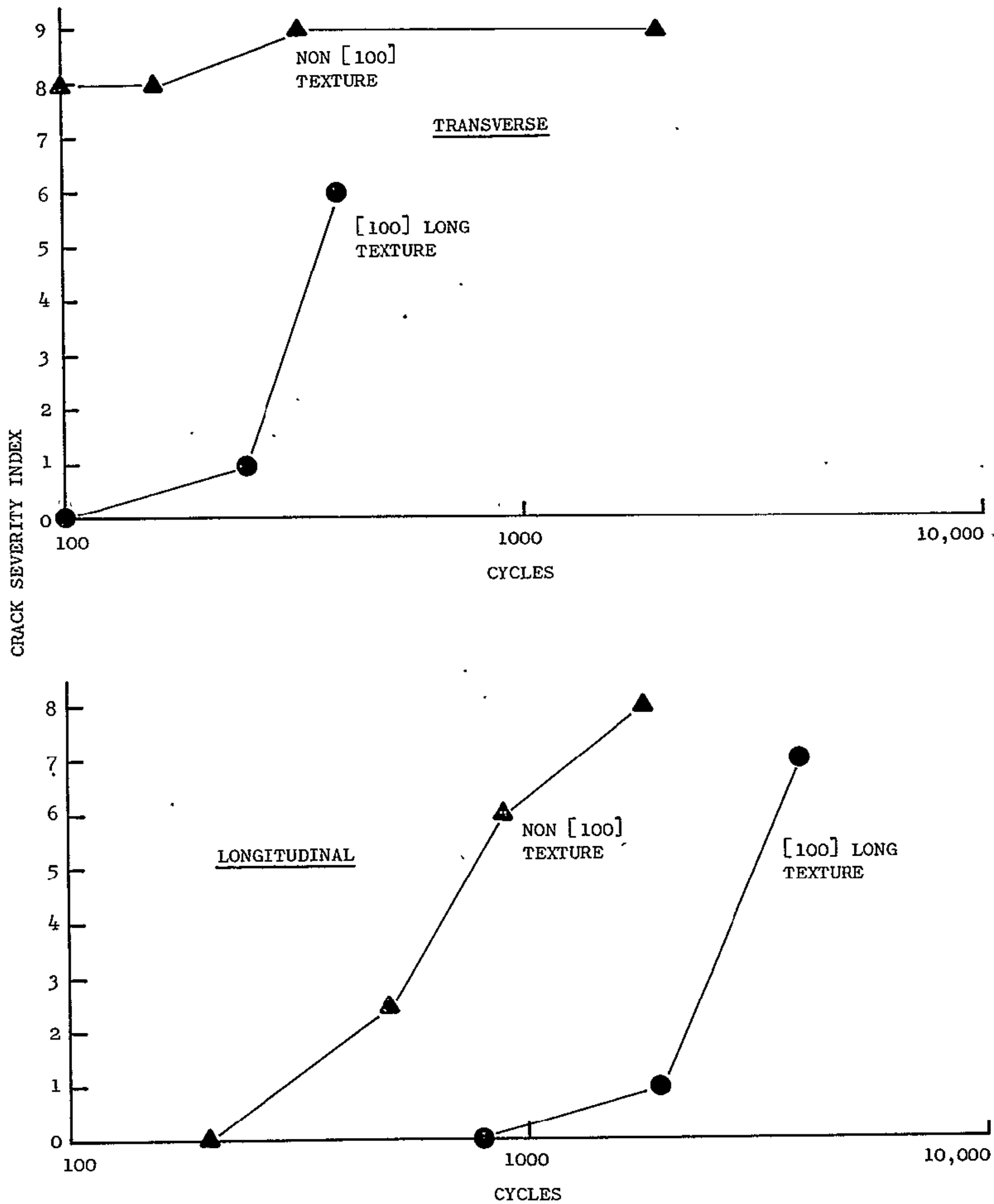

Figure 21 Thermal Fatigue of YD NiCrAl

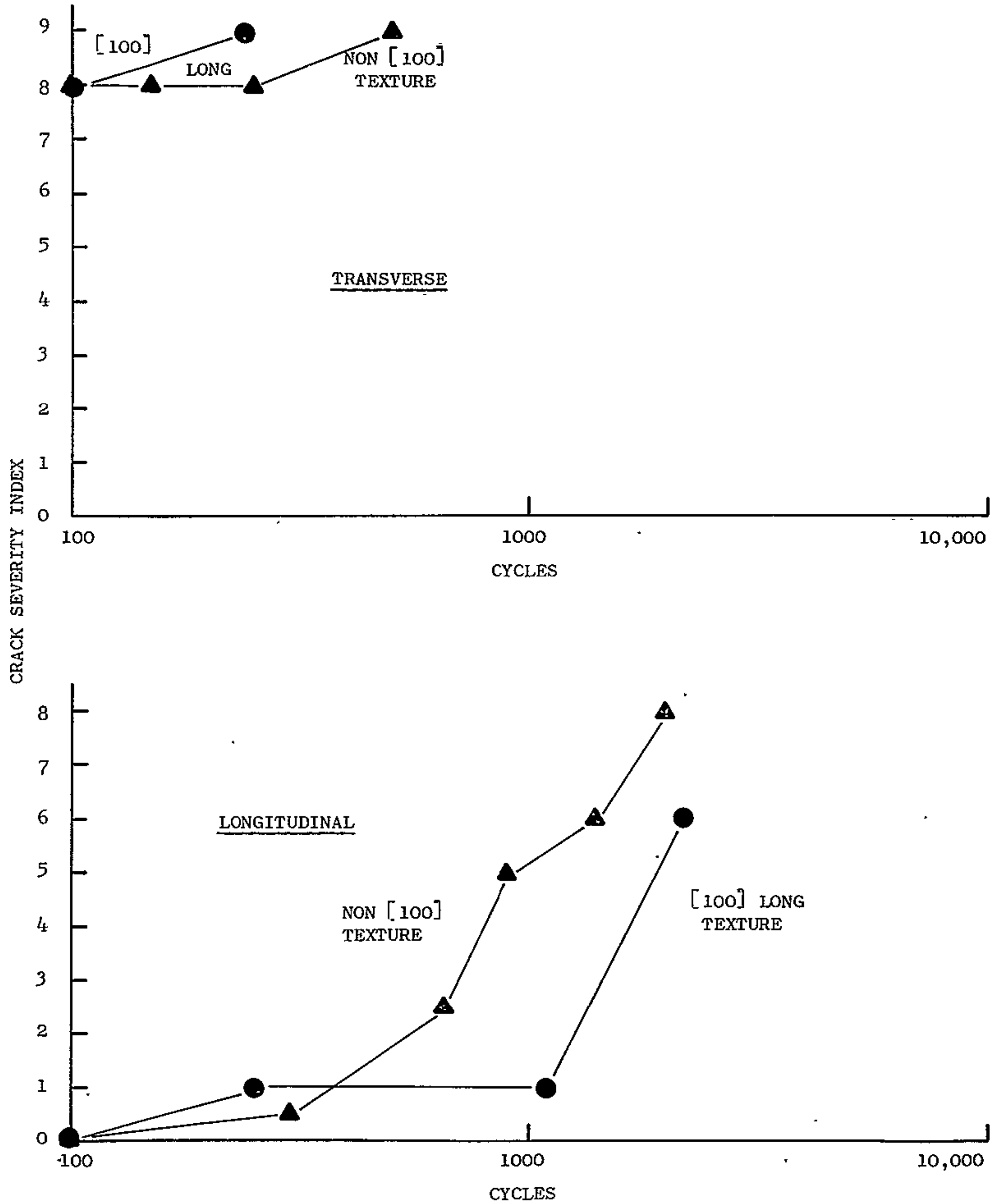

Figure 22 Thermal Fatigue of HPT Type HDA 8077

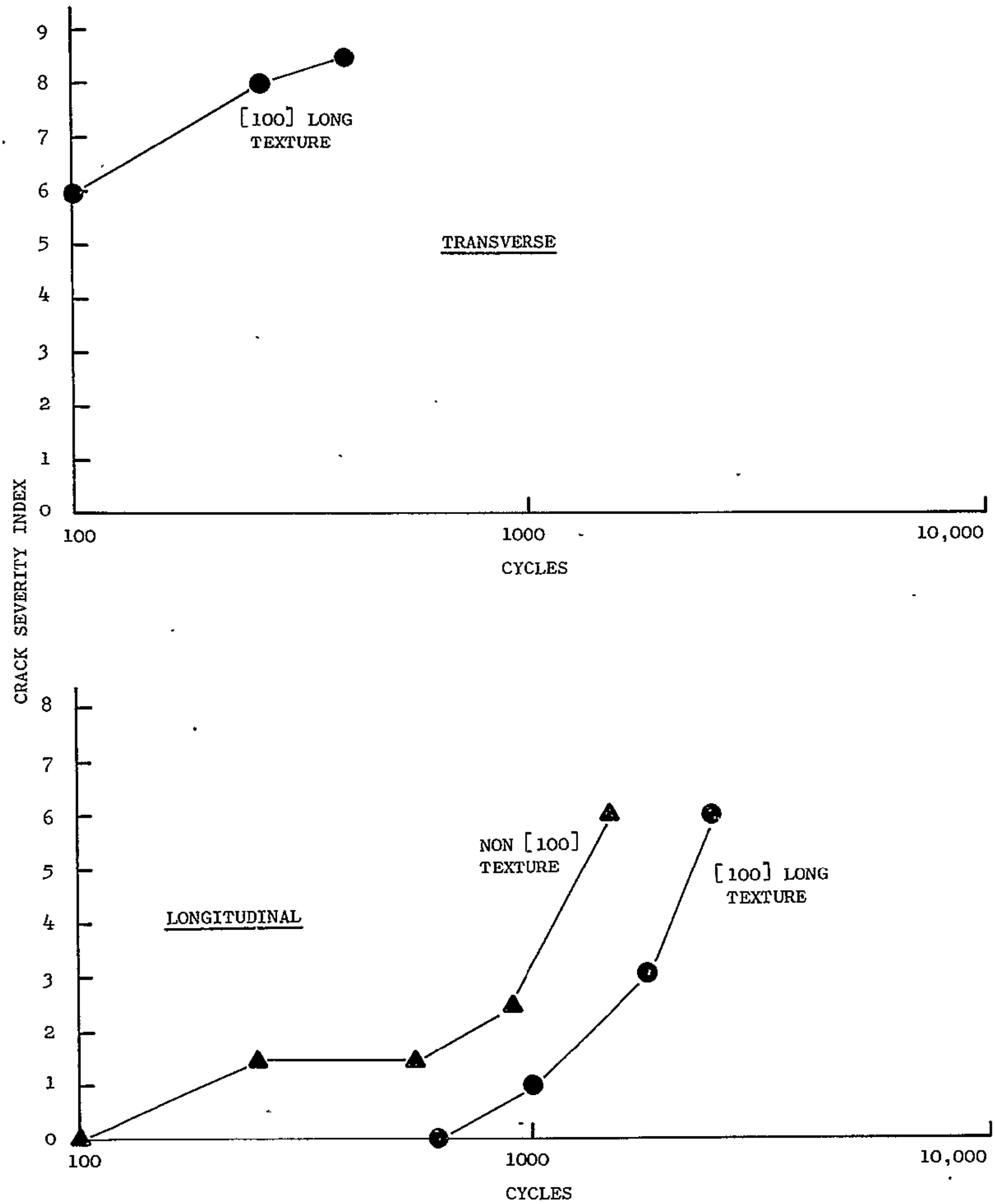

Figure 23 Thermal Fatigue of LPT Type HDA 8077

- MA 953 has only fair thermal fatigue resistance and MA 956 is quite poor.

3.1.11 Low Cycle Fatigue Testing

Strain-controlled, low-cycle, fatigue (LCF) testing is commonly used for turbine vane alloys. Strain control is selected over load control because the major vane stresses are induced by thermal-gradient-caused strains, not mechanical loads. Actual stresses are not necessarily predictable, being a function of how the material absorbs the strains, and whether it resists or relaxes. Low cycle testing is used because the cyclic periods relate to flight cycles and not engine rotational speed. Thermal strains can only be approximated, because they result from complex combinations of through-the-vane-wall and between-cooling-hole thermal gradients.

The LCF testing was done at an A ratio (alternating strain/mean strain) of 1.0. Testing was done at 871°, 1093°, and 1204° C (1600°, 2000°, 2200° F). The data are recorded in Table 10 and plotted in Figures 24 through 27. The figures also include a number of data points for MA 754 and DS NiCr obtained outside of the program. A number of observations can be made:

- Longitudinal lives for a given alloy, temperature, and strain exceed the transverse lives.
- The maximum strain values decrease with increasing temperature.
- Though there is considerable spread between the two heats of YD NiCrAl testing, the data show the following trend in ranking at 1093° C (2000° F):

  YD NiCrAl

  MA 754

  HDA 8077-HPT

  DS NiCr

  HDA 8077-LPT

- In the 1093° C (2000° F) transverse testing, the values for all alloys appear to converge at ~0.7% strain and 2000 cycles. For the other temperature/directions, there is either little divergence or insufficient data to establish trends.
- Based on these LCF data, YD NiCrAl and HDA-type HPT were judged suitable for vane use and acceptable for engine testing.

Table 10. Low Cycle Fatigue Data.

Alloy	Heat No.	Temperature ° C (° F)	Test Direction	Alternating Strain, %	Cycles to Crack Initiation (N_i)	Cycles to Failure (N_f)
8077-LPT	202	871 (1600)	L	0.41	790	1008
	202	871 (1600)	L	0.30	14008	16087
	202	871 (1600)	T	0.27	1242	1370
	202	1093 (2000)	L	0.24	1165	1597
	202	1093 (2000)	L	0.19	1067	1617
	202	1093 (2000)	L	0.095	---	52750 runout
	202	1093 (2000)	L	0.14	4827	9160
	202	1093 (2000)	L	0.095	---	63007 runout
	202	1093 (2000)	T	0.1	0.5	15
	202	1093 (2000)	T	0.075	0	---
	202	1093 (2000)	T	0.075	39010	70575 runout
	202	1093 (2000)	T	0.15	0.5	20
	202	1204 (2200)	L	0.16	937	1646
	202	1204 (2200)	L	0.18	1103	1300
	202	1204 (2200)	T	0.07	---	73
8077-HPT	203	871 (1600)	L	0.32	8449	9654
	203	871 (1600)	L	0.19	---	111172
	203	871 (1600)	T	0.28	3026	3150
	203	1093 (2000)	L	0.19	2476	2712
	203	1093 (2000)	L	0.23	781	921
	203	1093 (2000)	T	0.08	5272	8778
		1093 (2000)	T	0.12	6126	7386
		1093 (2000)	T	0.24	17	19
	203	1204 (2200)	L	0.14	8549	10145
	203	1204 (2200)	L	0.15	4392	5466
	203	1204 (2200)	T	0.07	---	5310
YD NiCrAl	---	871 (1600)	L	0.28	24450	26800
	---	871 (1600)	L	0.37	2004	3474
	---	871 (1600)	T	0.28	1078	1354
	---	871 (1600)	T	0.27	272	347
	X-40	1093 (2000)	L	0.24	1837	2918
	X-40	1093 (2000)	L	0.19	1830	3540
	X-40	1093 (2000)	T	0.076	5072	10155
	X-40	1093 (2000)	T	0.15	729	1337
	X-40	1093 (2000)	T	0.10	3047	5894
	X-40	1093 (2000)	T	0.077	18232	19144
	X-77	1093 (2000)	T	0.079	208	297
	223	1093 (2000)	T	0.103	18134	18818
	223	1093 (2000)	T	0.35	1328	1604
	---	1204 (2200)	T	0.072	33915	38052
	---	1204 (2200)	T	0.077	23107	28307
DS NiCr	Medium Grain	1093 (2000)	T	0.09	---	28
	Coarse Grain	1093 (2000)	T	0.12	18	74
	Coarse Grain	1093 (2000)	T	0.12	---	644

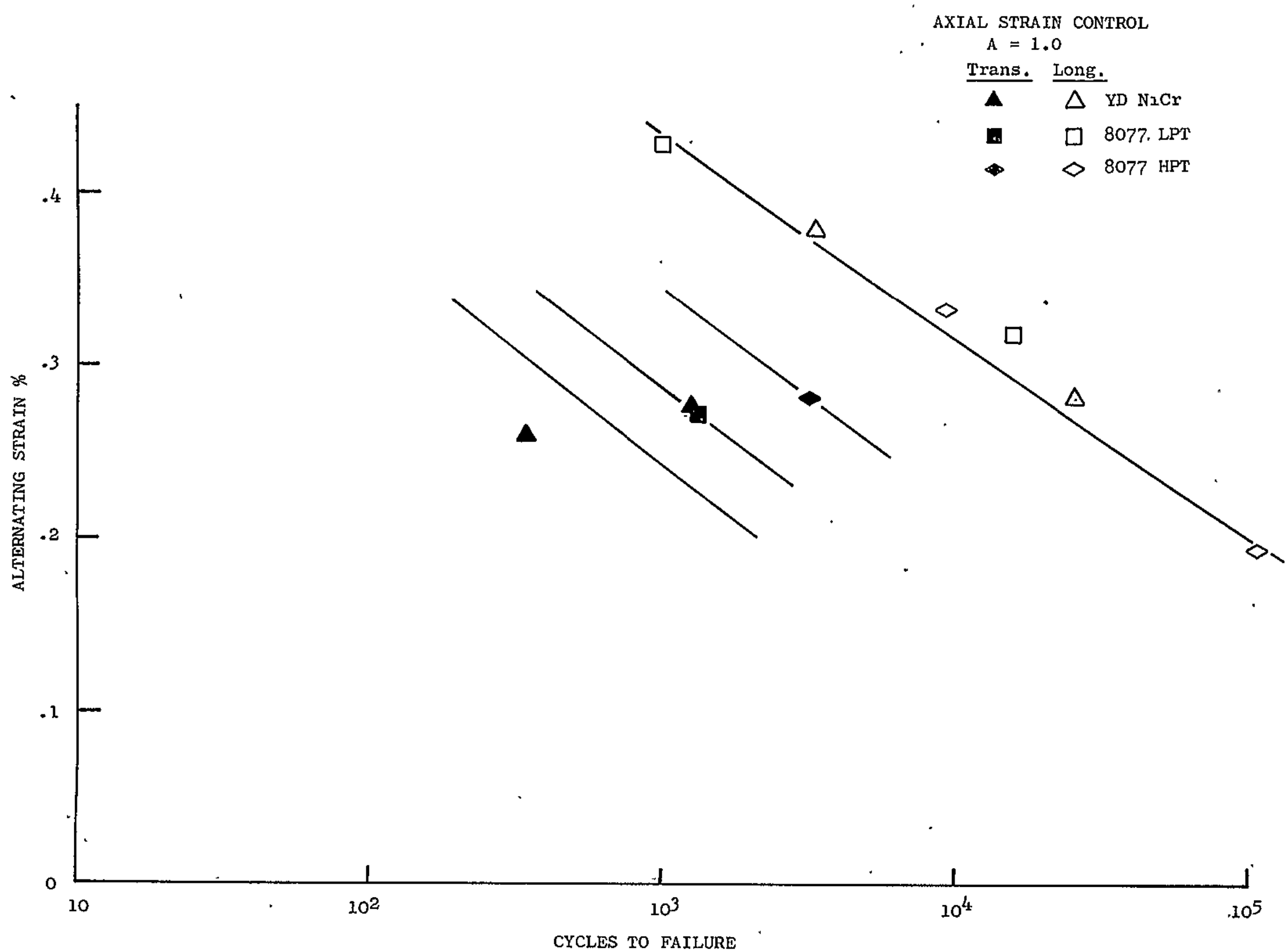

Figure 24 Low Cycle Fatigue 871°C (1600°F)

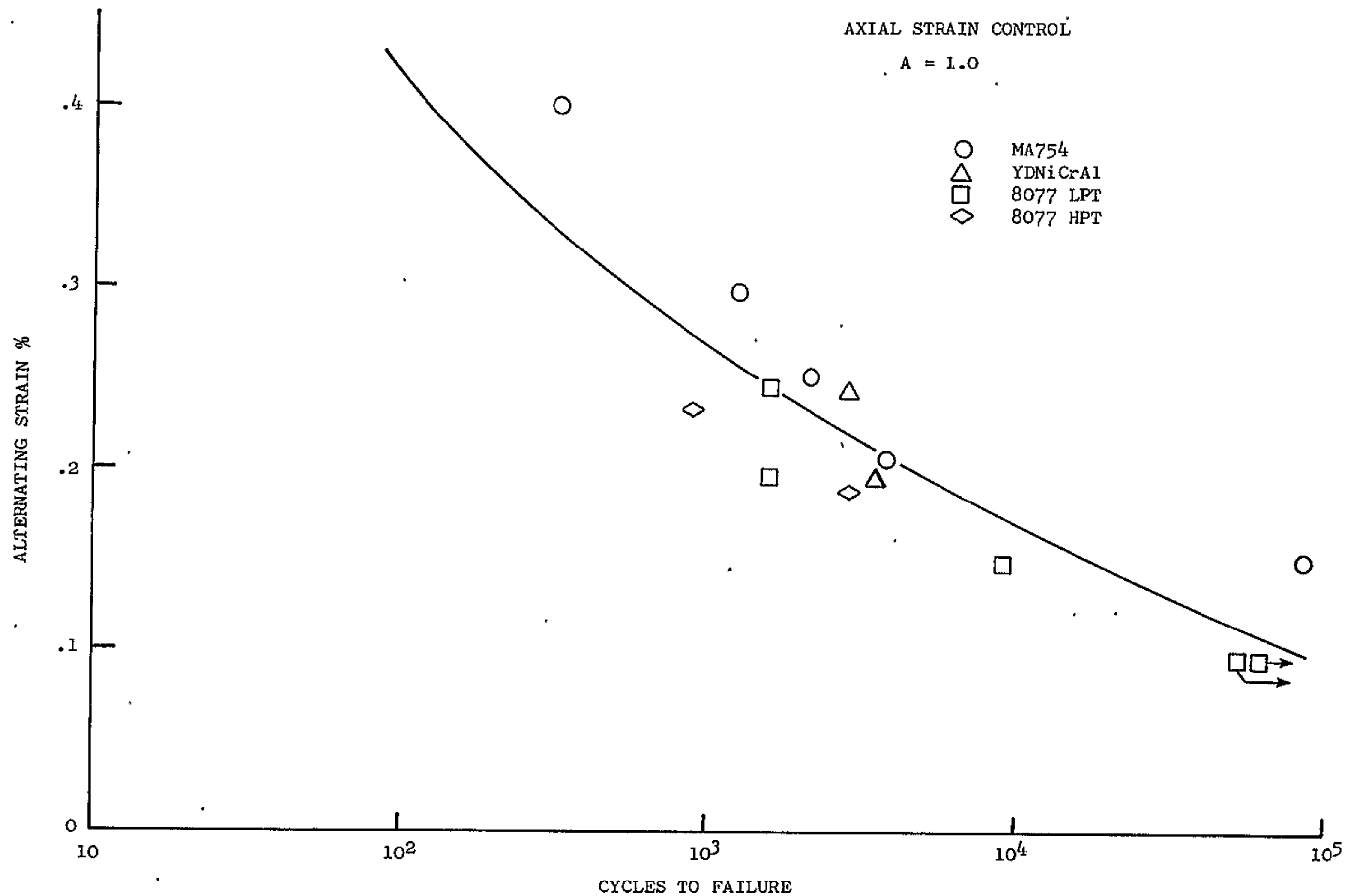

Figure 25 Longitudinal Low Cycle Fatigue 1093°C (2000°F)

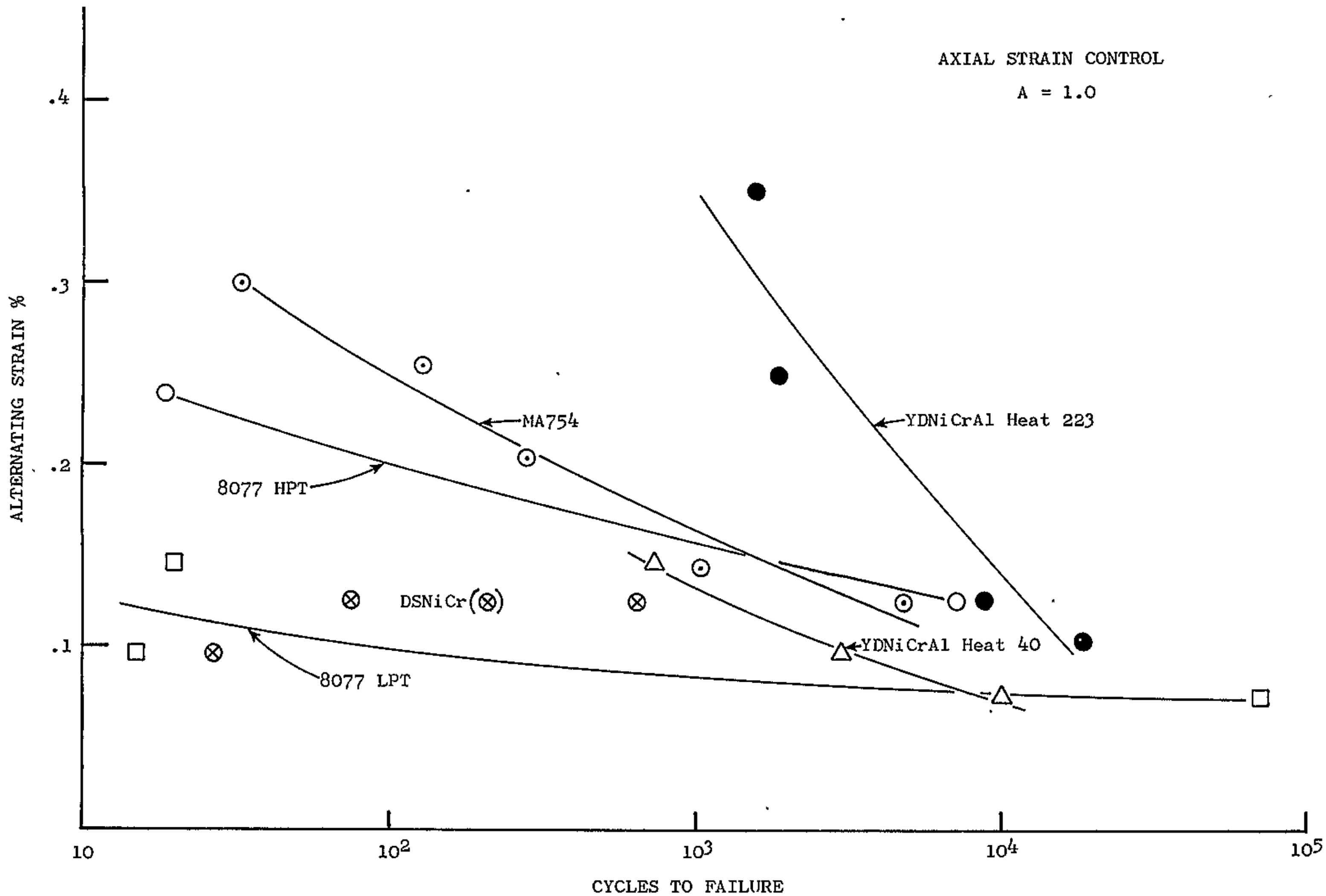

Figure 26 Transverse Low Cycle Fatigue 1093°C (2000°F)

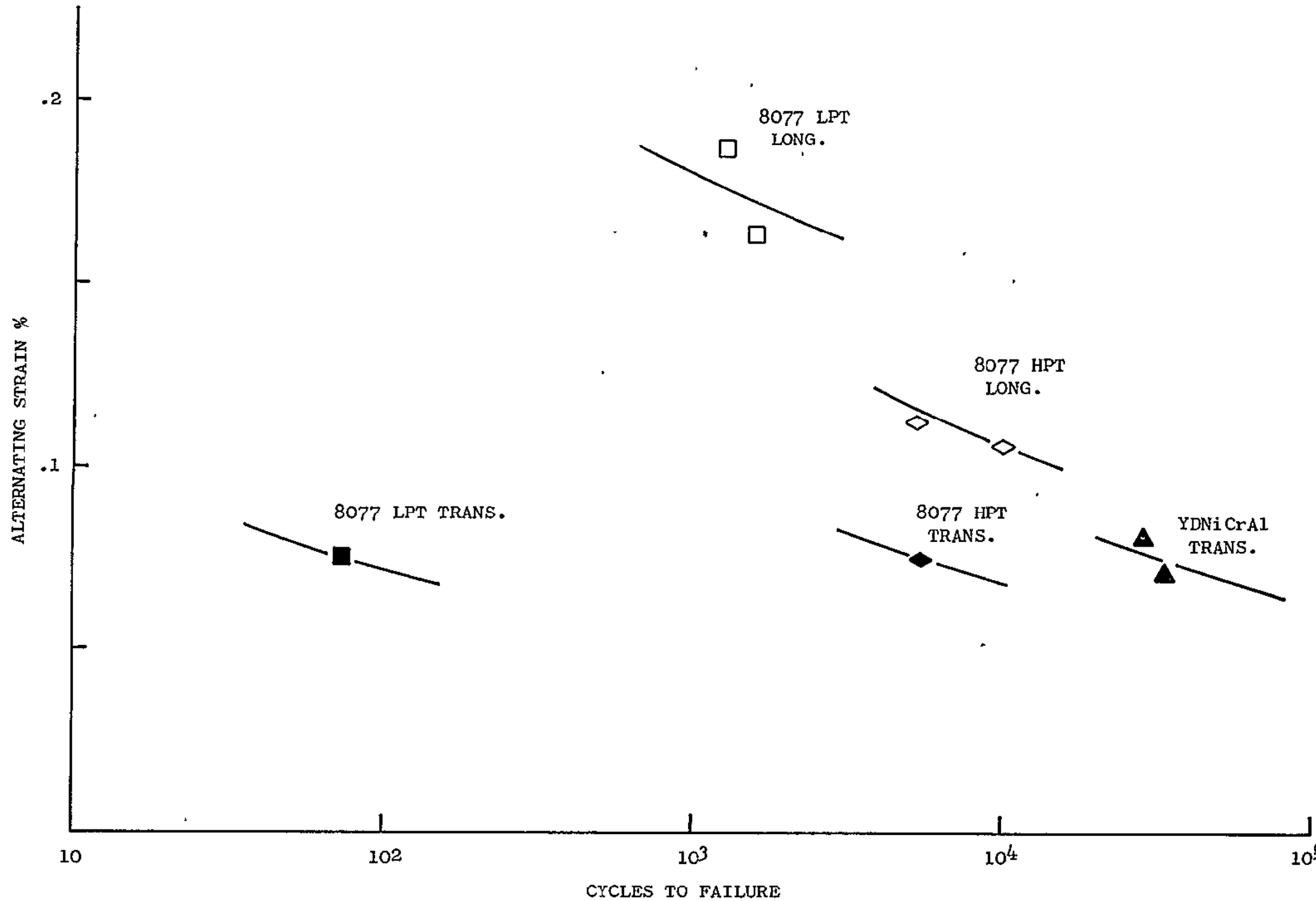

Figure 27 Low Cycle Fatigue 1204°C (2200°F)

3.1.12 Nil Strength Testing

"Nil Strength" is a test utilized to estimate melting point by measuring the maximum load-bearing temperature of a material. It is conducted in a stress rupture machine by loading to a minimal stress level, e.g., 2.07 MPa (300 psi) and heating from an intermediate temperature till failure occurs. The temperature at failure is the "Nil Strength Temperature." In ODS alloys, it has been observed that the nil strength usually is slightly above the predicted melting point. Table 11 lists the nil strength measured for several program alloys together with their estimated melting points. MA 956 could not be tested because its estimated melting point of over 1480° C (2700° F) exceeds the temperature capability of the testing equipment. The data indicate that HDA 8077 and YD NiCrAl meet the vane alloy melting point goal of 1371° C (2500° F), while MA 953 does not.

Table 11. Nil Strength of Program Alloys.

Alloy	Measured Nil Strength		Estimated Melting Point	
	° C	(° F)	° C	(° F)
YD NiCrAl	1382	(2520)	1371	(2500)
	1390	(2535)	---	---
HDA 8077	1390	(2535)	1371	(2500)
MA 953	1368	(2495)	1349	(2460)
	1362	(2483)	---	---

3.1.13 Oxidation Testing

Oxidation testing was conducted at both low and high velocities. The former was used to screen alloys for selection of the most promising candidates, and the latter was used to determine whether the advanced alloys would meet vane goals. Both series of tests indicated excellent oxidation resistance for MA 956, HDA 8077, and YD NiCrAl. The other alloys did not perform satisfactorily, especially in the high velocity testing.

Low Velocity Oxidation Testing

The low velocity oxidation testing consisted of 200 hours of cyclic exposure at 1204° C (2200° F) under Mach 0.05 conditions in a flame tunnel. The cycling was six times per hour with approximately 54 minutes of hot time per hour. The specimens were 3 mm (1/8 inch) diameter by 39 mm (1 1/2 inches) long. Four samples of each alloy were run:, two longitudinal and two transverse, except for the MA 956 for which transverse samples were not run.

The weight changes listed below were recorded from starting pin weights of approximately 2.4 grams (2.3 for MA 953 and 2.2 for MA 956 because of lower densities). Estimated 1093° C (2000° F) Mach 1 surface recessions were well within the 0.06-mm (0.0025-inch) goal. Actual surface recession measurements were not possible because, through oversight, the original pin diameters were not recorded.

Alloy	Weight Change, Mg/cm^2		Estimated 1093° C (2000° F) Mach 1 Surface Recession in 500 Hours	
	Minimum	Maximum	mm	(inch)
HDA 8077 (2% Y_2O_3)	-4.7	-6.0	0.02	(0.0007)
HDA 8077 (0.6% Y_2O_3)	-1.3	-1.6	0.005	(0.0002)
YD NiCrAl	-0.8	-1.0	0.003	(0.0001)
MA 953	-2.0	-12.4	0.04	(0.0015)
TD NiCrAl	+0.09	+ 0.5	0.03	(0.001)
MA 956	+0.5	+ 0.7	0.03	(0.001)

Microstructural examination, Figures 28 through 33, showed uniform and minimal oxidation on HDA 8077, YD NiCrAl, and MA 956 with occasional spike oxidation on TD NiCrAl and gross local attack on MA 953. The weight loss difference between the two Y_2O_3 levels in HDA 8077 is not understood, though the higher dispersoid level with its less perfect <100> texture may have had some effect. In any case, the projected Mach 1 surface recession values are well below the aim of 0.06 mm (0.0025 inch).

High Velocity Oxidation Testing

This testing was conducted in the General Electric (Lynn, Mass.) high velocity rig under Mach 1 airflow conditions with hourly cycling to approximately 93° C (200° F) for 5 minutes. Two 500-hour tests were run, at 982° C (1800° F) and 1204° C (2200° F).

In the 982° C (1800° F) test, weight loss/gain data were gathered, and metallography was done on the exposed samples. Visual observation showed varying degrees of attack ranging from essentially none on MA 956, low on

200X

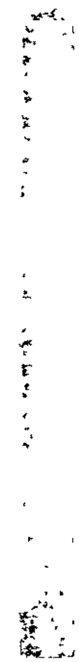

2X

LONGITUDINAL SAMPLE

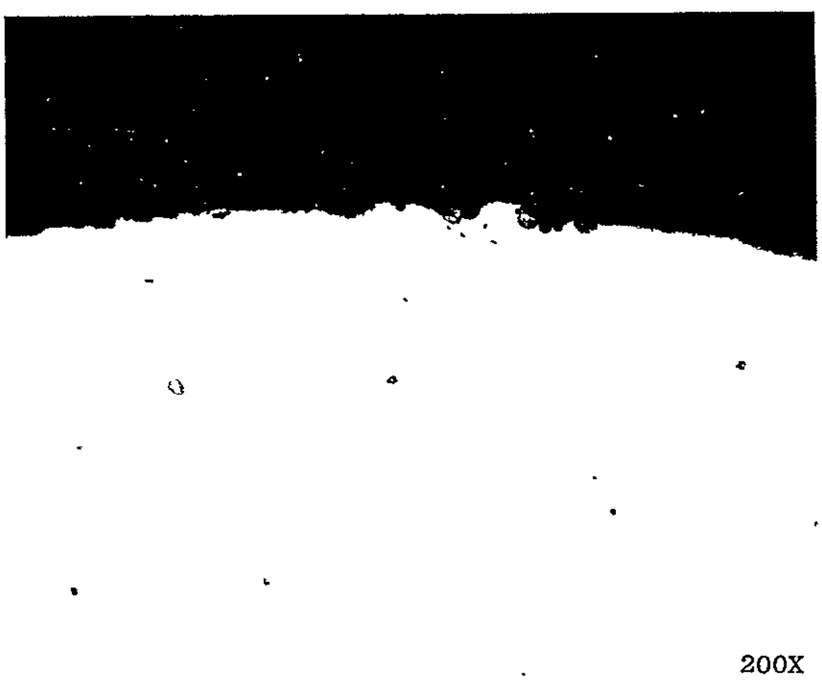

200X

2X

TRANSVERSE SAMPLE

Figure 28 YDNiCrAl Low Velocity Oxidation Pins

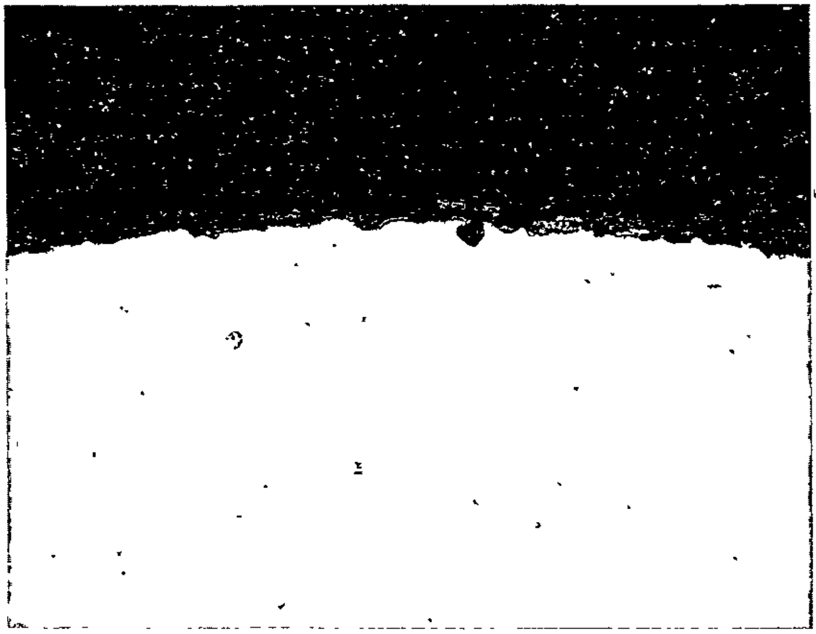

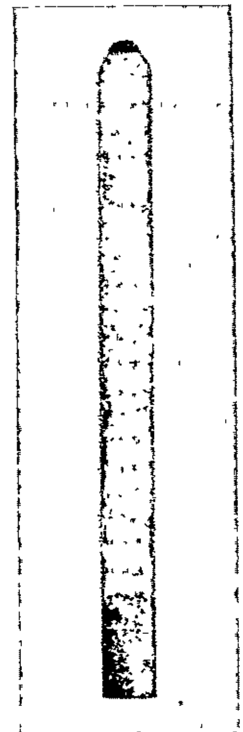

200X

LONGITUDINAL SAMPLE

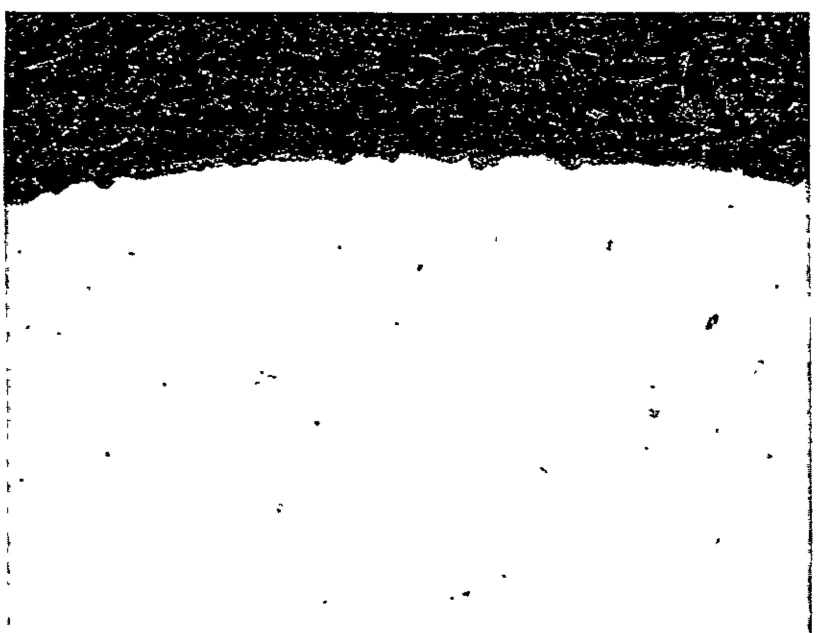

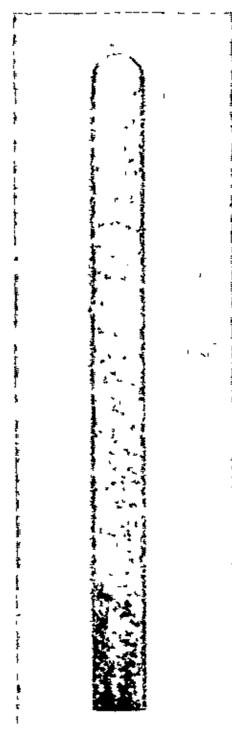

200X

2X

TRANSVERSE SAMPLE

Figure 29 HDA 8077 HPT Low Velocity Oxidation Pins

200X 2X

LONGITUDINAL SAMPLE

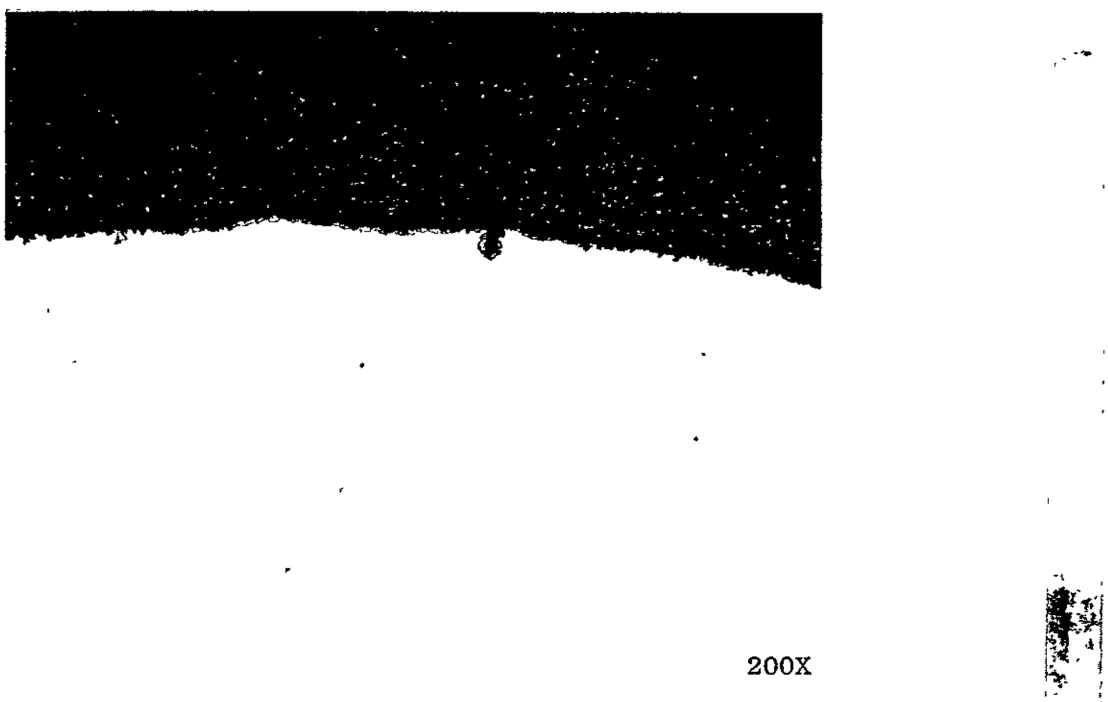

200X 2X

TRANSVERSE SAMPLE

Figure 30 HDA 8077 LPT Low Velocity Oxidation Pins

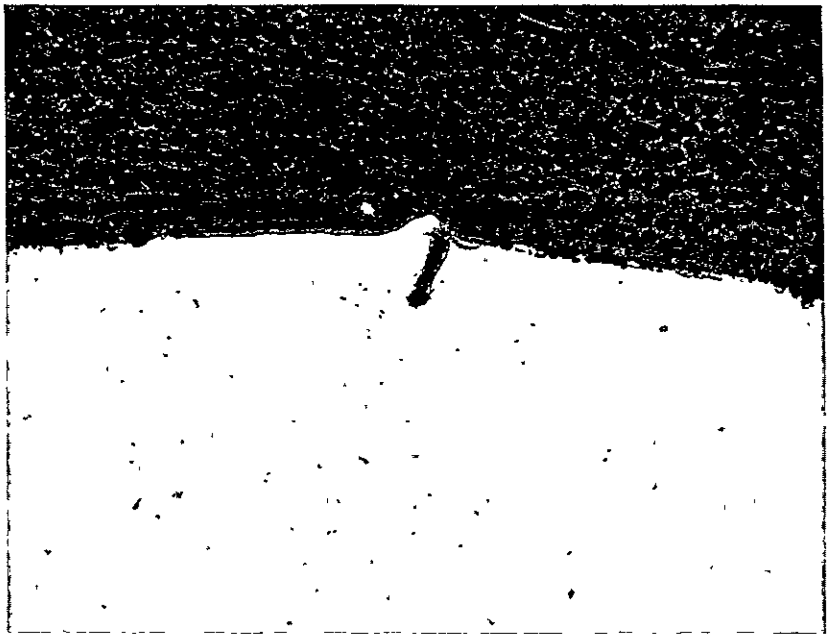

200X

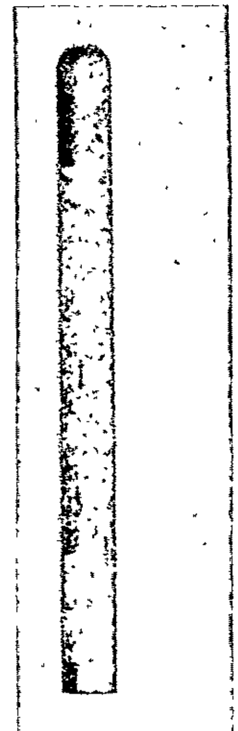

2X

LONGITUDINAL SAMPLE

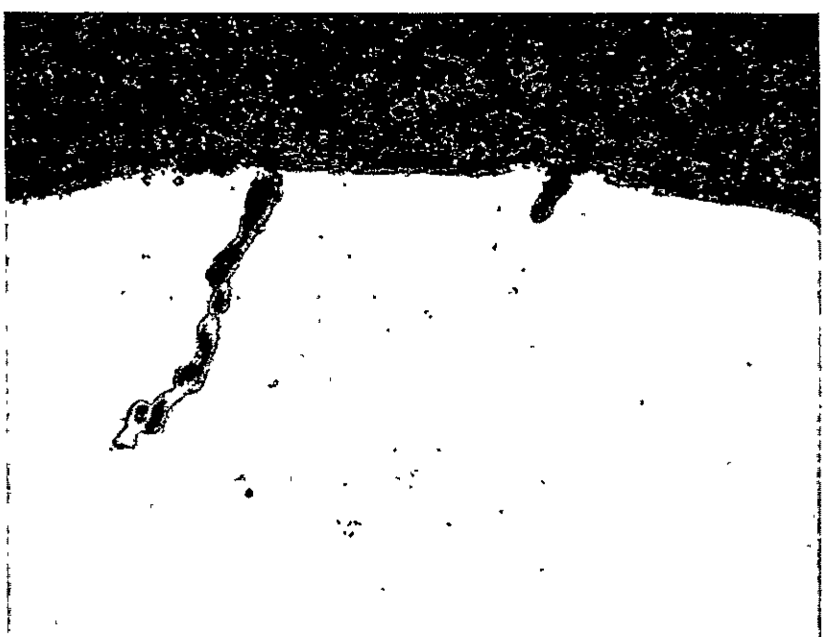

200X

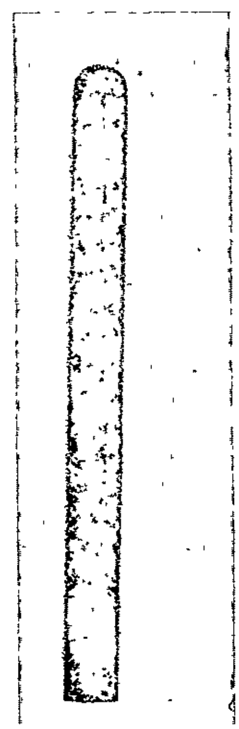

2X

TRANSVERSE SAMPLE

Figure 31 TDNiCrAl Low Velocity Oxidation Pins

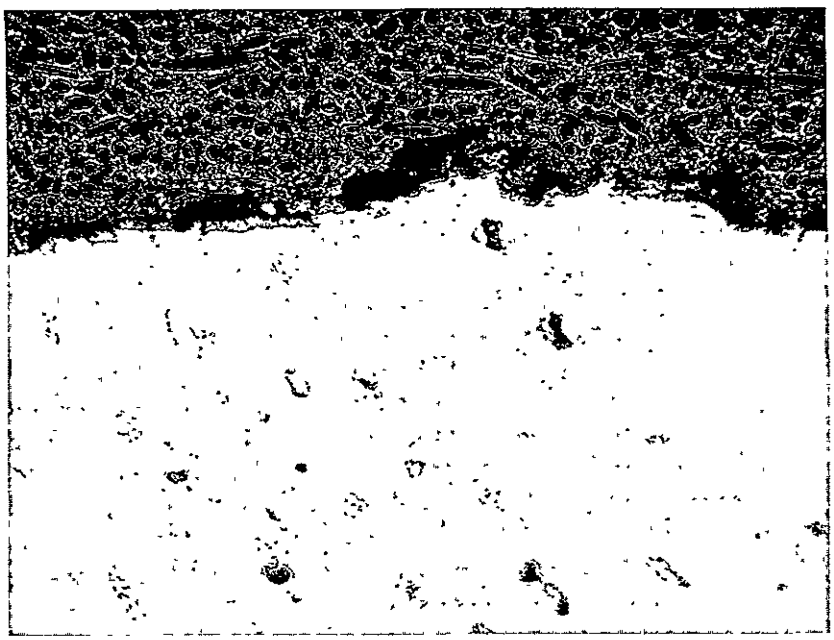

200X

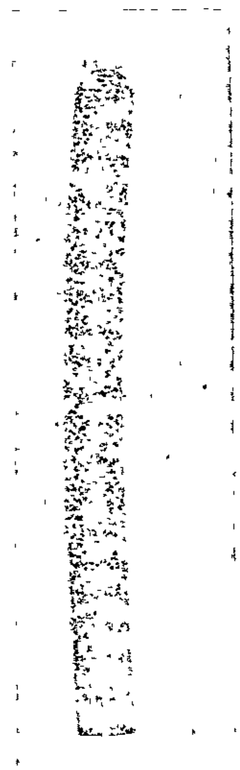

2X

LONGITUDINAL SAMPLE

Figure 32 MA956 Low Velocity Oxidation Pin

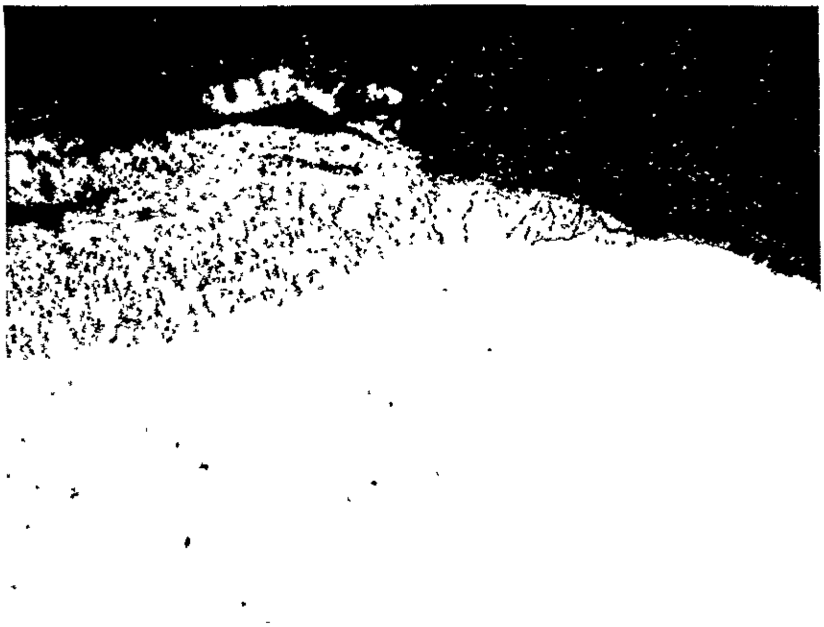

200X

2X

LONGITUDINAL SAMPLE

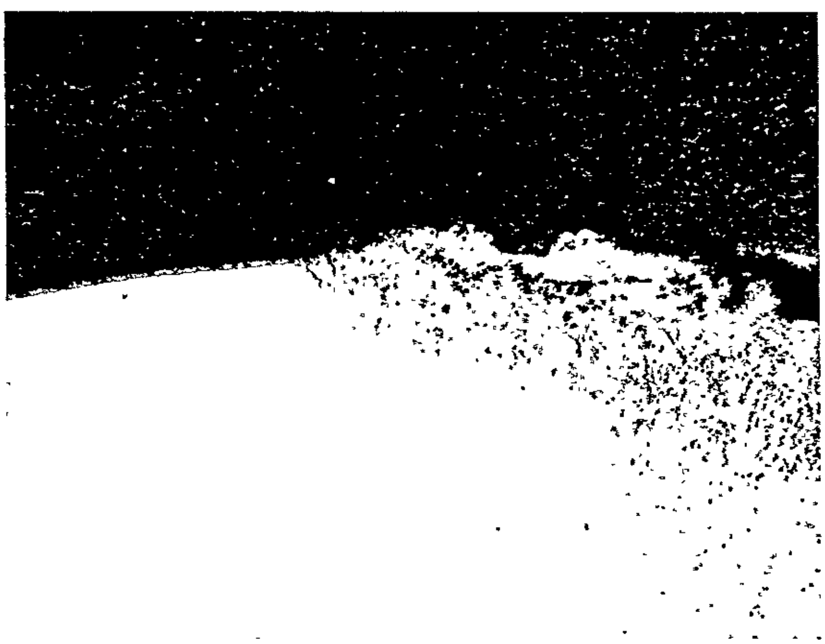

200X

2X

TRANSVERSE SAMPLE

1204°C (2200°F) MACH .05 200 HRS CYCLIC

Figure 33 MA953 Low velocity Oxidation Pins

YD NiCrAl and HDA 8077, to uneven and noticeable on MA 953. Weight loss/gain data are as follows:

Alloy	Mg Wt Change in 509 Hrs in Mach 1, 982° C (1800° F) Cyclic Oxidation	
	Sample 1	Sample 2
MA 956	+9	+8
YD NiCrAl	-59	-71
8077-202	-104	-115
8077-203	-40	-30
MA 754	-284	-260
MA 953	-126	-177
DS NiCrAl	-90	-48
Typical nickel-base blade alloys	-800 to 1400	

An overtemperature at an estimated 1200° C (2200° F) for 10 hours and 45 minutes occurred but it is not believed to have significantly affected the test results.

More extensive evaluation was done of the 1204° C (2200° F) test specimens. Testing under these conditions has shown dramatically the improved oxidation resistance of the aluminum-containing ODS alloys. Figure 34 depicts the samples at 113, 355, and 510 hours. The selected alloys HDA 8077 and YD NiCrAl clearly are superior to the other alloys except the MA 956 Fe-Cr-Al alloy. The comparison with MA 754 Ni-Cr alloy is especially significant. The relatively poor performances of DS NiCrAl and MA 953 are believed to be due to inhomogeneities, since good oxidation resistance is predicted for both compositions. Huntington Alloys' explanation of the poor MA 953 behavior is based on an analysis showing a free-Al content below the aim.

Continuation of the severe 1203° C (2200° F), Mach 1 oxidation testing beyond the ~200-hour point showed unexpected surface deterioration in both HDA 8077 and YD NiCrAl. In the same test, Sherritt-Gordon DS NiCrAl and MA 953 (early nonhomogeneous materials) were nearly consumed; these and other effects are shown in Figure 35. MA 956 (Fe-Cr-Al) continued to show excellent oxidation resistance. MA 754 was removed at the 208-hour point because of serious material loss, also shown in Figure 35.

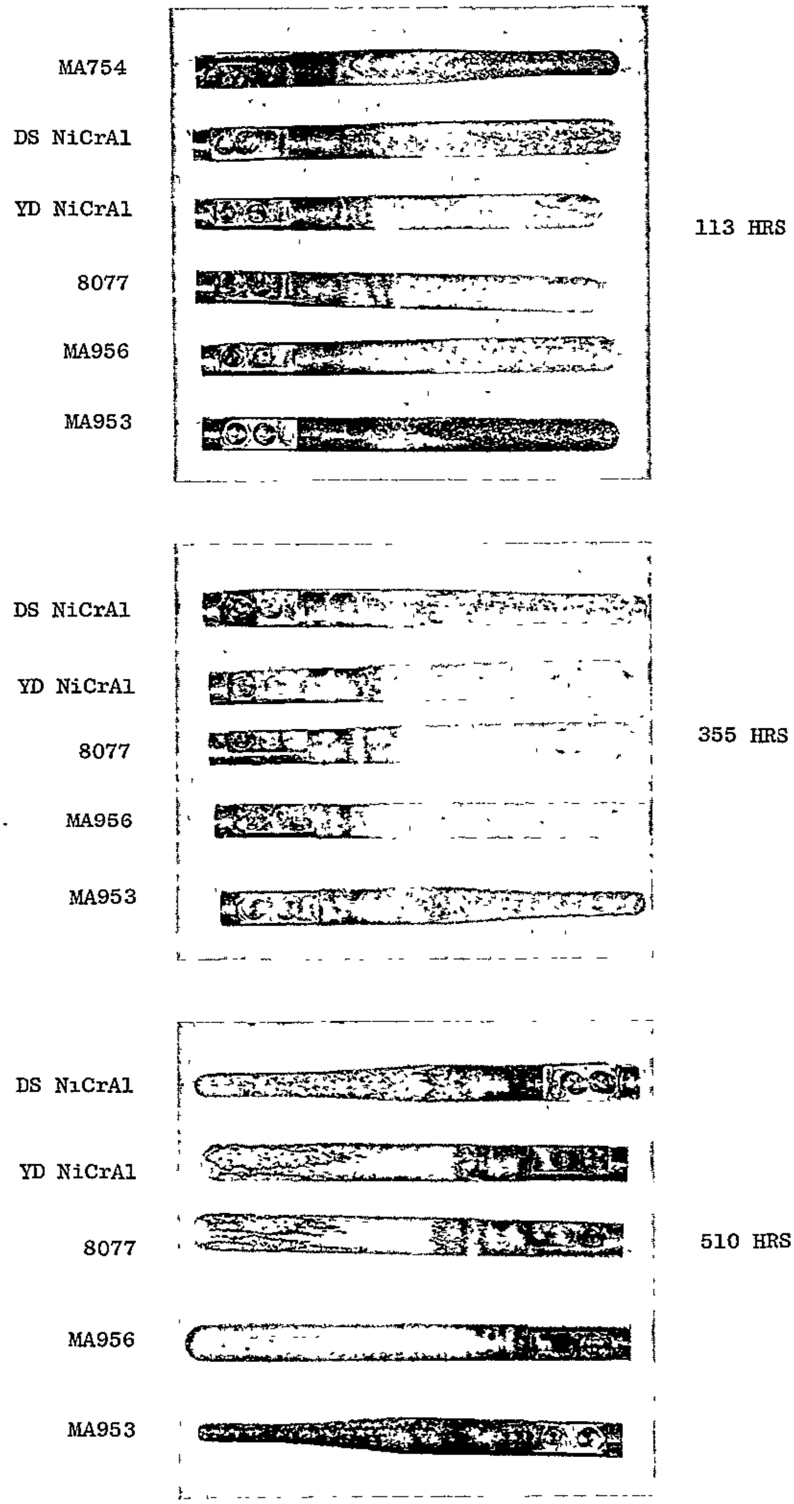

Figure 34 High Velocity 1204° C (2200° F) Oxidation Pins at 113, 355, 510 Hrs

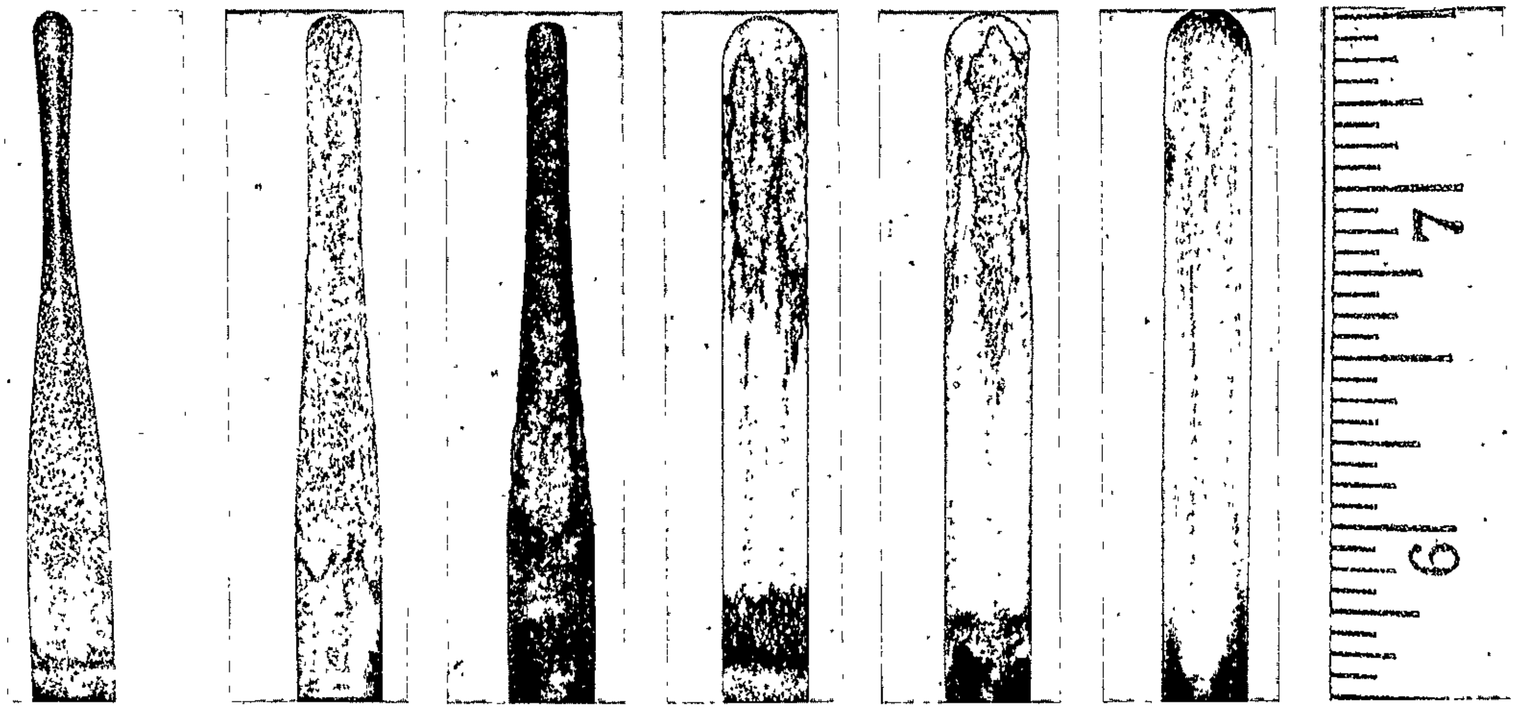

MA754	DSNiCrAl	MA953	8077-202	YDNiCrAl	MA956
208 HRS	510 HRS	510 HRS	510 HRS	510 HRS	510 HRS

Figure 35 Selected 1204° C (2200° F) High Velocity Oxidation Pins at 2X

Microanalyses by metallographic and probe techniques show the 8077/ YD NiCrAl behavior to be related to thermal cracking in this extremely severe cyclic test rather than to a failure of oxidation resistance. The thermal cracks apparently disrupted the protective Al_2O_3 surface layer, allowing formation of the less protective Cr_2O_3 and resulting in chromium loss.

One striking feature of the surface attack is that it occurred on 90°-apart faces of the 1/4-inch-diameter pins. These 90° faces had earlier exhibited thermal cracks. Figure 36 portrays the relationships. The 90° crack locations may be a function of the preferred orientation of the samples. These longitudinal (extrusion-direction) pins would have alternating low modulus <100> transverse texture and high modulus <100> transverse texture every 45° around the periphery of their transverse cross sections. The 50% modulus difference may have resulted in thermal stresses high enough to cause cracking. The MA 956, which has no preferred low modulus texture in any direction, may not have seen the excessive thermal strains. Rechecking of prior experience with other alloys on the high velocity rig has uncovered similar examples of 90° cracking but without any more rigorous explanation of the cause.

Microprobe traces for chromium (and oxides) and aluminum (and oxides) were illuminating. A representative transverse trace of 8077 (in Figure 37) after 252 exposure hours shows the expected matrix composition all the way to the surface and the adherent Al_2O_3 with no Cr_2O_3. Samples of 8077 and YD NiCrAl showed no measurable surface recession by metallographic examination at this stage. Probe analysis of a small crack at the 252-hour point (Figure 38) shows the presence of chromium oxide but still a predominance of aluminum oxide.

Microprobe traces after 510 exposure hours (in Figures 39 and 40) show predominantly chromium oxide on an eroded surface and aluminum oxide on the unattacked surface. Diametral measurements across the unattacked areas still show minimal surface recession. The eroded surface shows major chromium loss to 0.003 inch gradually decreasing to the original 16% at 0.030 inch. Only minor aluminum loss was observed. The unattacked surface also shows chromium and aluminum depletion that was not observed at 252 hours.

3.1.14 Hot Corrosion Testing

Hot corrosion (sulfidation) testing was carried out in the General Electric, Lynn, Mass., low velocity (Mach 0.07) test rig. The test conditions were 926° C (1700° F) with an addition of 5 ppm synthetic sea salt to the fuel. Two fuel/cyclic conditions were used: diesel fuel with an hourly cooldown, and JP-5 with a daily cooldown. The macro surface photos and cross-sectional photomicrographs in Figures 41 through 45 show no gross behavioral differences between the two fuel/cycle conditions. Minimal attack occurred on HDA 8077 (Ni-Cr-Al), MA 754 (Ni-Cr), and MA 956 (Fe-Cr-Al), but significant erosion occurred on MA 953 (Ni-Fe-Cr-Al) and YD NiCrAl (Ni-Cr-Al). The difference between the two Ni-Cr-Al alloys was quite unexpected.

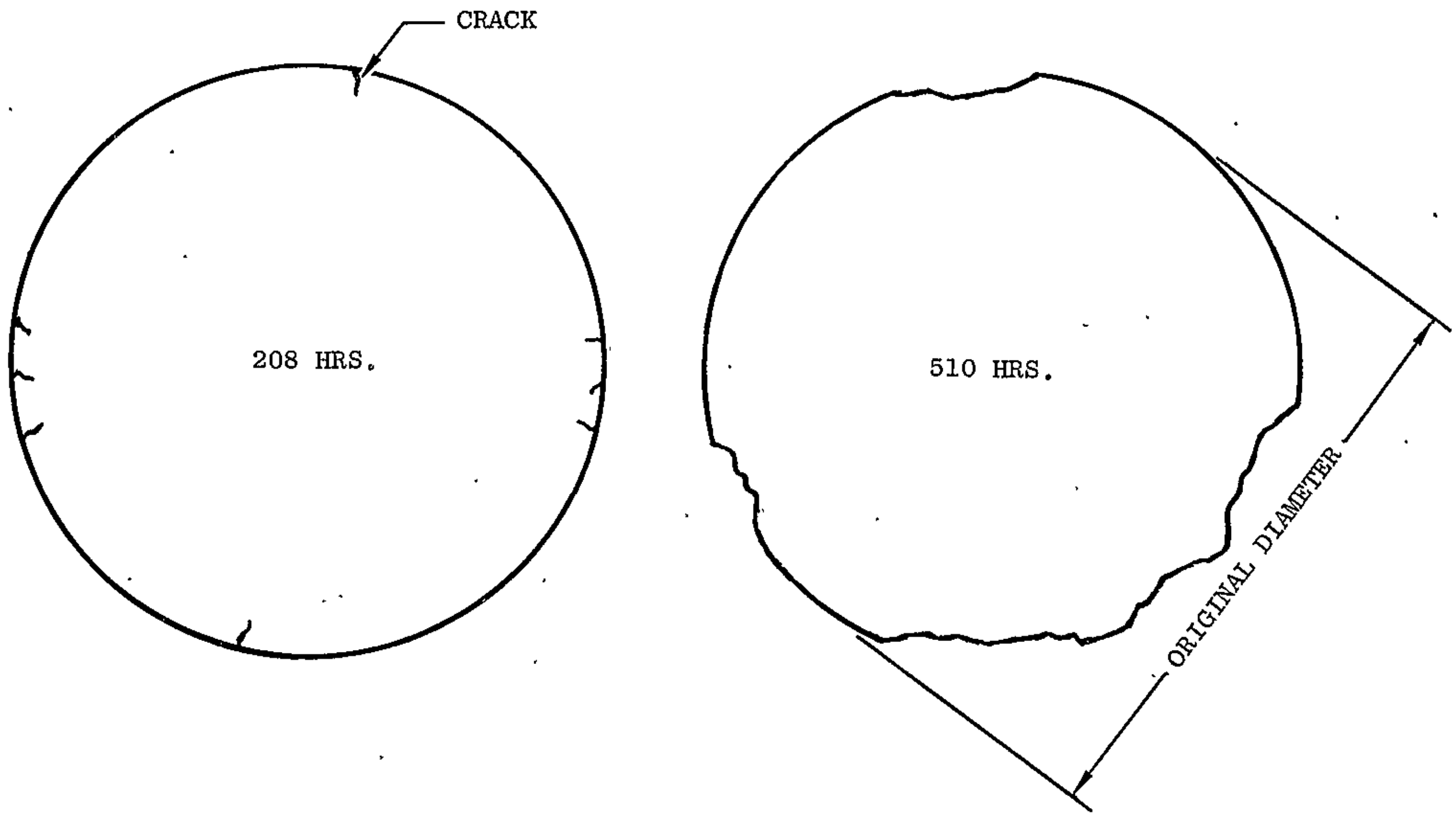

Figure 36 HDA 8077/YDNiCrAl 1204°C (2200°F) High Velocity Oxidation Specimen Cross Sections

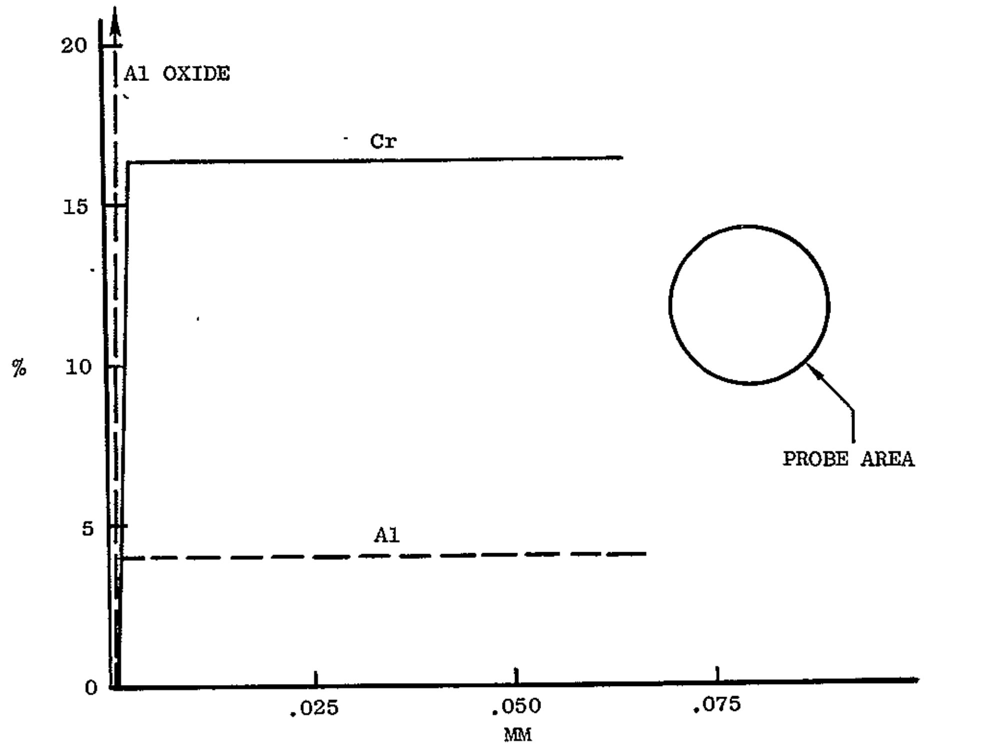

Figure 37 Microprobe Trace of 252 Hour YDNiCrAl Specimen Surface

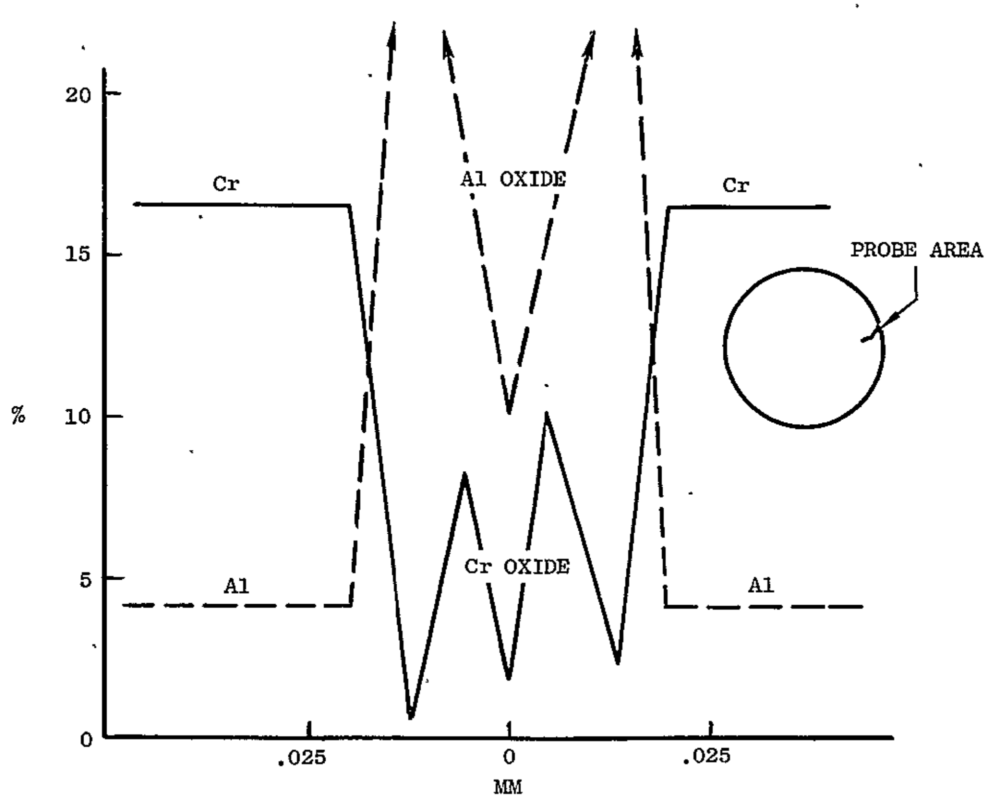

Figure 38 Microprobe Trace of 252 Hour YDNiCrAl Specimen Crack

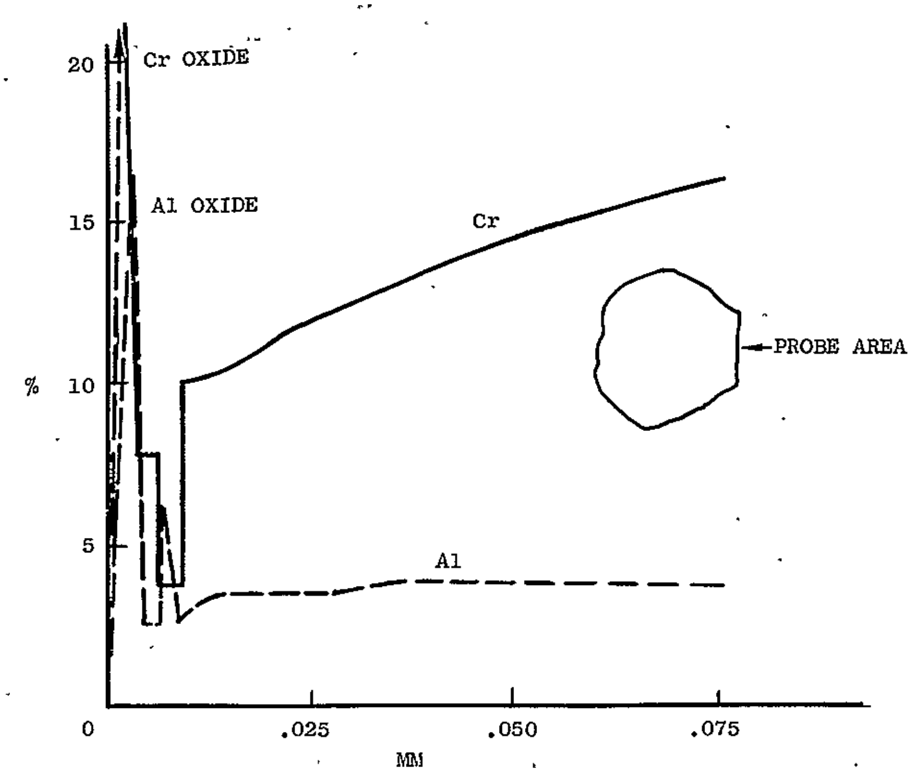

Figure 39 Microprobe Trace of 510 Hour 8077 Specimen Eroded Surface

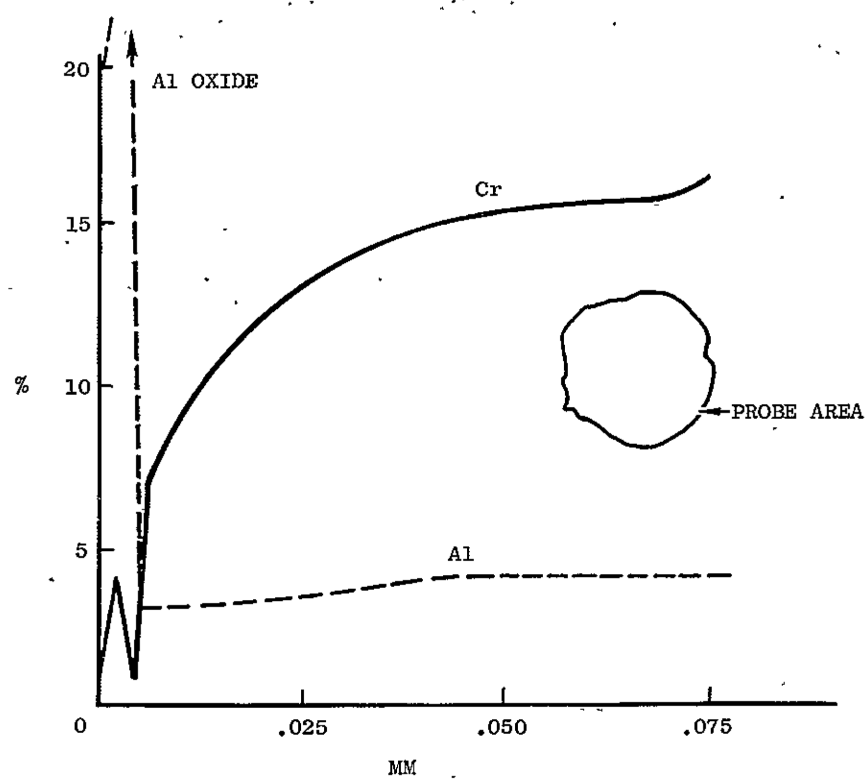

Figure 40 Microprobe Trace of 510 Hour 8077 Specimen

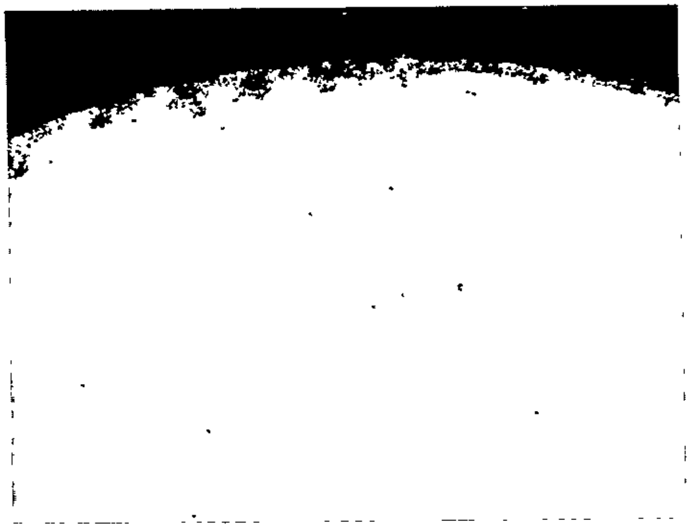

100X

1043 HRS DIESEL FUEL - HOURLY CYCLING

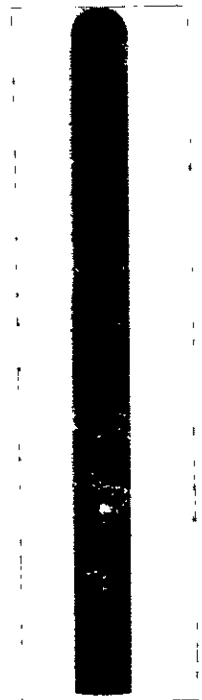

2X

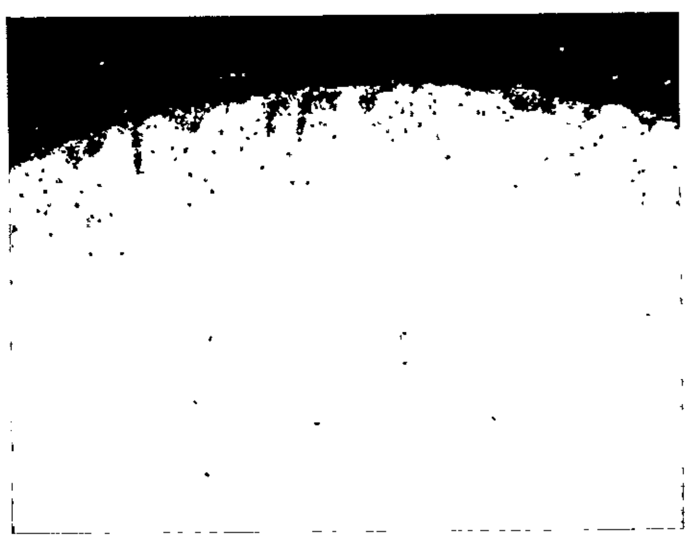

100X

1018 HRS JP5 FUEL - DAILY CYCLING

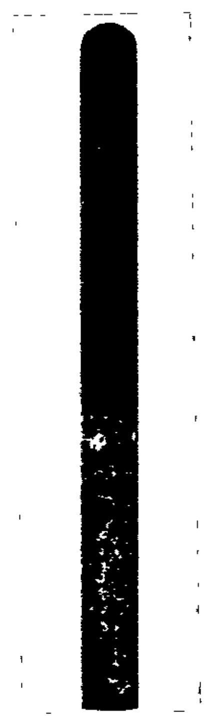

2X

926°C (1700°F) - 5 PPM SALT - LOW VELOCITY

Figure 41 HDA 8077 LPT Hot Corrosion Pins

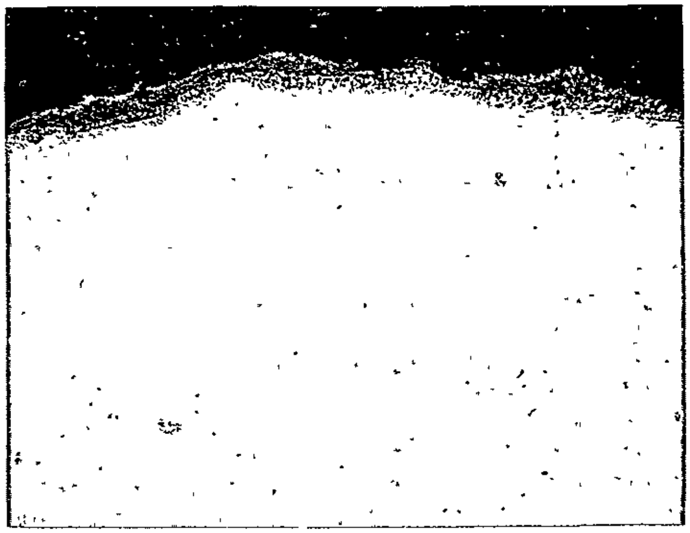

100X

550 HRS DIESEL FUEL - HOURLY CYCLING

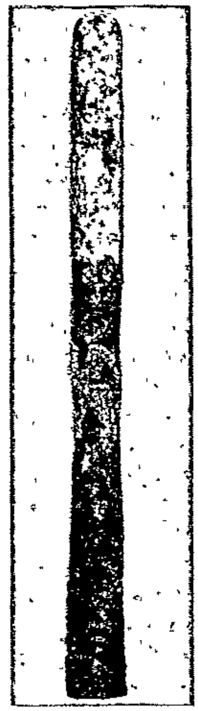

2X

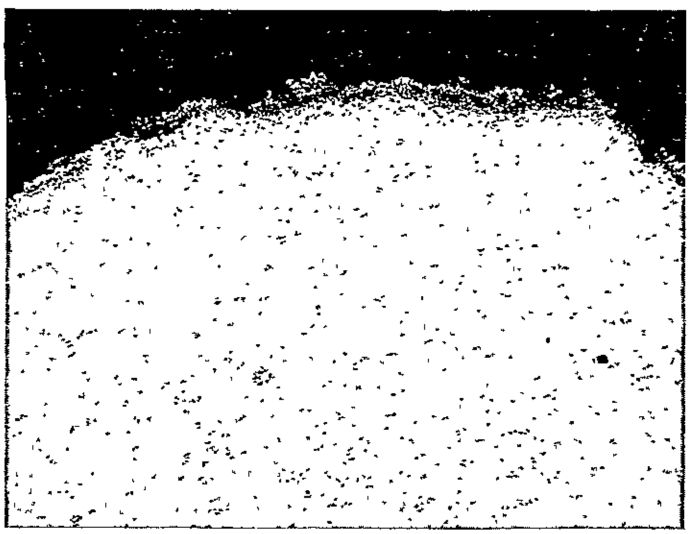

100X

449 HRS JP5 FUEL - DAILY CYCLING

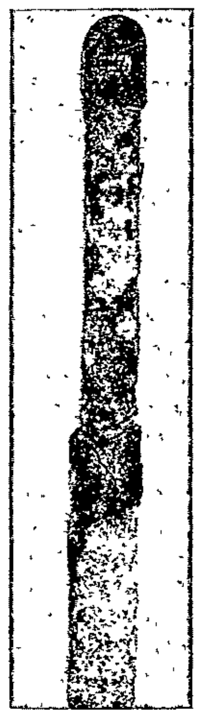

2X

926°C (1700°F) - 5PPM SALT - LOW VELOCITY

Figure 42 YDNiCrAl Hot Corrision Pins

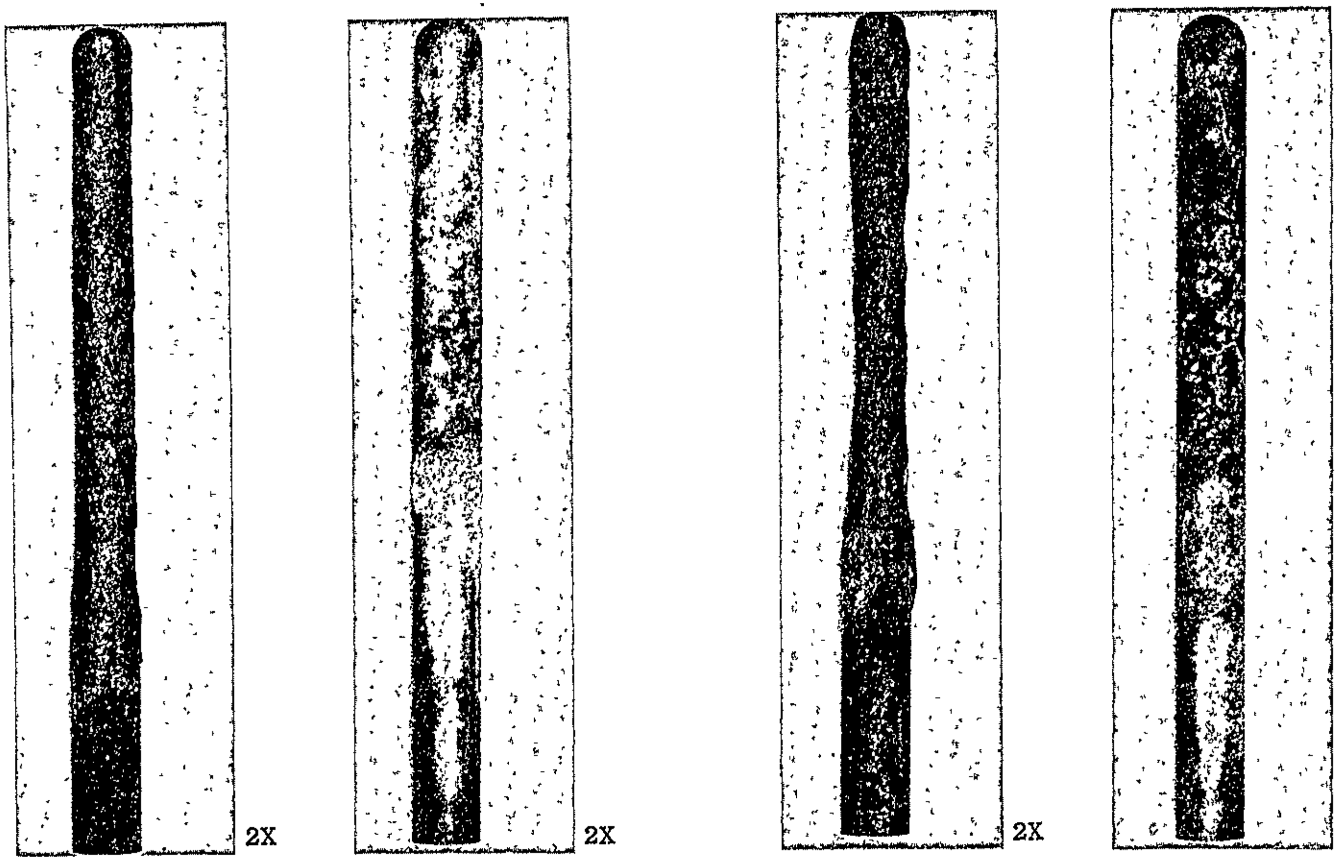

926°C (1700°F) - 5 PPM SALT - LOW VELOCITY

Figure 43 MA953 and MA956 Hot Corrosion Pins

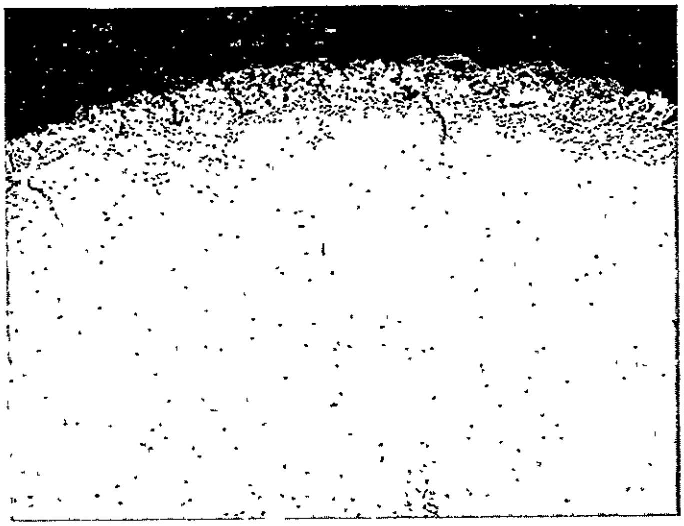

100X

885 HRS DIESEL FUEL - HOURLY CYCLING

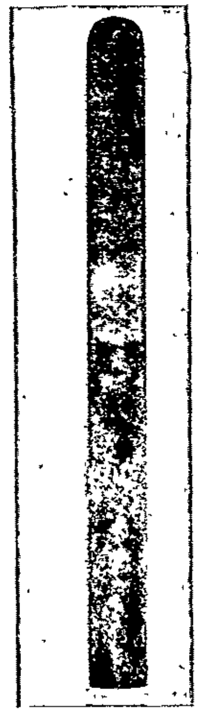

2X

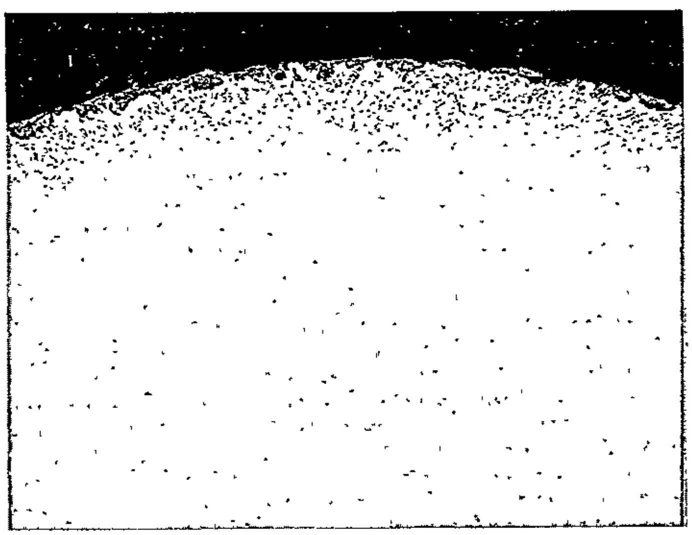

100X

1018 HRS JP5 FUEL - DAILY CYCLING

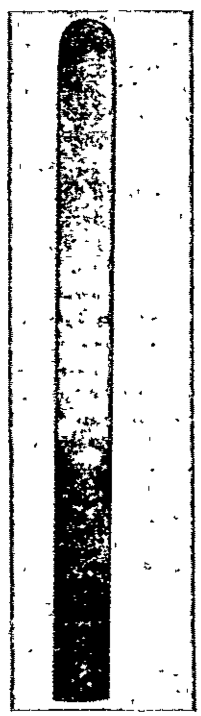

2X

926°C (1700°F) - 5PPM SALT - LOW VELOCITY

Figure 44 MA754 Hot Corrosion Pins

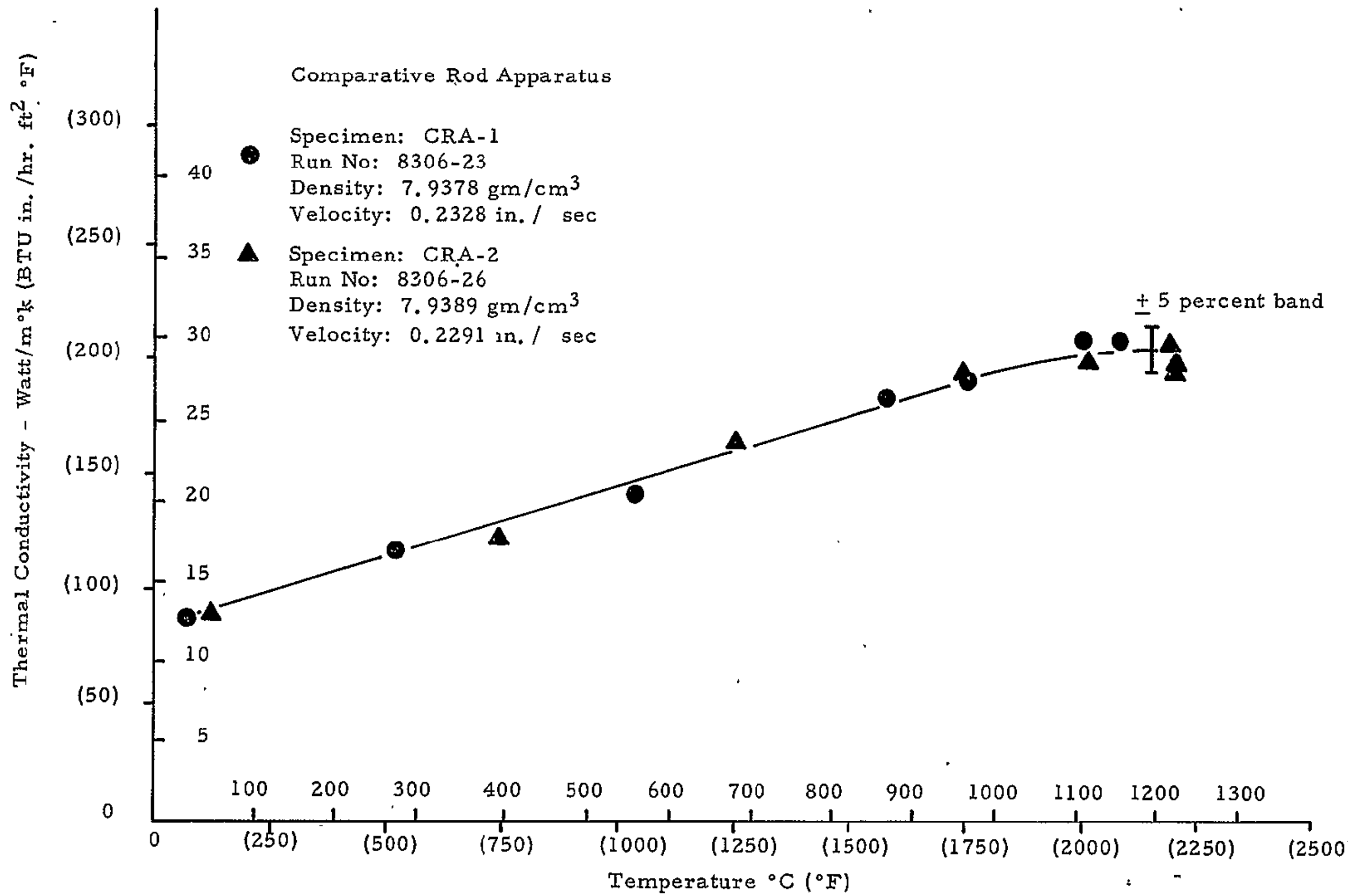

Figure 45 Thermal Conductivity of HDA 8077

Microexamination of the samples revealed subsurface attack on the HDA 8077 and MA 754 that was not evident from visual inspection. Estimates of average surface attack depth for these two alloys and MA 956 are as follows:

Alloy	Surface Attack		Test Conditions
	mm	inch	
HDA 8077	0.20 5o 0.25	0.008 to 0.010	1043 hours hourly cycling
	0.15 to 0.20	0.006 to 0.008	1018 hours daily cycling
MA 754	0.18 to 0.23	0.007 to 0.009	885 hours hourly cycling
	0.18 to 0.23	0.007 to 0.009	1018 hours daily cycling
MA 956	0.05 to 0.08	0.002 to 0.003	1043 hours hourly cycling
	0.03 to 0.05	0.001 to 0.002	1018 hours daily cycling

Further tests, outside of the program at General Electric and NASA, have added to the uncertainties about the hot corrosion resistance of the ODS Ni-Cr-Als (HDA 8077, YD NiCrAl, and Huntington Alloys' recent offering MA 757 nominal composition Ni-16Cr-4Al-0.7 Y_2O_3). The General Electric additional testing, Table 12, shows all the ODS-NiCrAls including the HDA 8077 LPT-type to be poor in hot corrosion and definitely not the equivalent of MA 754 as was shown in the tests in this program. The recent tests do show HDA 8077-LPT with its higher Y_2O_3 content slightly better than HDA 8077-HPT and YD NiCrAl with their lower Y_2O_3 contents. It is speculated that, in the program testing, the HDA 8077-LPT achieved a critical Al_2O_3 protective coating that was somehow enhanced by the additional Y_2O_3. Enough testing was done in the additional program to convince General Electric that the ODS-NiCrAls with their lower chromium contents are inferior to the ODS-NiCrs in hot corrosion when tested in the General Electric rig.

In direct contrast to General Electric testing, NASA showed the ODS-NiCrAls excellent in hot corrosion and better than the ODS-NiCrs(8,9). Exchange of information showed NASA testing to be at a significantly higher velocity (Mach 1) than General Electric Testing (Mach 0.07). Discussions between NASA and General Electric hot corrosion experts have not explained the differing results except to produce a speculation that the NASA testing had a larger component of oxidation exposure due to higher velocity delivering more oxygen to the sample than the General Electric test did. Another anomoly in test comparisons is that, for the ODS alloys, 1000 hours of testing resulted in similar surface recessions in both NASA and General Electric tests. For most conventional superalloys (e.g., Inconel 792), similar surface recessions were obtained in 100 hours at NASA and 1000 hours at General Electric. The questions are not expected to be resolved until the mechanics of corrosion are better defined under the test conditions used, and actual

Table 12. General Electric Additional Hot Corrosion Testing.

Conditions: 926° C (1700° F) 5ppm salt.
Uncoated Samples

Alloy	Surface Recession per Side	
	mm	(mils)
MA 754	0.23	9
HDA 8077-LPT	0.51	20
HDA 8077-HPT	0.76	30
YD NiCrAl	0.84	33
Typical Co-base Vane Alloy	0.13	5
Typical Ni-base Blade Alloy	0.30	12

engine testing shows what type of rig tests are more representative. It should be noted that the engine testing in this program was not conducted under conditions expected to produce hot corrosion effects.

3.1.15 Physical Property Testing

To provide physical property data applicable to vane design, thermal conductivity, thermal expansion, density, and dynamic modulus tests were conducted on HDA 8077 and YD NiCrAl. In general, the data showed that these two ODS-NiCrAl alloys were similar to the ODS-NiCr, MA 754.

Thermal Conductivity

The thermal conductivity of HDA 8077 was determined from room temperature to 1204° C (2200° F) on specimen blanks supplied by General Electric to Southern Research Institute. Gravimetric bulk density and ultrasonic velocity were measured on each blank before thermocouple holes were drilled in it. The results of these nondestructive evaluations are presented with the thermal conductivity data.

The thermal conductivity was determined from RT to about 1204° C (2200° F) in a comparative rod apparatus.

The specimen was placed between two references of known conductivity. For these measurements, references made of 316 stainless steel were used. Heat transfer occurred axially through the column of references and specimen, and radial losses were minimized by means of radial guard heaters wound on a ceramic tube. These losses are kept within ±5 percent for a given measurement by matching the temperature profile in the column and guard heaters.

The specimen configuration used on this program was 1.27 cm (1/2 inch) diameter by 2.54 cm (1 inch) length with the conductivity measurement being lengthwise. The heat transfer through the stacked assembly of references and specimen was calculated from the measured temperature gradients and the known conductivities of the references. Temperatures were measured with thermocouples placed in radially drilled holes in each specimen and reference.

The thermal conductivity of HDA 8077 is shown in Figure 45. Figure 46 shows the thermal conductivity of several nickel-base alloys evaluated at Southern Research Institute.

The data indicate that the thermal conductivity of HDA 8077 increases linearly from a value of 12.7 watt/m ° K at RT to about 28.8 watt/m ° K at 1052° C (1925° F). Above 1052° C, the curve flattens out to a value of about 29.4 watt/m ° K at 1204° C (2200° F). The data scatter was within ±5 percent over the entire temperature range, indicating good agreement between the two specimens evaluated. The almost linear behavior of the thermal conductivity as a function of temperature was as expected. This behavior is common for metallic alloys within the temperature range investigated.

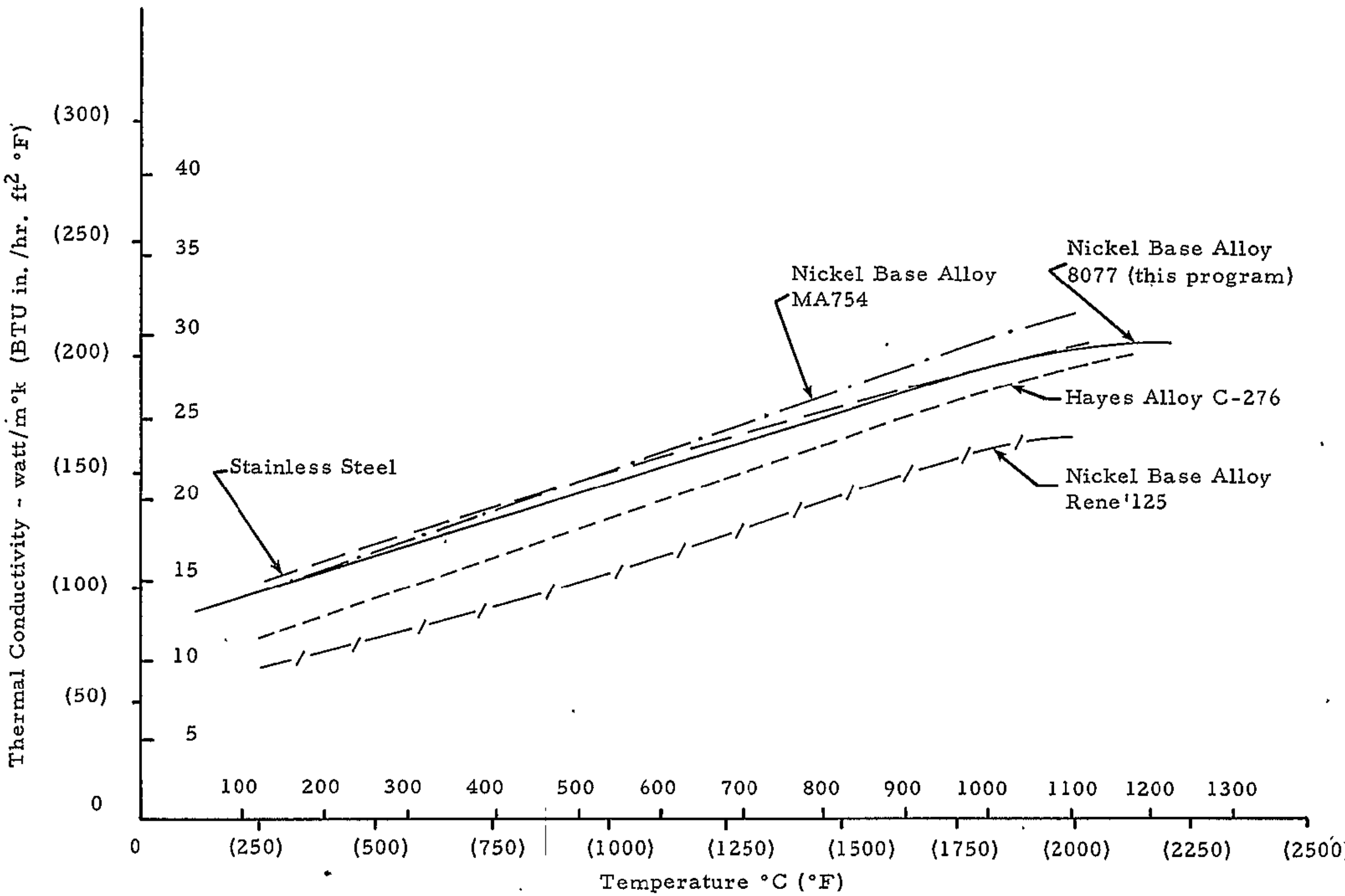

Figure 46 Thermal Conductivity of Stainless Steel and Several Nickel-Base Alloys

Thermal Expansion

Thermal expansion measurements were made by General Electric on two ODS-NiCrAl alloys, YD NiCrAl and MA 757. The latter is produced by Huntington Alloys using Mechanical Alloying, the same powder process as is used for HDA 8077.

Thermal expansion was measured using a Chevenard Model 50 Mechanical Dilatometer. Expansion coefficients are determined by comparing the test bar with a standard bar having known total and coefficient of thermal expansion values. The standard specimen used is 0.38 cm (0.150 inch) diameter by 6.5 cm (2.56 inches) long. The heating rate is 315° C (600° F) per hour.

The thermal expansion values plotted in Figures 47 and 48 are very similar to other common nickel-base alloys.

Dynamic Modulus

Modulus of elasticity measurements were carried out on several of the candidate alloys early in the program, before Task II selections had been made. Measurements were made in both longitudinal and transverse directions on TD NiCrAl, YD NiCrAl, HDA 8077 (LPT-type), and MA 953.

The method employed produces a "dynamic" modulus value which can differ from the "static" modulus determined from tensile stress-strain curves. In the test, one end of a precisely machined cylindrical specimen is subjected to a sonic input signal. To the other end of the specimen, a phono crystal is attached. By varying input frequency, the natural frequency of the specimen is determined. Substitution in the following equation produces the dynamic modulus:

$$E = \frac{KWL^3f^2}{D^4}$$

For SI and English units, the following apply:

Symbol	Parameter	Units	
		SI	English
E	Dynamic Modulus	Pa	psi
K	Constant	1.607×10^{-1}	4.1627×10^{-3}
W	Weight	gm	pounds
L	Length	cm	inches
D	Diameter	cm	inches
f	Frequency	cycles/sec	same

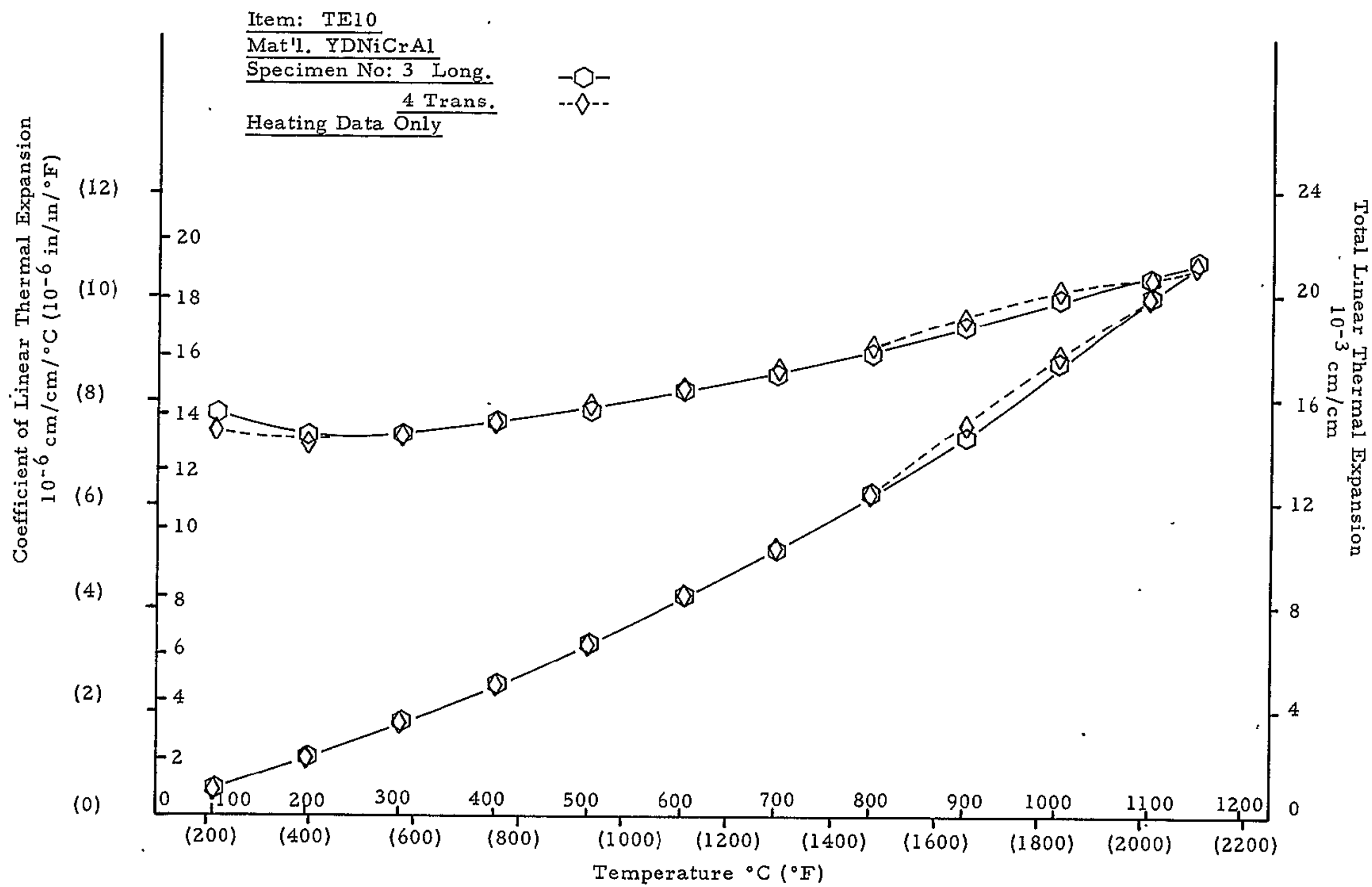

Figure 47 YDNiCrAl Thermal Expansion Curves

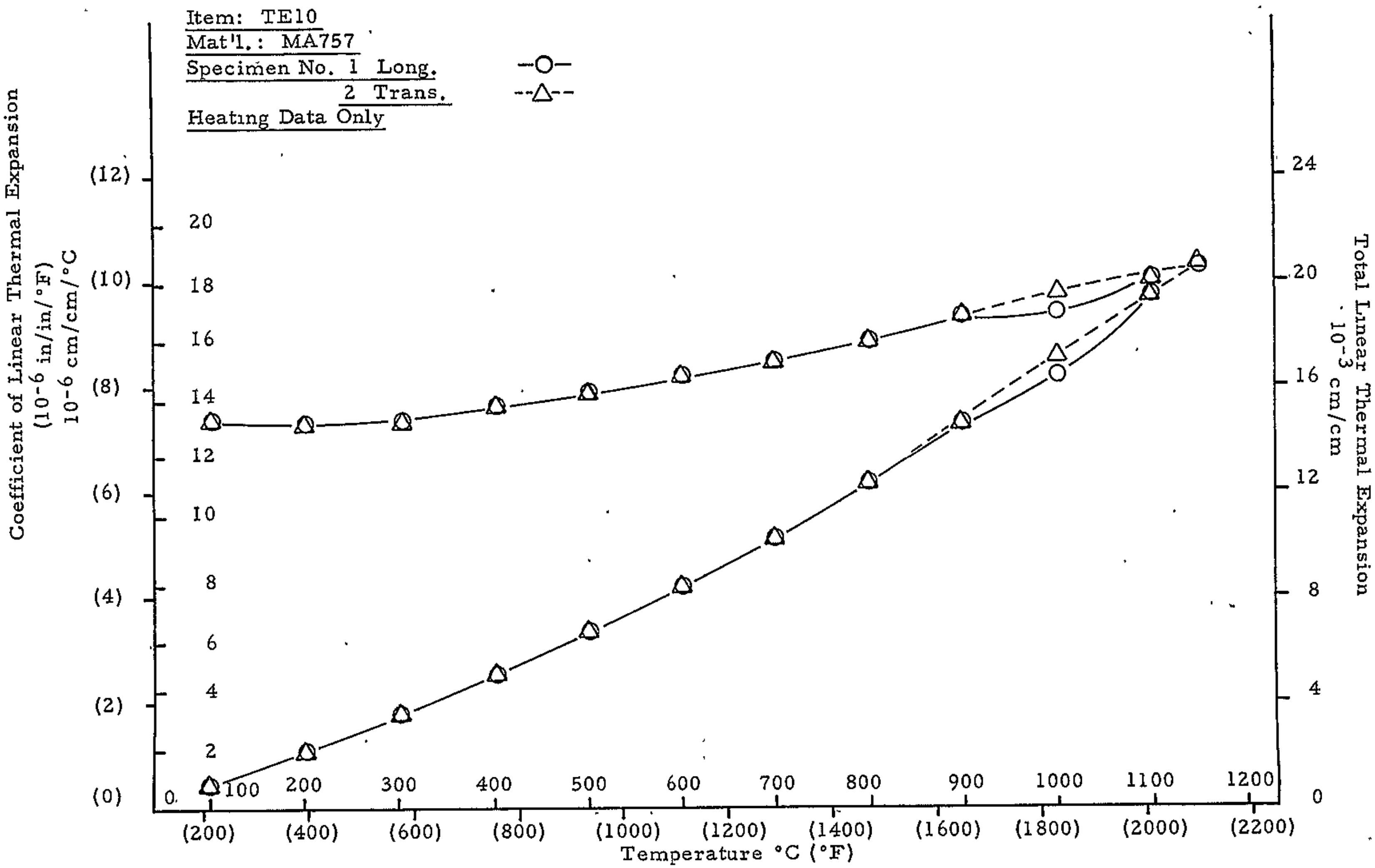

Figure 48 MA757 Thermal Expansion Curves

By suspending the specimen within a clamshell furnace, the measurement at elevated temperatures is accomplished readily.

The results are plotted separately for longitudinal and transverse directions in Figures 49 and 50. The most significant fact is that the longitudinal moduli are lower than the transverse. This is because of the developed <100> longitudinal texture. The beneficial effect of this low-modulus texture is to improve thermal fatigue resistance because of lower thermal stresses for given thermal strains. The TD NiCrAl values appear reasonable since the <100> texture was not achieved in this alloy. The HDA 8077 and MA 953 values appear low in both longitudinal and transverse directions. There is no reason why they should be substantially different than the YD NiCrAl, because their crystallographic orientations are the same. The YD NiCrAl values correlate well with previous measurements on TD NiCr, DS NiCr, and MA 754.

Density

In addition to the measurements of density obtained at Southern Research Institute in connection with the thermal conductivity determinations, densities of HDA 8077 and YD NiCrAl were independently measured at General Electric using a water-displacement method. The values listed below are in close agreement with the HDA 8077 data from Southern Research.

Alloy	Density	
	gm/cc	$lb/in.^3$
HDA 8077-LPT	7.9342	0.2867
YD NiCrAl	7.9384	0.2868

3.1.16 Chemistry and Dispersoid Morphology

Chemical analyses were run, and dispersoid characteristics were determined with early program material. MA 956 and DS NiCrAl were not included because they were supplied considerably later than the other alloys. The chemical analyses are listed in Table 13. Nickel, aluminum, lanthanum, and thorium were determined gravimetrically; iron by redox titration; yttrium gravimetrically; titanium by spectrophotometry; sulfur by combustion and titration; argon by mass spectrometry; and, nitrogen/oxygen by vacuum fusion. The values appear reasonable except for the yttria and lanthana in HDA 8077-HPT and MA 953, which appear low. The minor iron contents in HDA 8077 result from the mechanical alloying process. The oxygen values are totals including that tied up in the dispersed oxide. As such, they all appear in line except for the high MA 953 value. Sulfur also appears high in this alloy. Argon was found only in MA 953, presumably a result of powder processing.

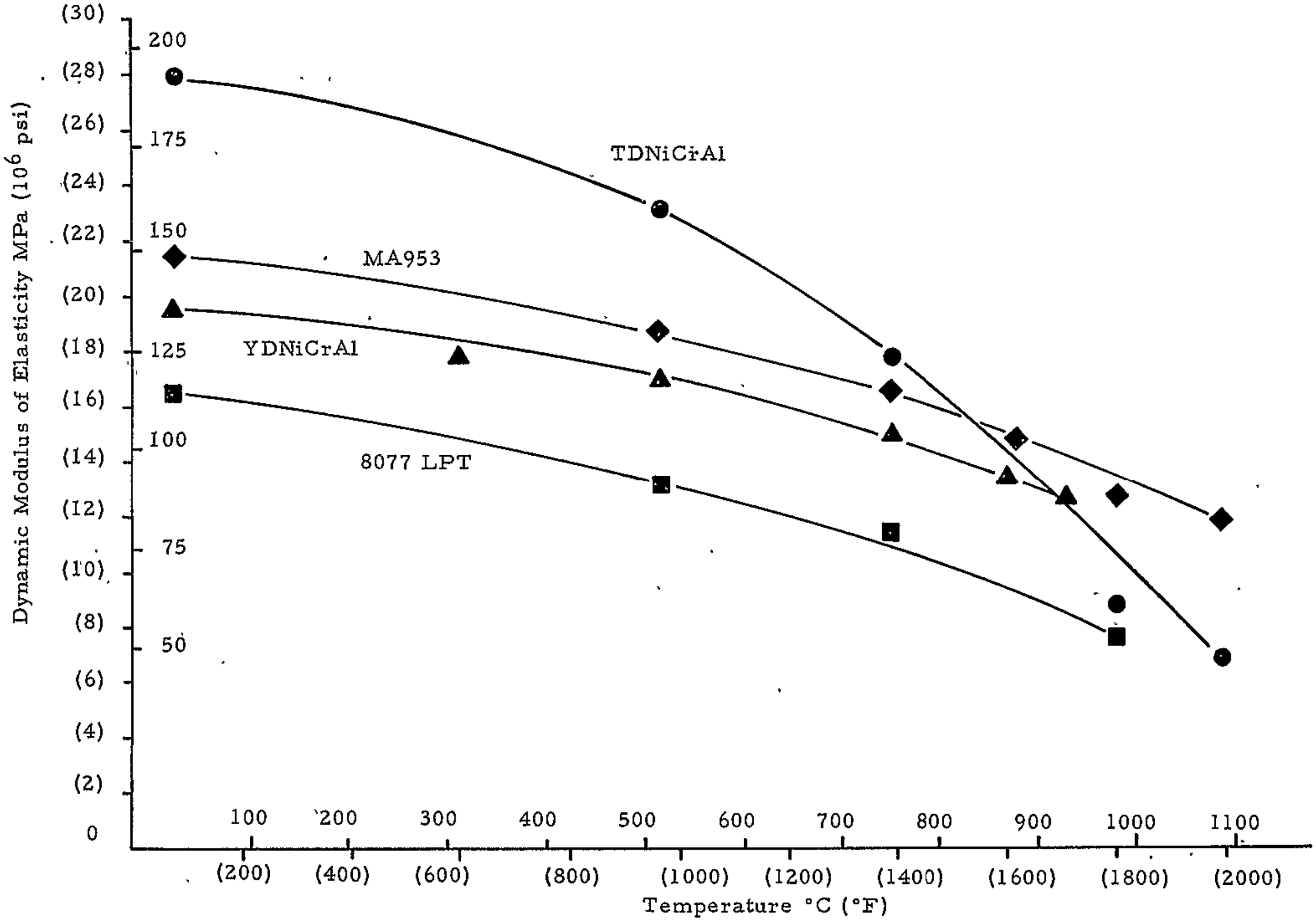

Figure 49 Longitudinal Dynamic Moduli

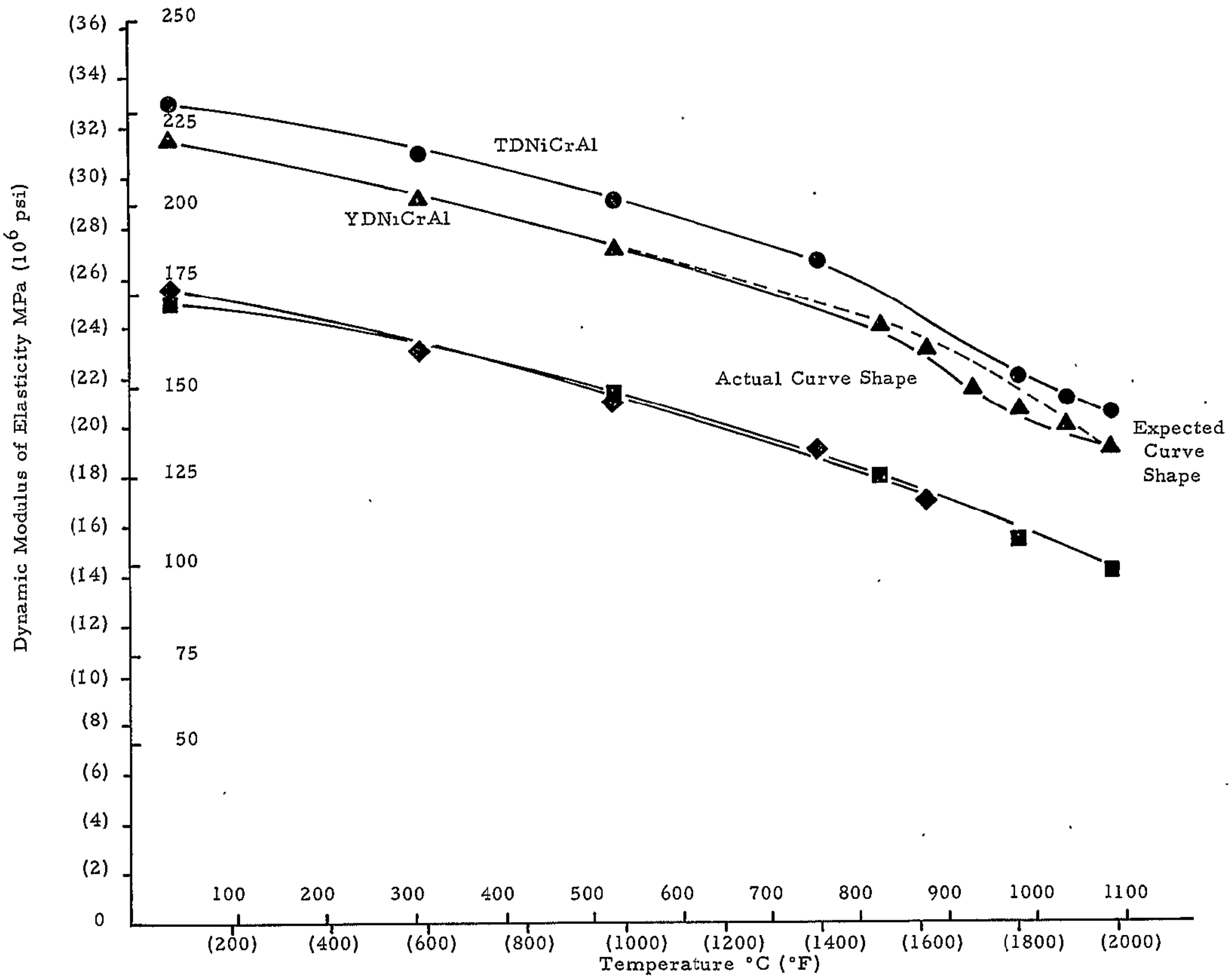

Figure 50 Transverse Dynamic Moduli

C-2

Table 13. Chemical Analyses of Program Alloys.

Alloy	Constituent % by Weight											
	Ni	Cr	Fe	Al	Ti	ThO_2	Y_2O_3	La_2O_3	S	O_2	N_2	A
TD NiCrAl	76.71	16.17	---	4.77	---	1.88	---	---	0.0032	0.399	0.0025	---
YD NiCrAl	78.13	15.66	0.15	4.53	---	---	0.98	---	0.0028	0.394	0.0077	---
HDA 8077-LPT	77.26	15.32	1.02	3.98	0.11	---	1.66	---	0.0025	0.510	0.0215	---
HDA 8077-HPT	77.98	16.30	1.13	4.04	0.05	---	0.47	---	0.0015	0.286	0.0003	---
MA 953	40.23	17.96	35.63	4.75	0.48	---	---	0.21	0.0101	0.790	0.0245	0.0026
						dispersoids						

Dispersoid characteristics were examined both for their physical distribution and chemical formulation. Figures 51 and 52, which are replica electrophotomicrographs, show marked similarity of dispersoid size and distribution between TD NiCrAl and the two HDA 8077 types. The lanthana in MA 953 appears coarser, though uniformly distributed. YD NiCrAl, on the other hand, has a considerably coarser, less-uniformly-distributed dispersoid.

Past experience had shown that thoria-dispersed alloys normally retain the chemical integrity of that dispersoid, but that yttria sometimes combines with other stable oxides such as alumina.

To determine the stability of the program alloy dispersoids, a small study was undertaken. The phases of MA 956, HDA 8077, YD NiCrAl, and MA 953 alloys were electrolytically separated using 10% $HCl-CH_3OH$ and 1% ammonium sulfate-1% citric acid electrolytes. The separated phases were identified by x-ray diffraction. The principal oxides were determined to be $AlYO_3$ in Fe-Cr-Al-Y_2O_3 and $Al_2Y_4O_9$ in HDA 8077. Phases containing lanthanum could not be identified in MA 953. Evidence of the presence of Y_2O_3 was inconclusive, since only one weak line in the diffraction patterns could be assigned to this oxide.

Weighed specimens were electrolytically dissolved in electrolytes of 10% $HCl-CH_3OH$ and in 1% citric acid-1% ammonium sulfate in distilled water. The separated phases were collected from the electrolytes on weighed Millipore filters, washed, dried, and weighed. The weight percent of the separated phases is shown in Table 14.

The separated phases were analyzed by the x-ray diffractometer method using filtered chromium radiation generated at a power setting of 40 kVp - 20mA. The phases identified are shown in Table 14.

To experimentally show the presence of Y_2O_3 in the alloys presents problems in isolating the oxide and in identifying it by x-ray diffraction. The electrolytes commonly used to electrolytically dissolve the matrix of an alloy probably dissolve Y_2O_3 to some degree. In the x-ray diffraction analysis of the phase material that is separated from the matrix, a conclusive identification of Y_2O_3 is doubtful unless the oxide is present in a relatively large amount in the phase material. A small amount of the oxide would not be detected because Y_2O_3 inherently produces a weak diffraction pattern.

The possibility of Y_2O_3 in the HDA 8077, as indicated by the presence in the diffraction pattern of the strongest line, 3.060 Å, is a stimulus to pursue the matter with experiments which might increase the sensitivity of detection of Y_2O_3 in the phase residue of this alloy and of others containing yttrium. Recommended experiments consist of phase separation using neutral electrolytes which should be more favorable for retaining Y_2O_3 than the acidic electrolytes used in this work. A neutral electrolyte (such as iron chloride in water) was suggested by Harry Beattie of General Electric, Schenectady.

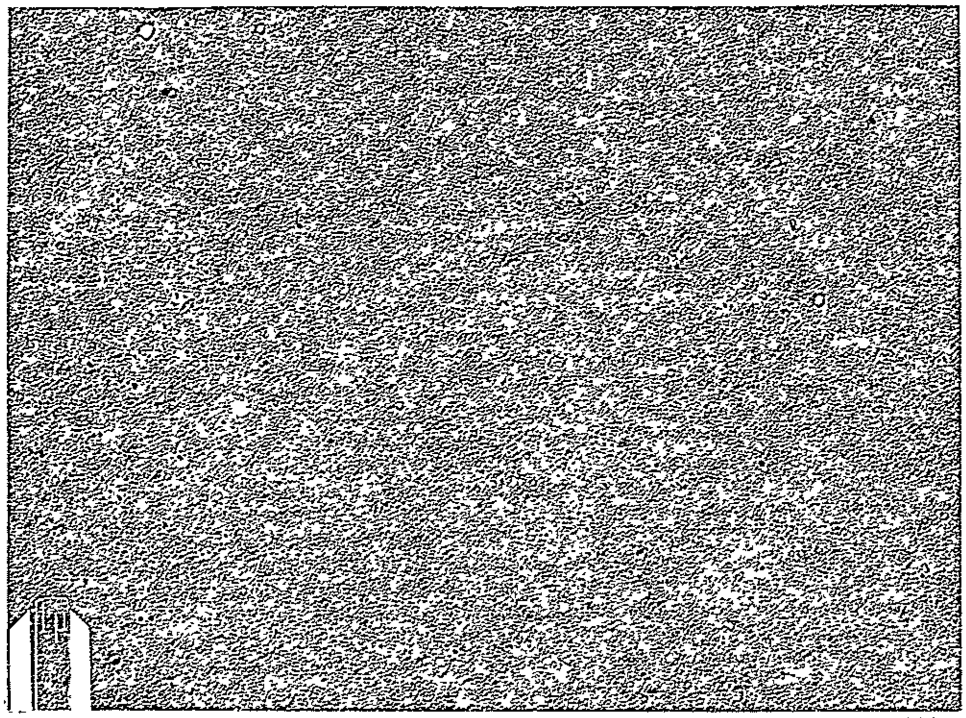

5000X

HDA 8077 - LPT

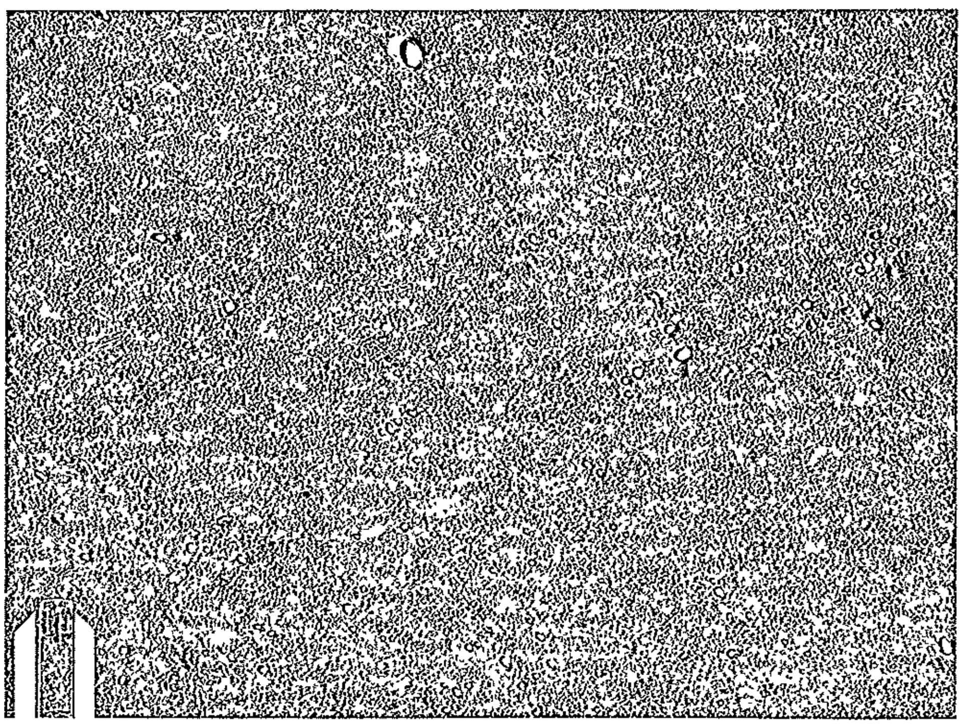

5000X

TDNiCrAl

Figure 51 Electron Photomicrographs HDA 8077 and TDNiCrAl

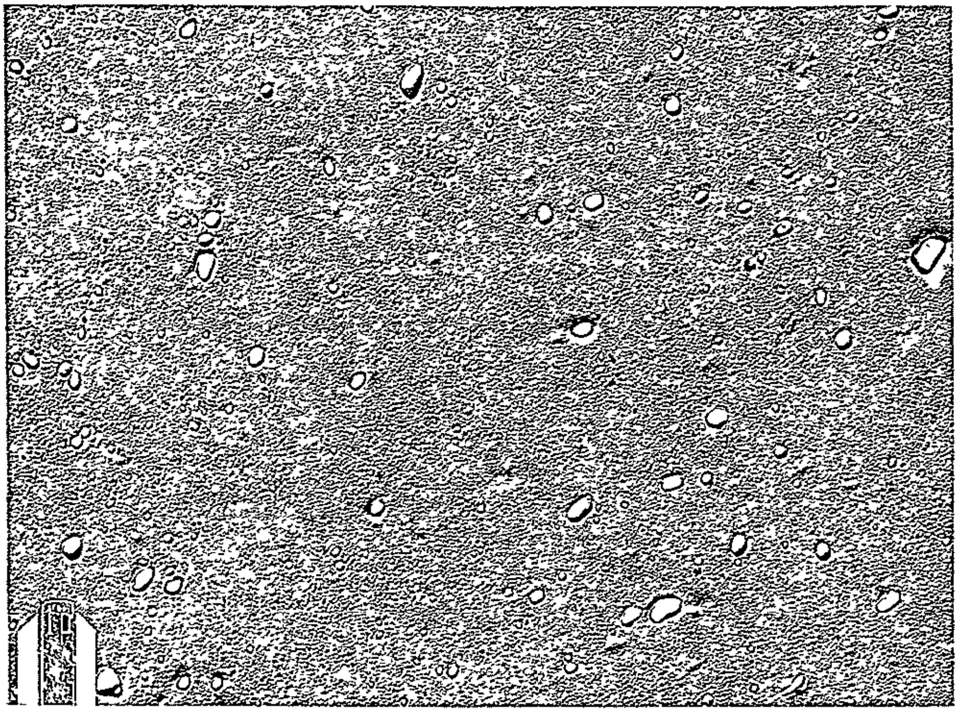

YDNiCrAl 5000X

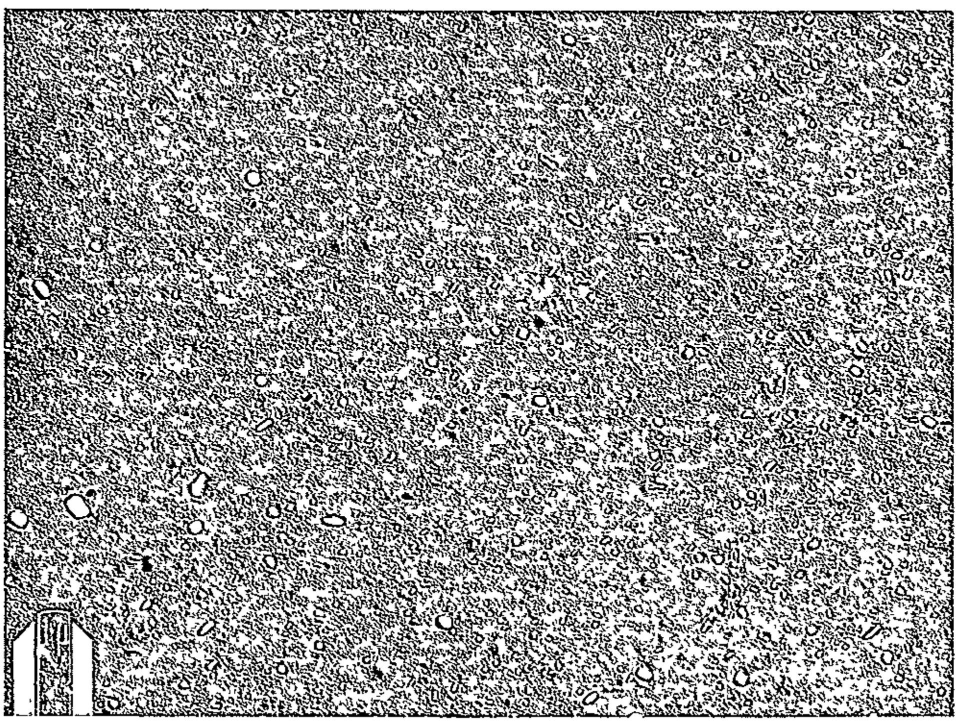

MA953 5000X

Figure 52 Electron Photomicrographs MA953 and YDNiCrAl

Table 14. Dispersoid Phase Extractions.

Alloy	Citric Acid-Ammonium Sulfate Phase Separation	Phases Wt %	HCl-CH_3OH Phase Separation	Phases Wt %
HDA 8077 (Ni-Cr-Al-Y_2O_3)	Face-Centered-Cubic Ni rich phase	15.9	$Al_2Y_4O_9$	0.91
	$Al_2Y_4O_9$	---	$AlYO_3$	---
		---	Y_2O_3 (possible) (JCPDS 5-0574)*	---
Fe-Cr-Al-Y_2O_3 (Similar to MA 956)	$AlYO_3$ (JCPDS 11-662)	1.6	$AlYO_3$	1.6
	$Al_2Y_4O_9$ (JCPDS 14-475)	---	$Al_2Y_4O_9$	---
	Al_2O_3 (JCPDS 10-173)	---	Al_2O_3 (questionable)	---
MA 953 (Ni-Fe-Cr-Al-La_2O_3)	NiAl (JCPDS 2-1261)	---	Al_2O_3	---
	Al_2O_3 (JCPDS 10-173)	---	---	---

*JCPDS = Joint Committee on Powder Diffraction Standards

The phase particles separated from an alloy differ in size, shape, and density. If the particles are dispersed in water, a partial separation of the individual phases may be accomplished by the difference in sedimentation rate. The method, if applied to the phases of the yttrium-containing alloys, might be successful in isolating more of the Y_2O_3 from the other oxides. If so, the increased concentration presents a much more favorable situation for a conclusive identification of the oxide in the fraction by x-ray diffraction.

3.2 TASK II - MANUFACTURING TECHNOLOGY

3.2.1 Selection of Alloys for Vane Manufacture and Engine Test

Based on attainment of the program goal properties, HDA 8077 and YD-NiCrAl were selected for vane manufacture and engine test. Stress rupture properties were met for both LPT and HPT vanes in HDA 8077 and for HPT vanes in YD NiCrAl. Thermal fatigue resistance equivalent to MA 754 was achieved in both alloys. Oxidation resistance at Mach 1 goal conditions was exceeded. The fabrication characteristics of brazeability, machinability, and formability are acceptable in both alloys as shown in Section 3.2.5 which follows. Melting temperatures ~1371° C (2500° F) were tested by the "nil strength" procedure. Hot corrosion testing showed satisfactory results for HDA 8077 but not for YD NiCrAl. Further hot corrosion testing outside the program showed further anomolies. This subject was discussed previously in detail in Section 3.1.14 of this report. Property retention in high temperature exposure was acceptable.

3.2.2 Vane Material Procurement

The Task II alloys were procured to material specifications negotiated with the two material vendors. These specifications were issued as "folder series" (preliminary) documents. The salient features of both specifications include the following:

Texture

- Maximum longitudinal room temperature modulus - 25×10^6 psi
- Macro examination - dull matte finish on etched transverse section which indicates attainment of the <100> longitudinal texture.

Brazeability

- Capability of 1204° C (2200° F) brazing test without voiding

Fluorescent Penetrant

Finished part capability

Stress Rupture

1093° C (2000° F) Stress for 20-Hour Life

Alloy	Longitudinal		Transverse		Short Transverse	
	MPa	ksi	MPa	ksi	MPa	ksi
YD NiCrAl	51.7	7.5	34.5	5.0	20.7	3.0
HDA 8077-LPT	75.8	11.0	31.0	4.5	---	---
HDA 8077-HPT	62.0	9.0	34.5	5.0	---	---

It was not possible to negotiate a short transverse stress rupture specification for HDA 8077 because Cabot had neither the capability nor the supporting data to back up a guarantee. Special Metals, on the other hand, was willing to accept the short transverse specification based on General Electric data.

3.2.3 Extrusion Shapes

The alloys were supplied in several different extruded shapes during the program. In Task I, YD NiCrAl and HDA 8077-LPT-type were supplied in the small rectangular shape shown at the top of Figure 53. The HPT-type HDA 8077 was extruded to the "Task I shape" shown in that figure. The other Task I alloys were produced in various rectangular shapes as described earlier. For Task II, the HDA 8077-LPT vanes were machined from existing Task I material. For the HPT vanes, a new YD NiCrAl extrusion shape was designed and the Task I HDA 8077 shape was modified as also shown in Figure 53.

3.2.4 Machinability Evaluation

The Ni-Cr-Al ODS alloys proved to be very machineable by both conventional and nonconventional metal-removal techniques. This capability stems in part from the relative simplicity of the alloys in contrast to the more highly alloyed superalloys. The presence of a dispersed phase interferes very little with machineability. Its major effect is a slight increase in ambient temperature hardness. The alloys, because of the presence of the dispersed phase, are quite stable microstructurally. This adds to their

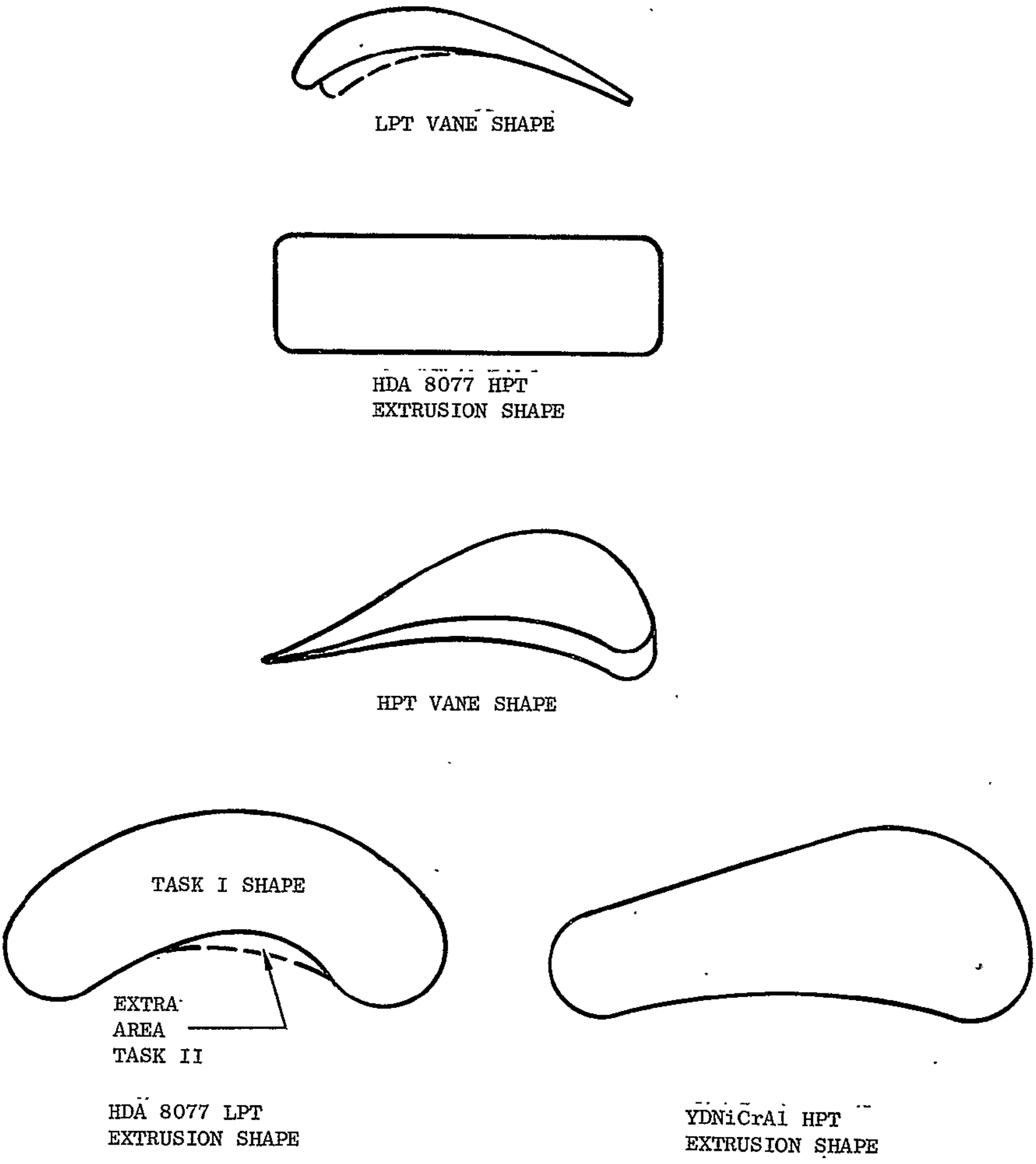

Figure 53 ODS-NiCrAl Vane and Extrusion Shapes for Task II

stability in response to drilling, turning, grinding, end milling, and Electro-Discharge Machining (EDM). The multifaceted sample is depicted in Figure 54, along with representative microstructures after a 1315° C (2400° F) exposure. It can be seen that the surface effects were nil with all of these machining techniques. In another study, the Electro-Chemical Machining (ECM) capability of the materials was shown to be excellent.

3.2.5 Brazeability Evaluation

The adaptability of the aluminum-containing alloys to various braze alloys was not as universal as was the adaptability to varied machining techniques, though satisfactory braze alloys were identified for all alloys. As the listing in Table 15 indicates, B93 proved suitable for HDA 8077 and YD NiCrAl. This is fortunate, since that alloy is the standard used for MA 754 vane brazing. For MA 953, the Cobalt-based H33 was workable; and, for the ODS-FeCrAl alloys, RA 333 (containing 18% iron) proved to be the most successful of the braze alloys evaluated. Representative microstructures of successful and unsuccessful braze joints are shown in Figures 55 through 57.

3.2.6 Vane Manufacture

This phase of the program proved to be almost routine, with the machining of the HDA 8077 and YD NiCrAl vanes fitting into the current MA 754 vane manufacturing cycles of the respective F101 engine machining vendors with no trouble. The only incident was an accidental one with two of the HPT YD NiCrAl vanes in which a tool grab occurred during the profile milling operation. The cutting tool grabbed and; before the mill could be stopped, one complete revolution occurred. This resulted in a groove approximately 0.020 inch deep around the entire airfoil. The depth of the groove was below finish size for the vane, therefore eliminating any chance of saving the airfoil through hand benching. Insufficient extra material was on hand to replace the vane stock. The remaining vanes looked excellent and passed the vendor's dimensional checks. The LPT vanes were machined without incident. Five HDA 8077-LPT vane blanks were supplied and five vanes were delivered. Machining of both F101 and CF6-50 HPT vanes and F101 LPT vanes was accomplished in approximately the same manner using the following sequence:

- Saw blanks to vane length plus grip stock
- Machine rough outer contour by profile milling
- Machine ends to size
- Hand finish outside to final contour
- EDM internal cavities
- EDM cooling holes.

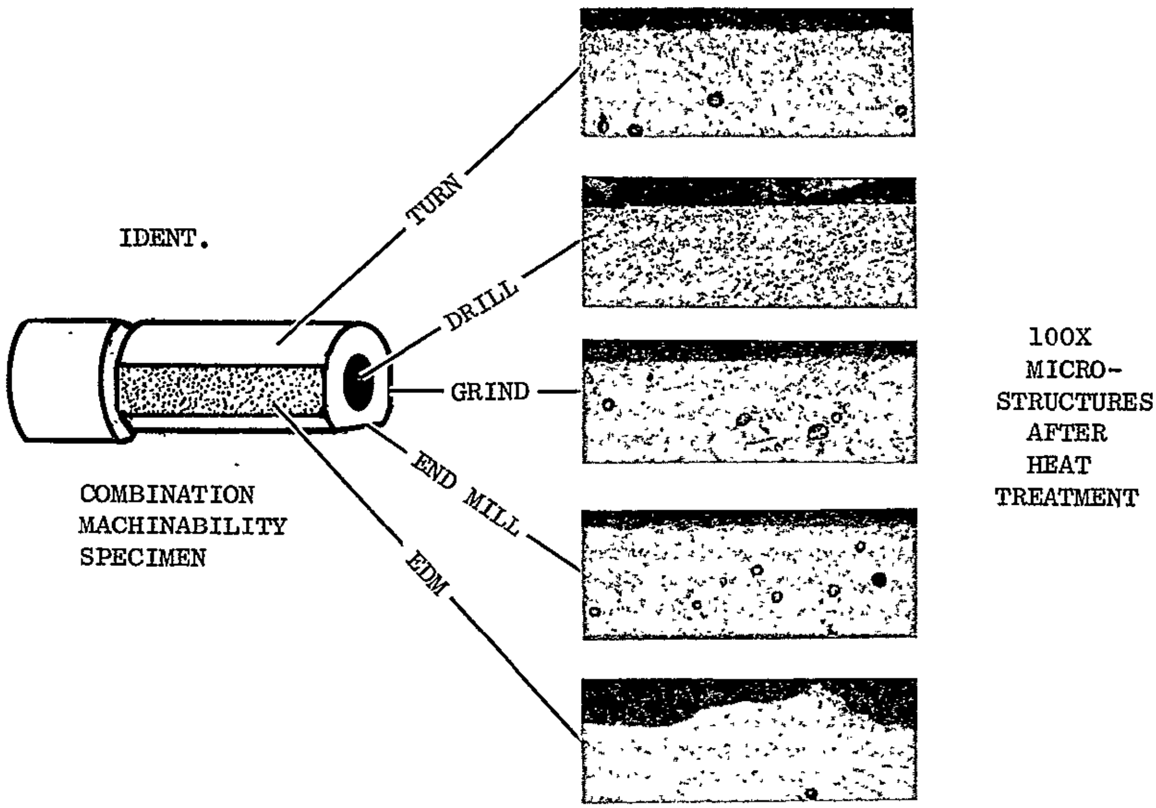

Figure 54 Microstability of HDA 8077 in Machining

Table 15. Brazing Test Results.

ODS Alloy	Braze Alloy	Results
HDA 8077 HPT	B93	Satisfactory
HDA 8077 HPT	TD6	Major Voids
HDA 8077 LPT	B93	Satisfactory
HDA 8977 LPT	TD6	Voids
YD NiCrAl	B93	Satisfactory
YD NiCrAl	TD6	Voids
TD NiCrAl	B93	Minor Voids
MA 953	B93	Voids
MA 953	TD6	Erosion and Voids
MA 953	H33	Satisfactory
MA 956	B93	No Wetting
MA 956	TD6	Major Erosion
MA 956	H33	Major Erosion
Fe-Cr-Al (Similar to MA 956)	RA333	Satisfactory

Braze Alloy Compositions

B93 = 55Ni, 14Cr, 9.5Co, 4.9Ti, 4W, 4Mo, 3Al, 4.5Si, 0.7B
TD6 = 54Ni, 15.5Cr, 16Mo, 4W, 6Fe, 4Si
H33 = 51Co, 19Cr, 17Ni, 4W, 8Si, 0.8B
RA 333 = 45Ni, 25Cr, 18Fe, 3Co, 3Mo, 3W, 1.5Mn, 1.5Si

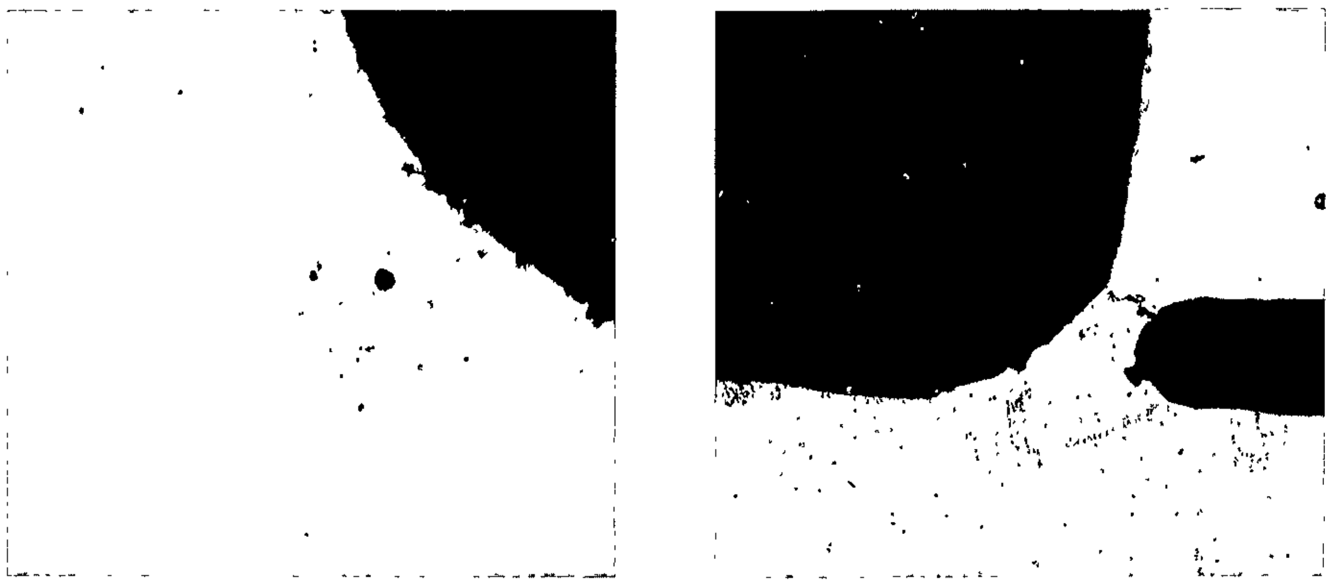

50X 50X

B-93 BRAZED JOINT TD6 BRAZED JOINT

Figure 55 HDA 8077 Brazed Sections

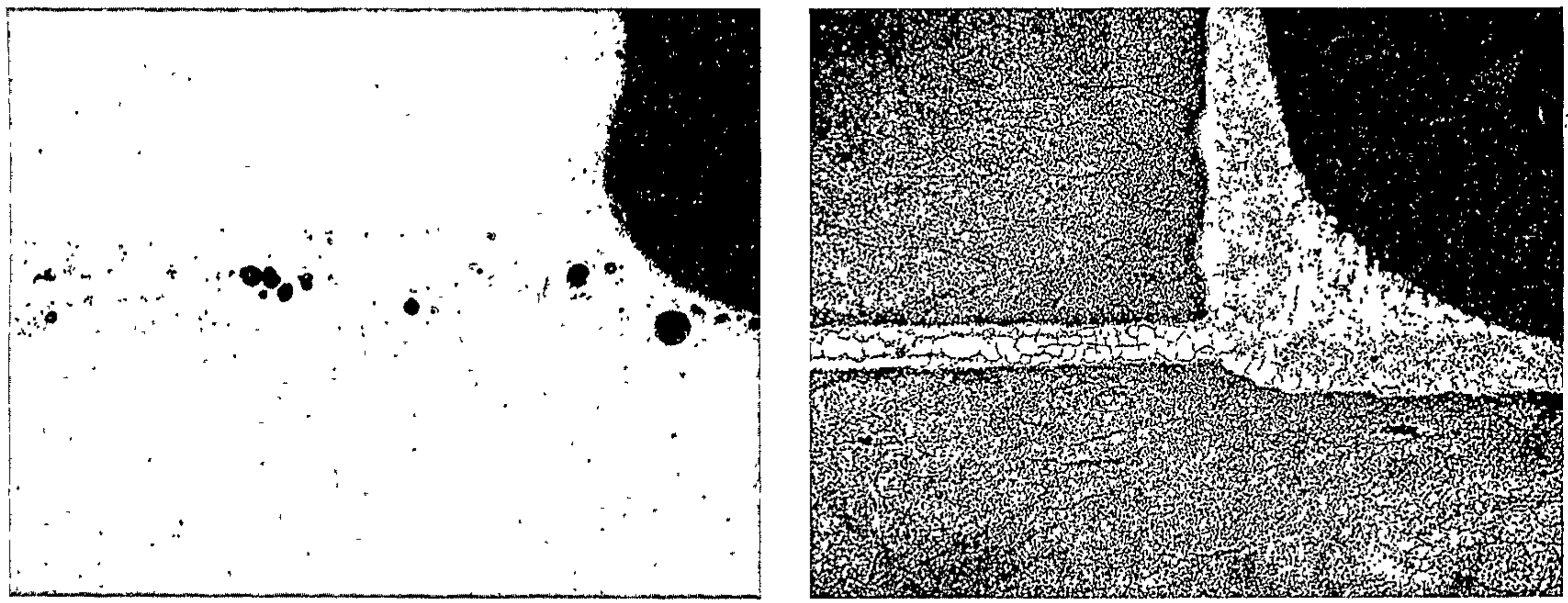

50X 50X

B93 BRAZED JOINT H33 BRAZED JOINT

Figure 56 MA953 Brazed Sections

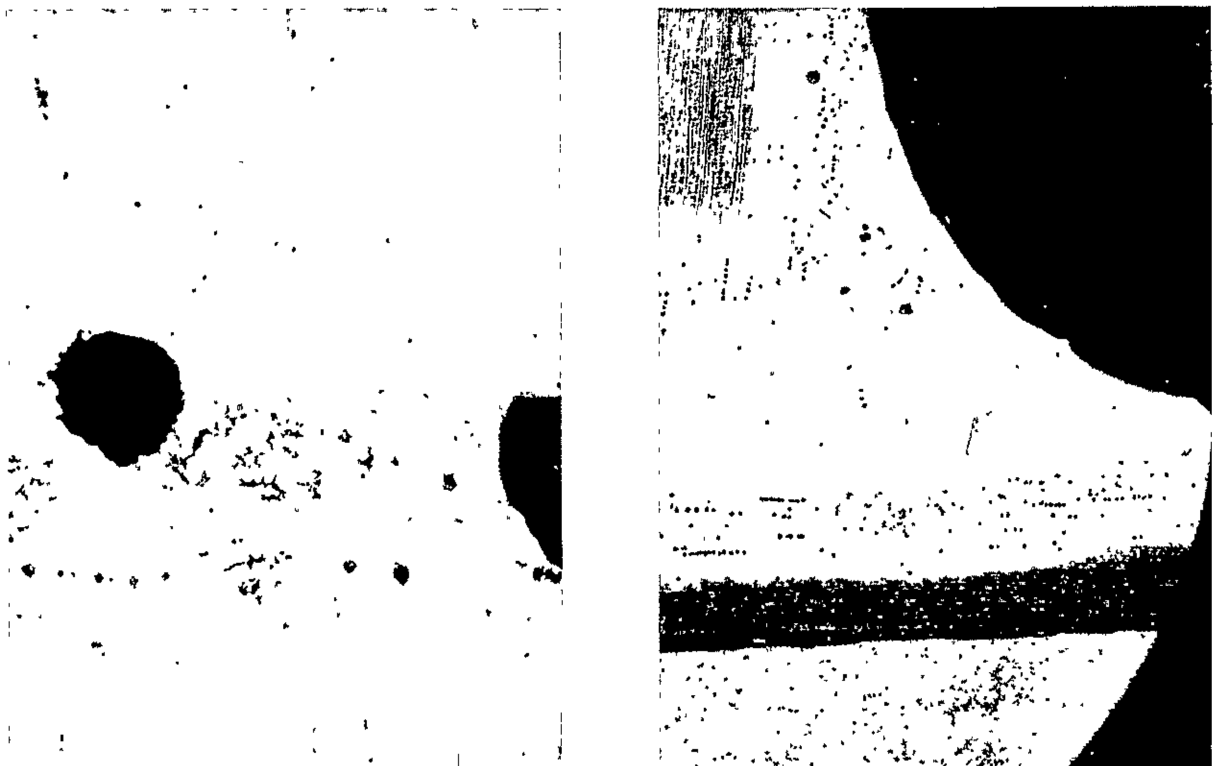

50X

MA956 - TD6

FeCrAl - RA333

Figure 57 ODS FeCrAl Brazed Sections

3.2.7 Nozzle Assembly

Nozzle assembly of the two F101 PV nozzles went very smoothly, demonstrating the excellent fabricability of the ODS-NiCrAl alloys. No further part losses were sustained after the two YD NiCrAl vanes were scrapped in machining.

The HDA 8077-HPT vanes were of the 0.6% Y_2O_3 HPT-type. The LPT-type 8077 alloy was not engine-tested in the HPT nozzle because it was not considered a viable HPT vane material. High temperature transverse ductility was considered marginal and Cabot found it difficult to reproducibly provide a low modulus recrystallization texture in this 2% Y_2O_3 alloy. The drawbacks of this type of HDA 8077 rendered it too great a risk for an F101 PV nozzle.

3.2.8 Nozzle Segment Repair

Responding to a request from F101 Turbine Design, the NASA Program Manager authorized the utilization of one of the HPT vanes in a retrofit/repair of existing MA 754 vanes in a nozzle segment. The retrofit/repair was successfully conducted using an HDA 8077 vane of the 0.5% Y_2O_3 HPT composition. The nozzle segment used was (originally) a discrepant part. The discrepant MA 754 vane was EDM'd from the segment. An HDA 8077 vane was inserted, alloyed, and brazed into place. The braze quality was very good. Brazing was done with B93 alloy. No evidence was seen of excessive flow of the braze alloy on the adjacent (MA 754) vane, which was not replaced.

Total change in flow-path radial height through all operations of the repair was less than 0.002 inch. This demonstration has shown that a vane can be replaced in a segment as a repair for damaged vanes.

3.3 TASK III - ENGINE TEST

The plan for engine testing the ODS alloys in this program included tests in three F101 turbine nozzles [two in the high pressure turbine (HPT) and one in the low pressure turbine (LPT)]. Because of delays encountered in preparing one of the HPT nozzles and the lack of a suitable test engine, a CF6-50 engine test was substituted for one of the F101 engine tests to fulfill the contract requirements.

The F101 nozzle configurations are depicted in Figure 58, showing the locations of HDA 8077, YD NiCrAl, and MA 754 (bare and coated) vanes.

3.3.1 F101 LPT Engine Test

The F101 LPT nozzle is composed of an inner band, an outer band, and 77 uncooled vanes. The current vane alloy is MA 754. The vane operates in an environment such that the principal mechanical stresses are in the engine

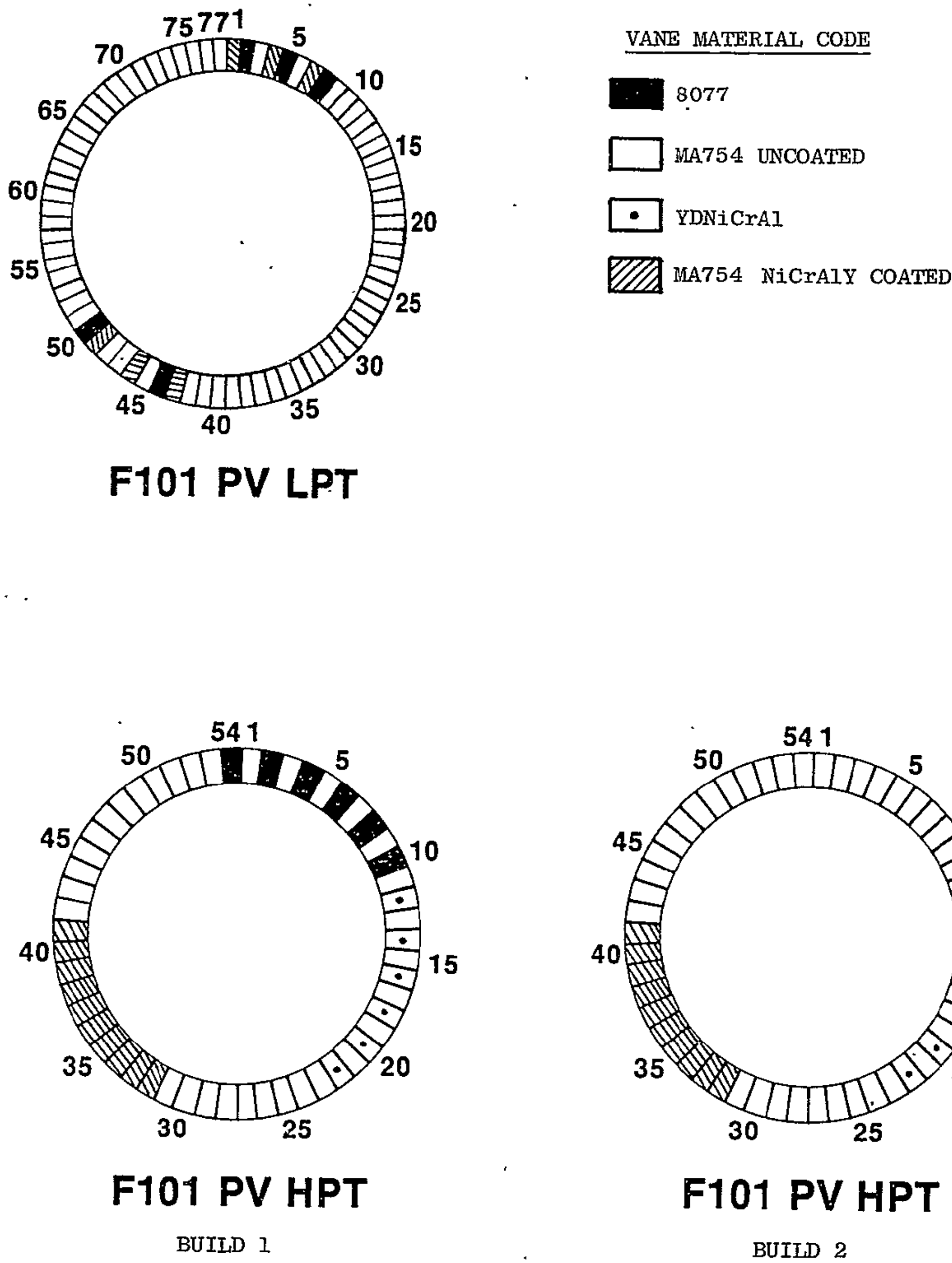

Figure 58 F101 PV Nozzle Vane Layouts

radial (vane longitudinal) direction. Through-the-wall thermal stresses are low because the vane is uncooled. It is estimated that maximum vane metal temperatures are 1204° C (2200° F) at the 70%-span section of the vane (hot-streak conditions, hot-day takeoff). Stress analyses indicate that the vane is stress-rupture-limited in the longitudinal direction.

The engine test was scheduled to run an accelerated mission test cycle; the profile is shown in Figure 59. The engine test was started and, after 60 hours (75 test cycles, 375 thermal cycles) of high temperature running, a subidle speed overtemperature condition occurred because of a fuel control malfunction. The overtemperature condition caused re-solutioning of much of the superalloy cast components in the turbines. The HDA 8077 and MA 754 LPT vanes were unaffected. Because of the overtemperature occurrence, the engine test for this part of the program essentially was ended, since possible salvage reheat treatment of the conventional superalloy nozzle bands would take more time than the engine test program could encompass.

All the ODS LPT vanes looked good on visual inspection as is shown in Figure 60, which depicts uncoated HDA 8077 vanes and bare and coated MA 754 vanes. On a negative note, what the photographs don't show is the green oxide on the HDA 8077 vanes in contrast to the silver color of the Ni-Cr-Al-Y coated MA 754 vanes. This indicates that the HDA 8077 vanes had not formed a protective Al_2O_3 surface, while the coated MA 754 vanes had. The HDA 8077 vanes did have a more uniform oxide film than the bare MA 754 vanes, however.

The overall judgment is that the HDA 8077 vanes performed satisfactorily, though the test time was too short to make a full assessment. Such an assessment would necessarily require additional engine testing and detailed metallographic examination. The absence of a protective Al_2O_3 film, however, is a negative factor.

3.3.2 F101 HPT Engine Test

The F101 HPT nozzle is composed of 27 vane-pair segments, each currently consisting of two MA 754 vanes and inner and outer MA 754 band segments. The vanes and bands are cooled. The vanes operate in an environment such that the principal stresses are caused by thermal gradients which produce thermal strains. The strains are complex in that they occur both through the vane wall and along it between cooling holes. It is estimated that maximum vane temperatures of 1126° C (2060° F) are reached at the pitch section of the vane at both leading and trailing edges (hot-streak conditions, hot-day take-off). Stress analyses indicate that the vane is LCF-limited at these locations. Meaningful rupture requirements are difficult to calculate using existing design techniques. The fact that the ODS alloys are not isotropic and the difficulty in handling stress relaxation in these creep-resistant alloys are additional complicating factors.

The engine test was planned for a total of 400 hours with 800 cycles. The cycle profile is shown in Figure 61. Each test cycle contains two thermal cycles.

ACCELERATED MISSION TEST CYCLE

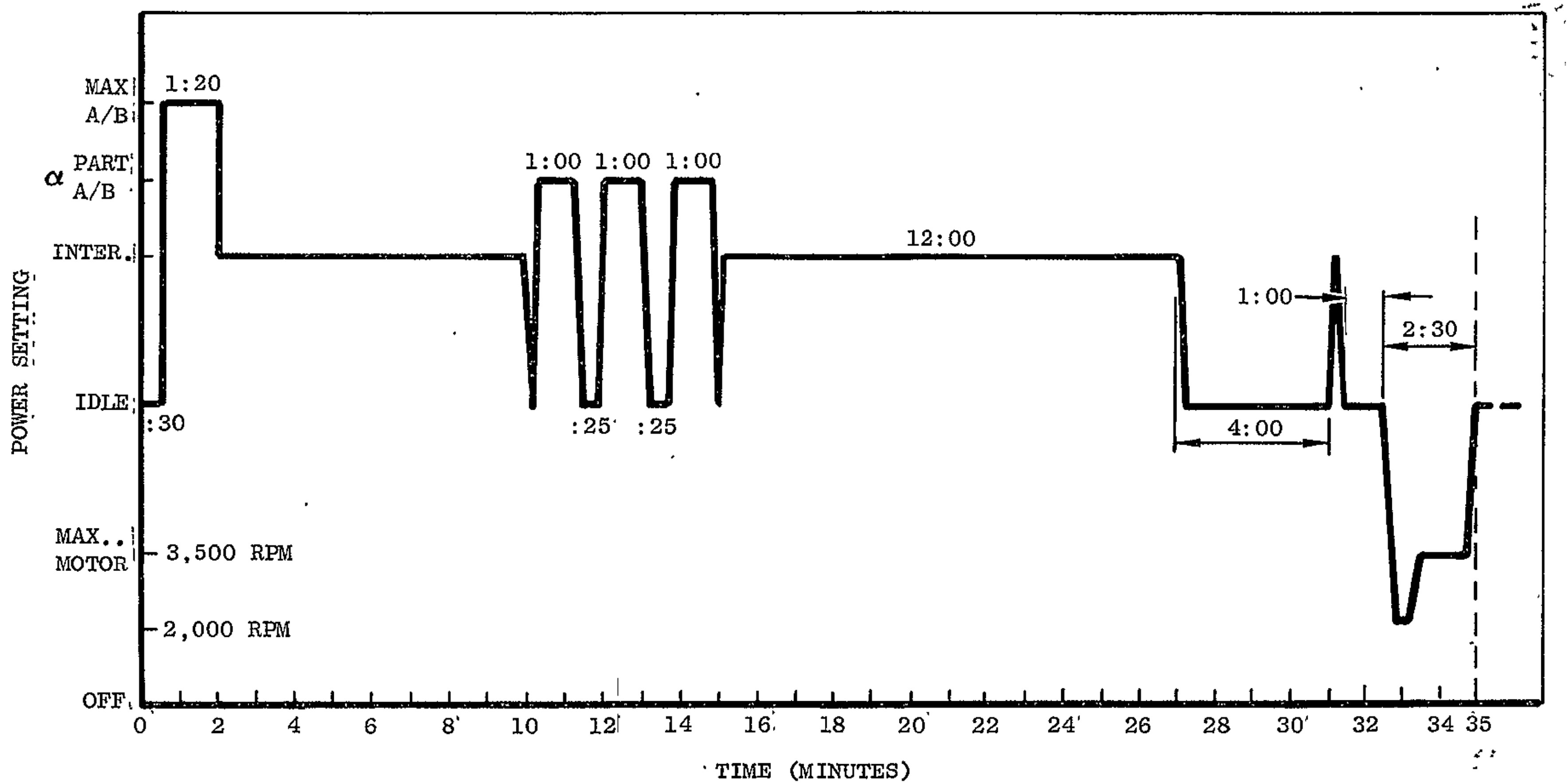

Figure 59 F101 LPT Engine Test Cycle

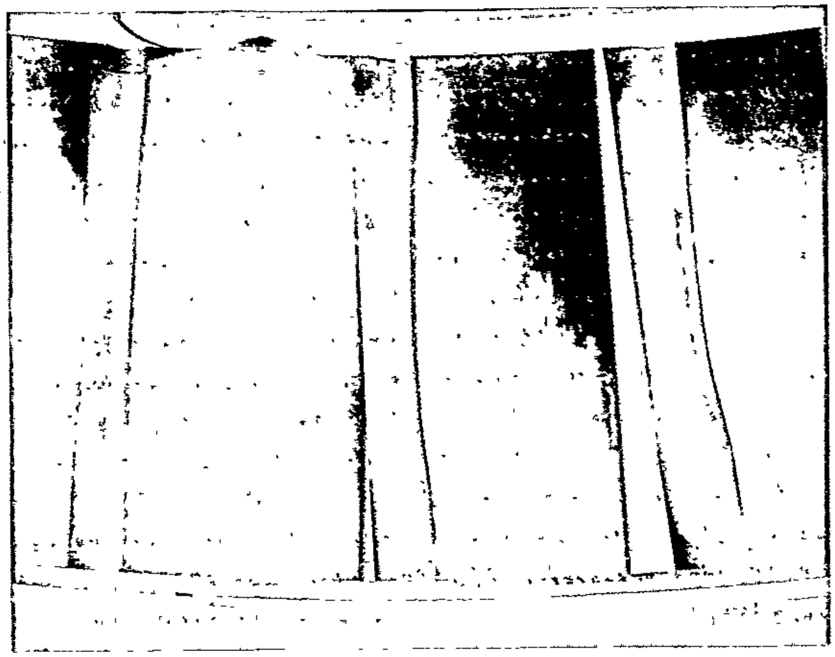

MA754 COATED | HDA8077 BARE | MA754 BARE

LEADING EDGES

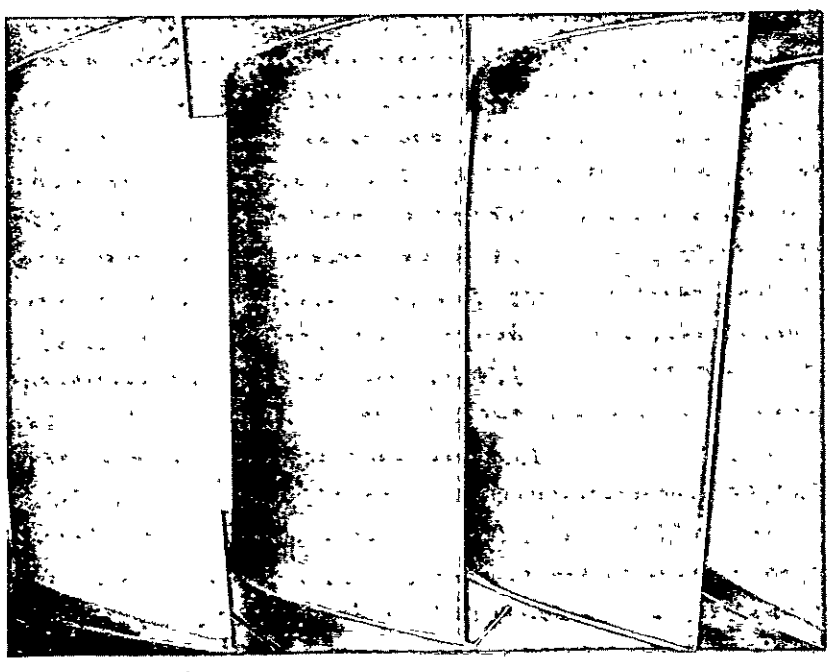

MA754 COATED | HDA8077 BARE | MA754 BARE

TRAILING EDGES

Figure 60 LPT Engine Test of HDA 8077, Bare & Coated MA 754 Vanes

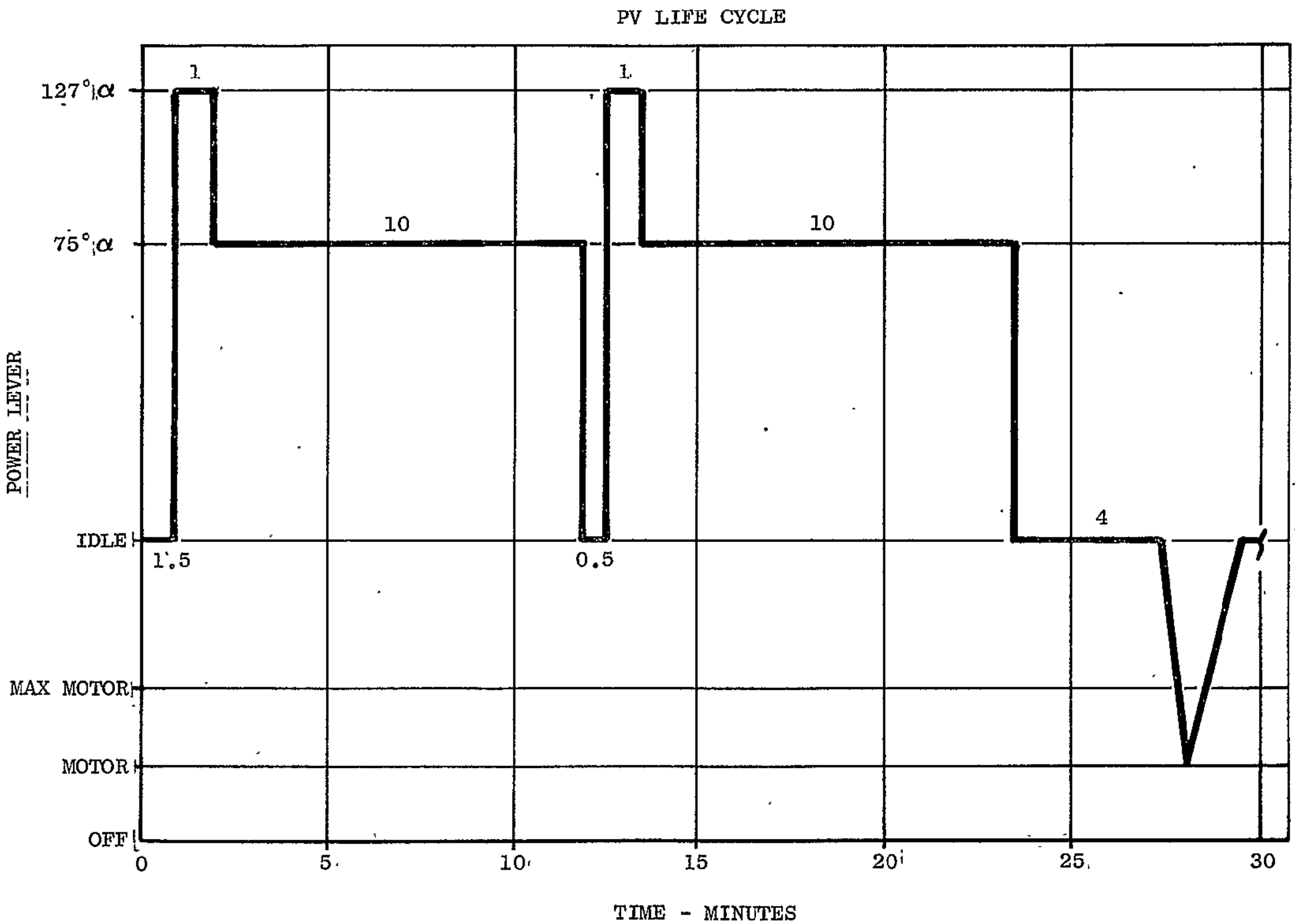

Figure 61 F101 HPT Engine Test Cycle

The engine was run for 105 hours and 200 cycles before the first teardown. Examination in the "dirty" condition showed the YD NiCrAl and MA 754 vanes in satisfactory condition, but the HDA 8077 vanes exhibited trailing edge bowing (Figure 62) and severe cracking. Two of the six HDA 8077 vanes had band-to-band suction-side (convex) cracks. Closeup views of two pressure-side hole rows in HDA 8077 and MA 754 vanes, Figure 63, show the absence of surface cracking in the MA 754 vanes.

Cutup of two of the HDA 8077 vanes showed considerable cracking in addition to that visible on the outer surfaces. Figure 64 shows the location of the major cracks. In Figures 65, 66, and 67, the cracks are shown in microsections of the leading edge/forward cavity, the aft cavity, and trailing edge, respectively. Similar views of the companion MA 754 vanes are shown in Figures 68 through 71. For outside surface closeups of the MA 754 vanes, refer back to Figure 63. The marked difference between the vane materials is clearly evident; the MA 754 vanes are not bowed, there are no through-the-wall fractures, and the secondary cracking is considerably less. Most of the HDA 8077 cracks occurred under tensile or rupture conditions. This is indicated by the fact that they followed the irregular grain boundaries. Several of the cracks, however, appear to be by low cycle fatigue as indicated by the straight-line transgranular propagation shown in Figure 67.

After removal of the HDA 8077/MA 754 vane segments, the engine test was continued to the 315-hour/699-cycle point and again torn down for examination. Macro examination of the vanes showed, unexpectedly, considerable distress on the YD NiCrAl vanes and still only minor effects on the MA 754. Figure 72 shows large displacement trailing edge bowing on the YD NiCrAl vanes and some also on the MA 754 vanes. Figure 73 shows surface cracking on the YD NiCrAl vanes. Figure 74 pictorially displays the location of cracking observed in the cut-up microexamination of the vanes. Typical microsections of the vanes are shown in Figures 75 through 77 in the same format as that done earlier for the HDA 8077 and MA 754 vanes.

In addition to the increased cracking observed in HDA 8077 and YD NiCrAl, relative to MA 754, several surface attack effects were noted. A subsurface oxide buildup occurred in the trailing-edge cooling-hole area that was not observed on MA 754. The effect is shown in Figure 78. This is one of the hotter zones of the vane. It should be noted that the effect occurs both on the outside vane surface and inside the cooling hole. The attack was observed to a distance of approximately 8.9 mm (0.35 inch) from the hole exit. A study employing Scanning Electron Microscopy (SEM) and Energy Dispersive Analysis of x-rays (EDAX), Figure 79, failed to pinpoint external contamination as a cause of the unusual attack. The SEM/EDAX analyses of the oxide particles show a substantial aluminum oxide content, indicating that they were formed by internal oxidation. The EDAX analyses of the areas between the particles show practically no aluminum from the vane surface through the oxide particle area. The chromium in this zone is depleted also. It is postulated that the engine environment prevented formation of a protective Al_2O_3 scale and that this lack of a protective scale allowed internal oxidation to take place.

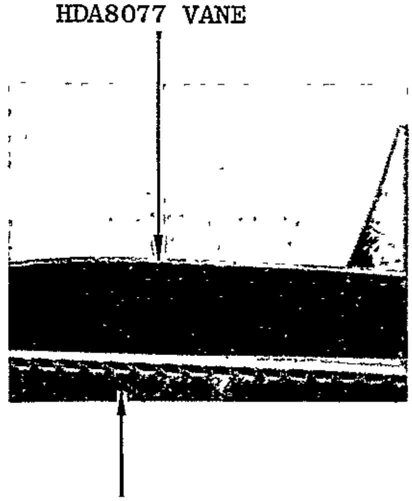

Figure 62 HDA 8077 Vane Trailing Edge Bowing, F101 HPT Test

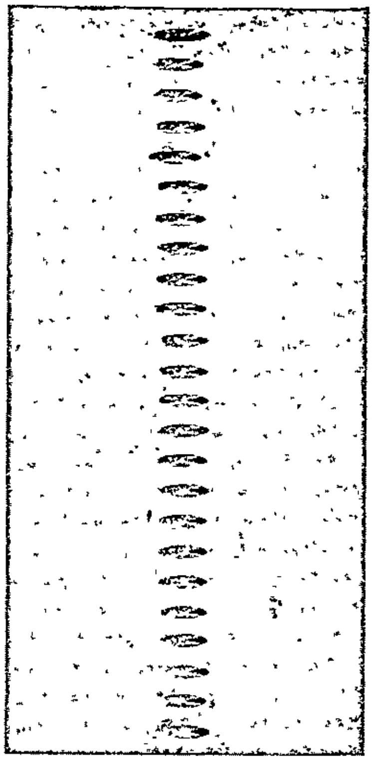

MA754
VANES

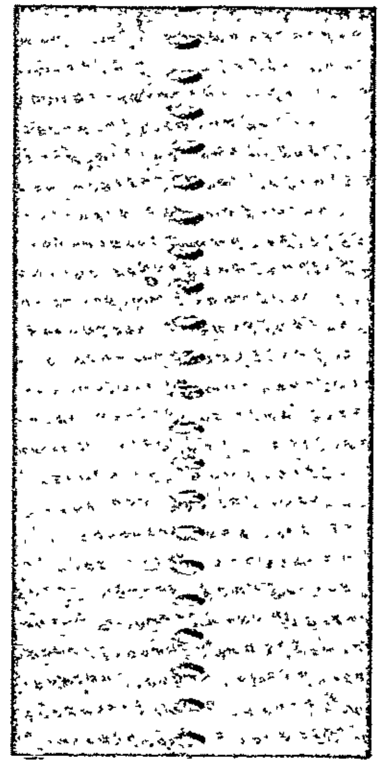

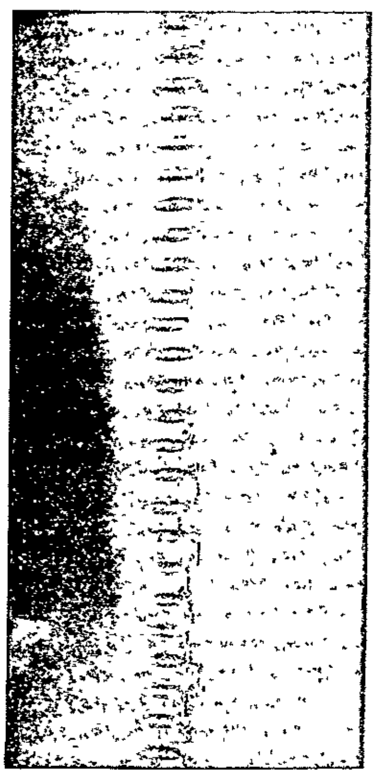

HDA8077
VANES

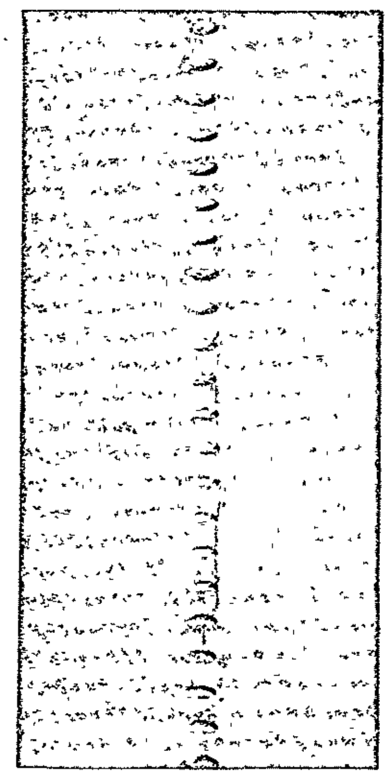

Figure 63 HDA 8077 and MA 754 Vane Pressure Side Closeups F101 HPT Test

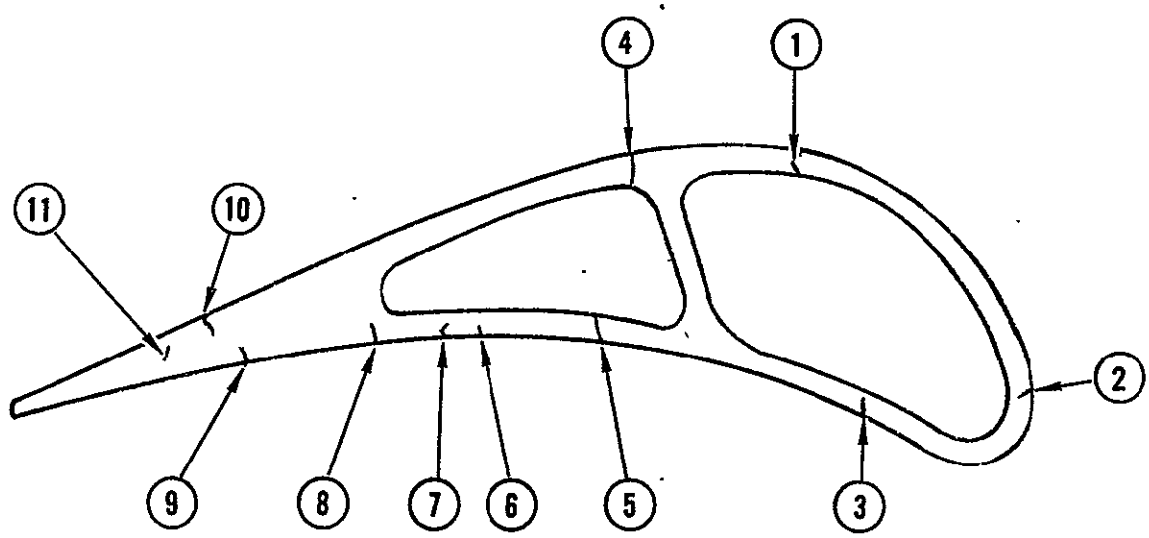

MICROSECTIONS SHOWN IN FIGURES 65, 66 and 67

Figure 64 HDA 8077 Vane Crack Locations, F101 HPT Test

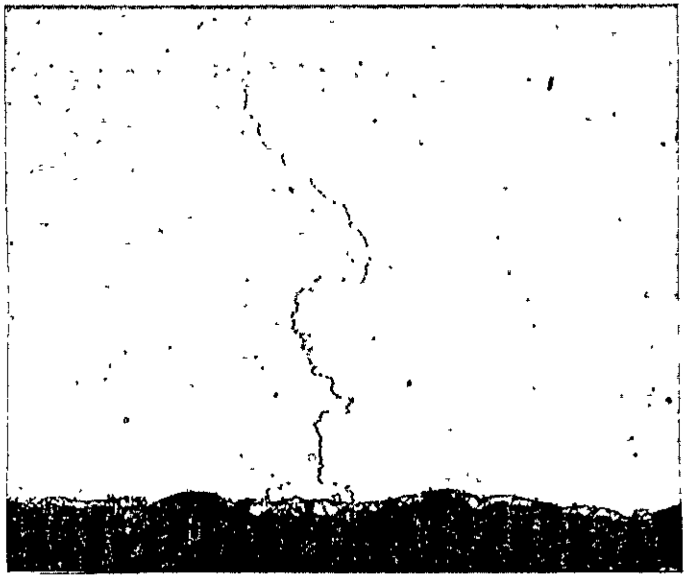

LOCATION 1 INNER WALL SUCTION SIDE

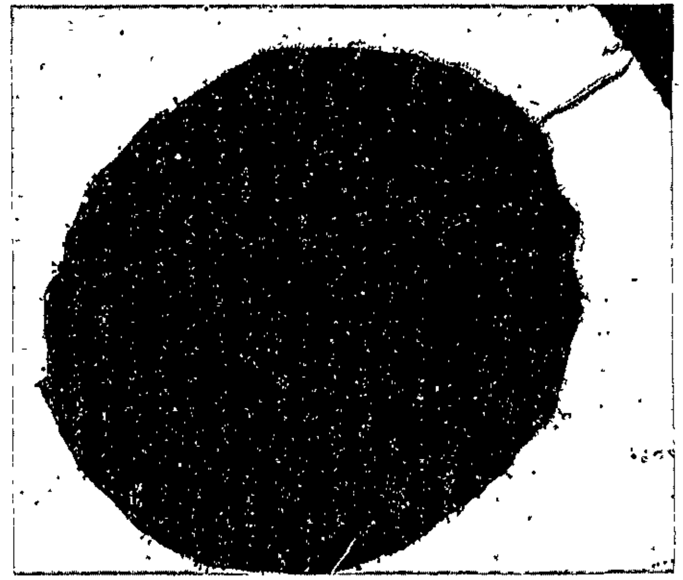

LOCATION 2 LEAD EDGE COOLING HOLE

LOCATION 3 OUTER WALL PRESSURE SIDE

Figure 65 HDA 8077 Lead Cavity Microsections F101 HPT Test

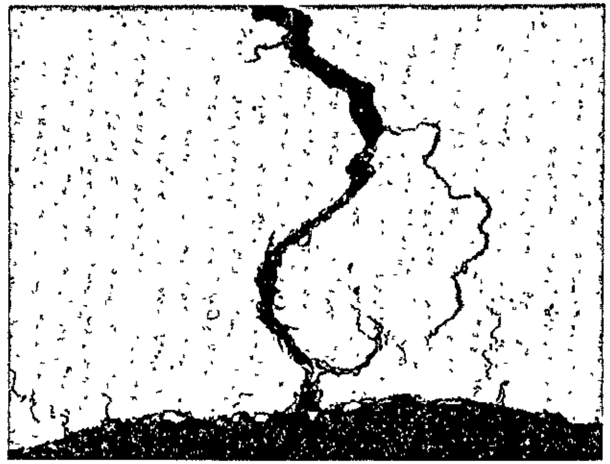

LOCATION 4 SUCTION SIDE THROUGH WALL FRACTURE

VANE LOCATIONS
REF. FIG. 64

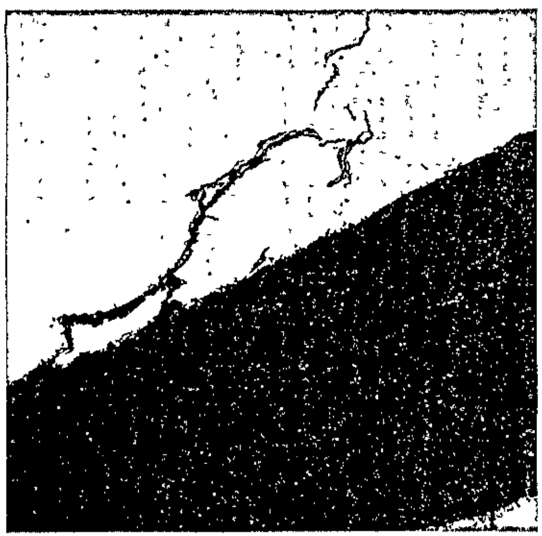

LOCATION 7 COOLING HOLE

LOCATION 6 PRESSURE SIDE OUTER SURFACE

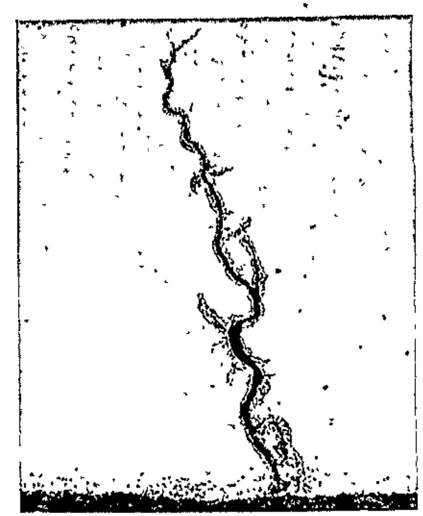

LOCATION 5 PRESSURE SIDE OUTER–SURFACE.

Figure 66 HDA 8077 Aft Cavity Microsections F101 HPT Test

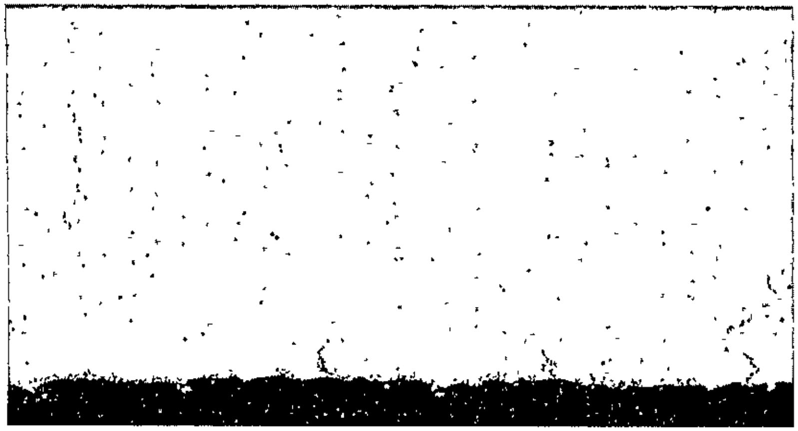

LOCATION 11 COOLING HOLE SURFACE

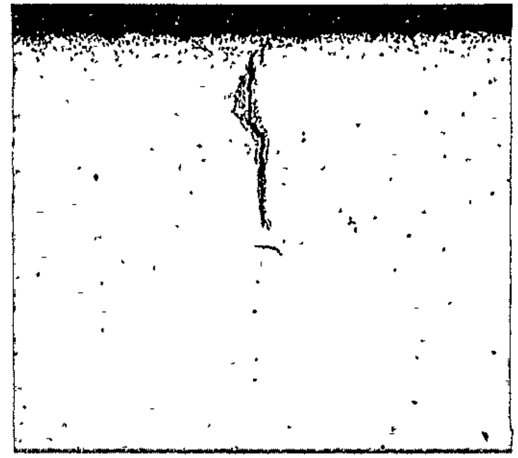

LOCATION 10 SUCTION SIDE OUTER SURFACE

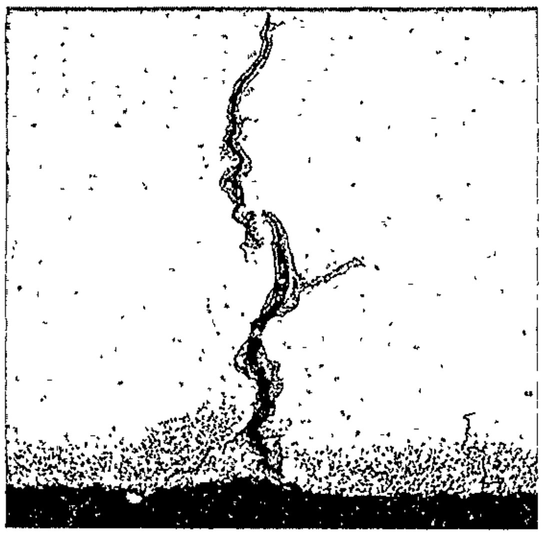

LOCATION 9 PRESSURE SIDE SURFACE

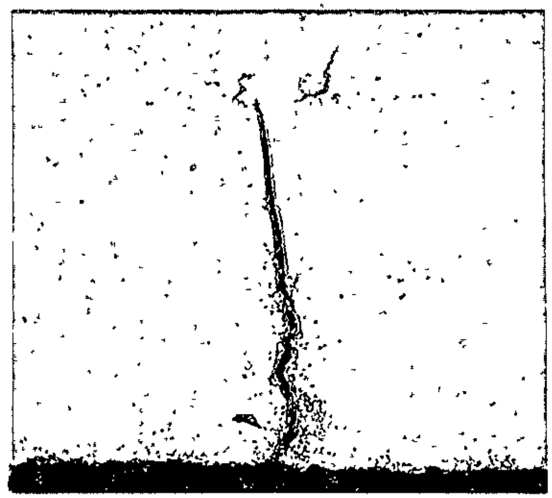

LOCATION 8 PRESSURE SIDE SURFACE

VANE LOCATIONS
REF. FIG. 64

Figure 67 HDA 8077 Trailing Edge Microsections F101 HPT Test

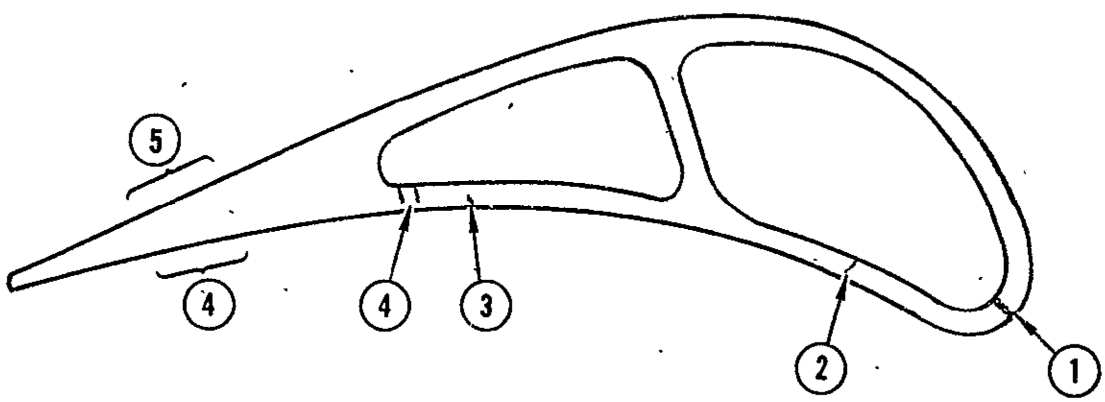

MICROSECTIONS SHOWN IN FIGURES 69, 70 AND 71

Figure 68 MA 754 Vane Crack Locations, F101 HPT Test

VANE LOCATIONS
REF. FIG. 68

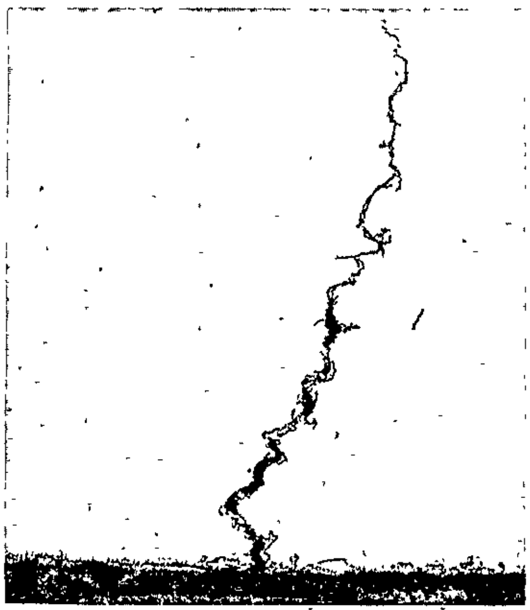

LOCATION 2 PRESSURE SIDE OUTSIDE SURFACE

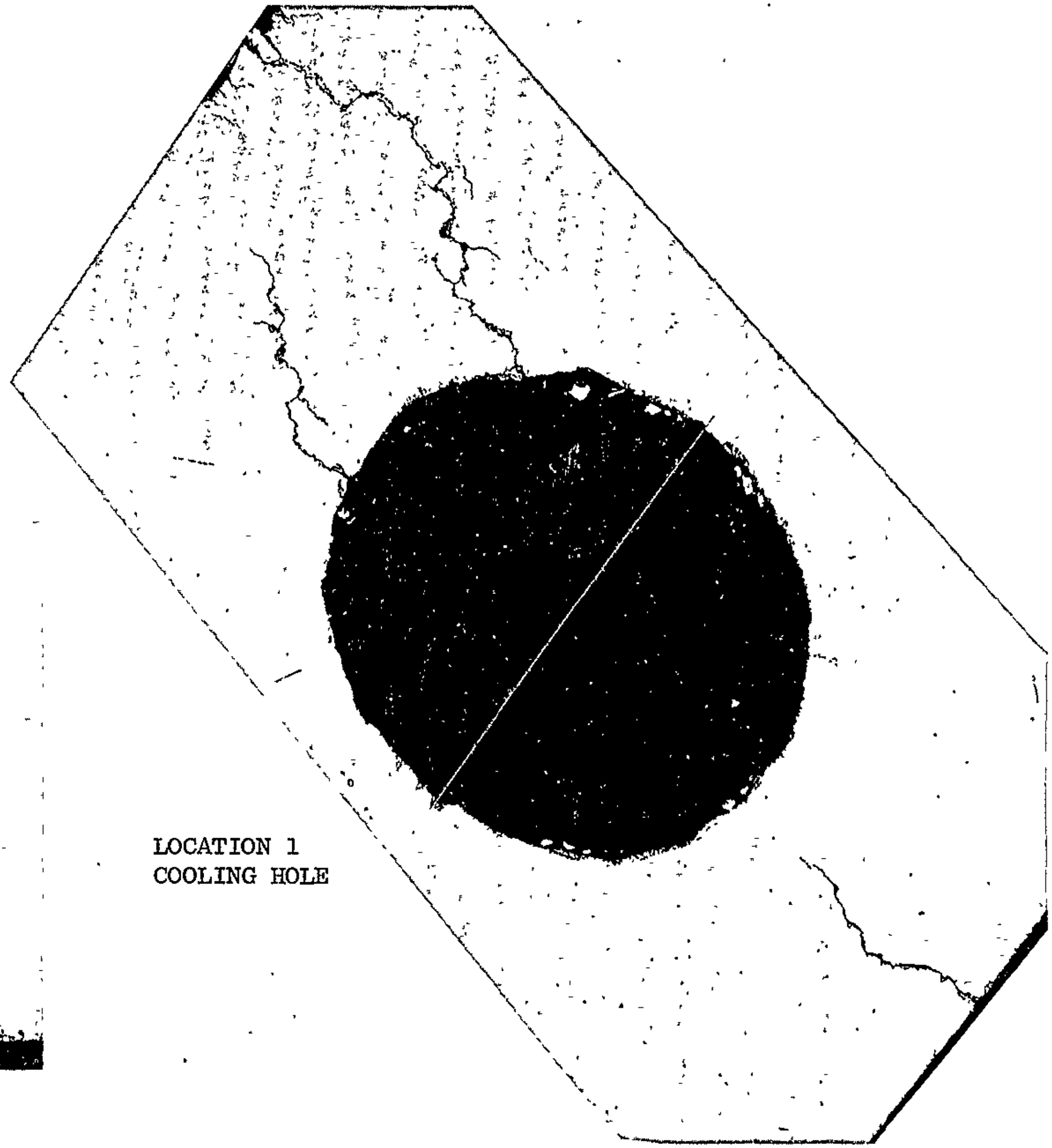

LOCATION 1 COOLING HOLE

Figure 69 MA 754 Lead Cavity Microsections F101 HPT Test

LOCATION 4 INNER SURFACE

VANE LOCATIONS
REF. FIG. 68

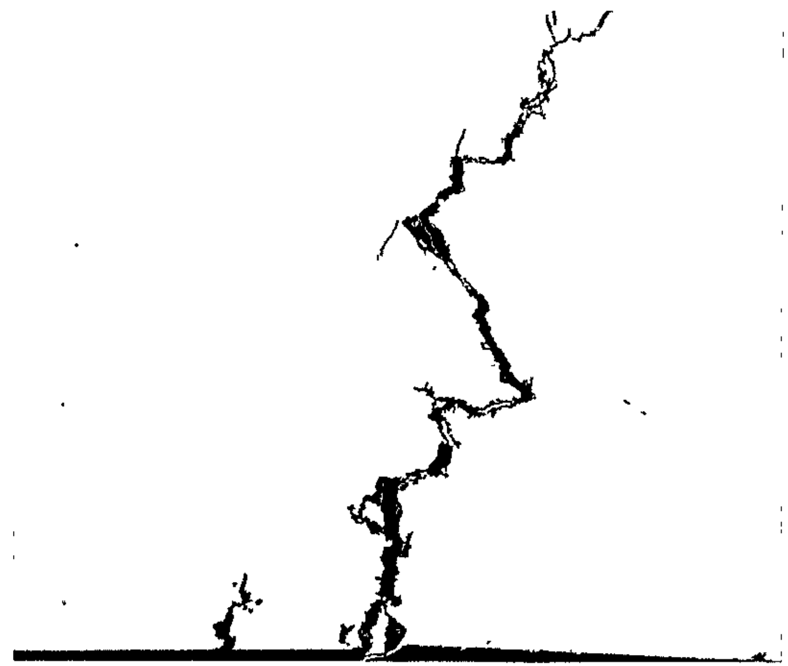

LOCATION 3 OUTER SURFACE

Figure 70 MA 754 Aft Cavity Microsections F101 HPT Test

ORIGINAL PAGE IS
OF POOR QUALITY

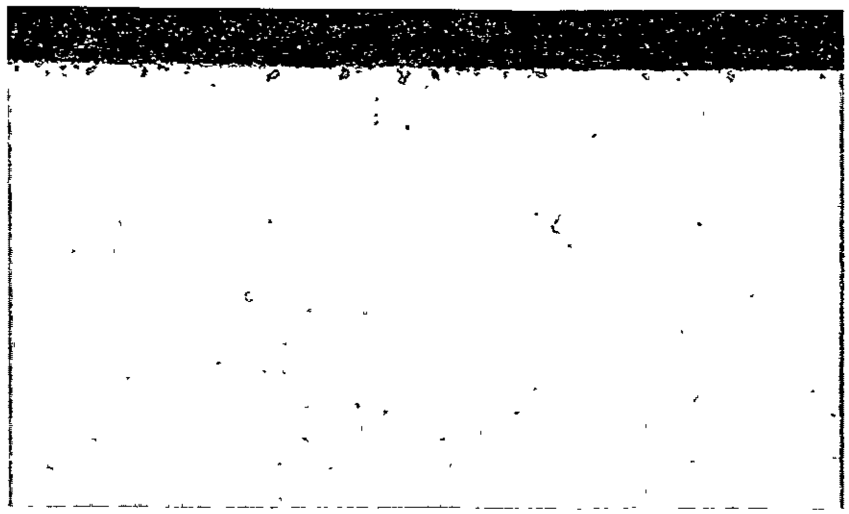

AREA 5
SUCTION
SIDE
SURFACE

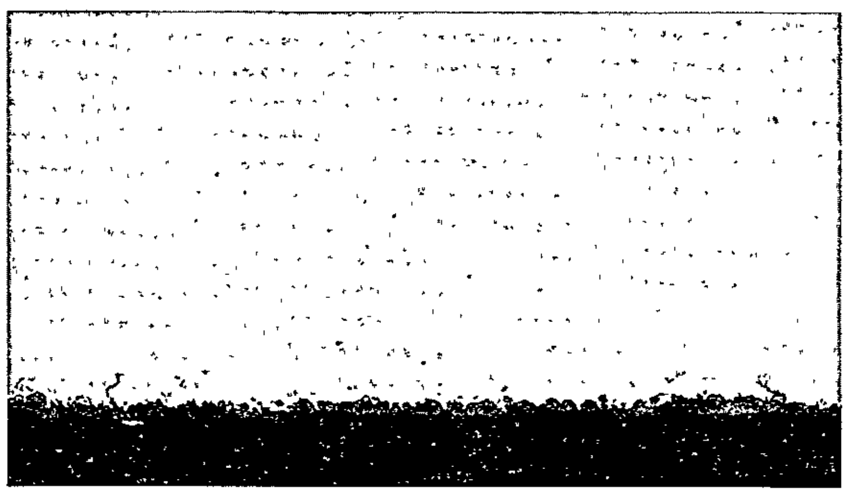

AREA 4
PRESSURE
SIDE
SURFACE

VANE AREAS
REF. FIG. 68

Figure 71 MA 754 Trailing Edge Microstructures F101 HPT Test

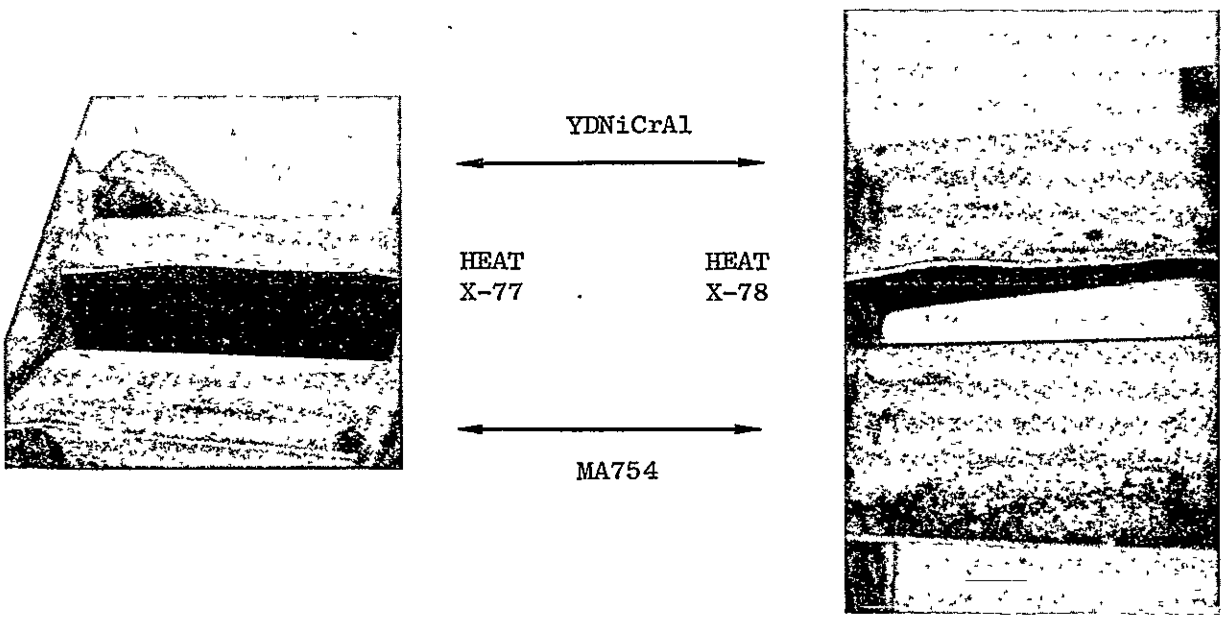

Figure 72 YD NiCrAl Trailing Edge Bowing F101 HPT Test

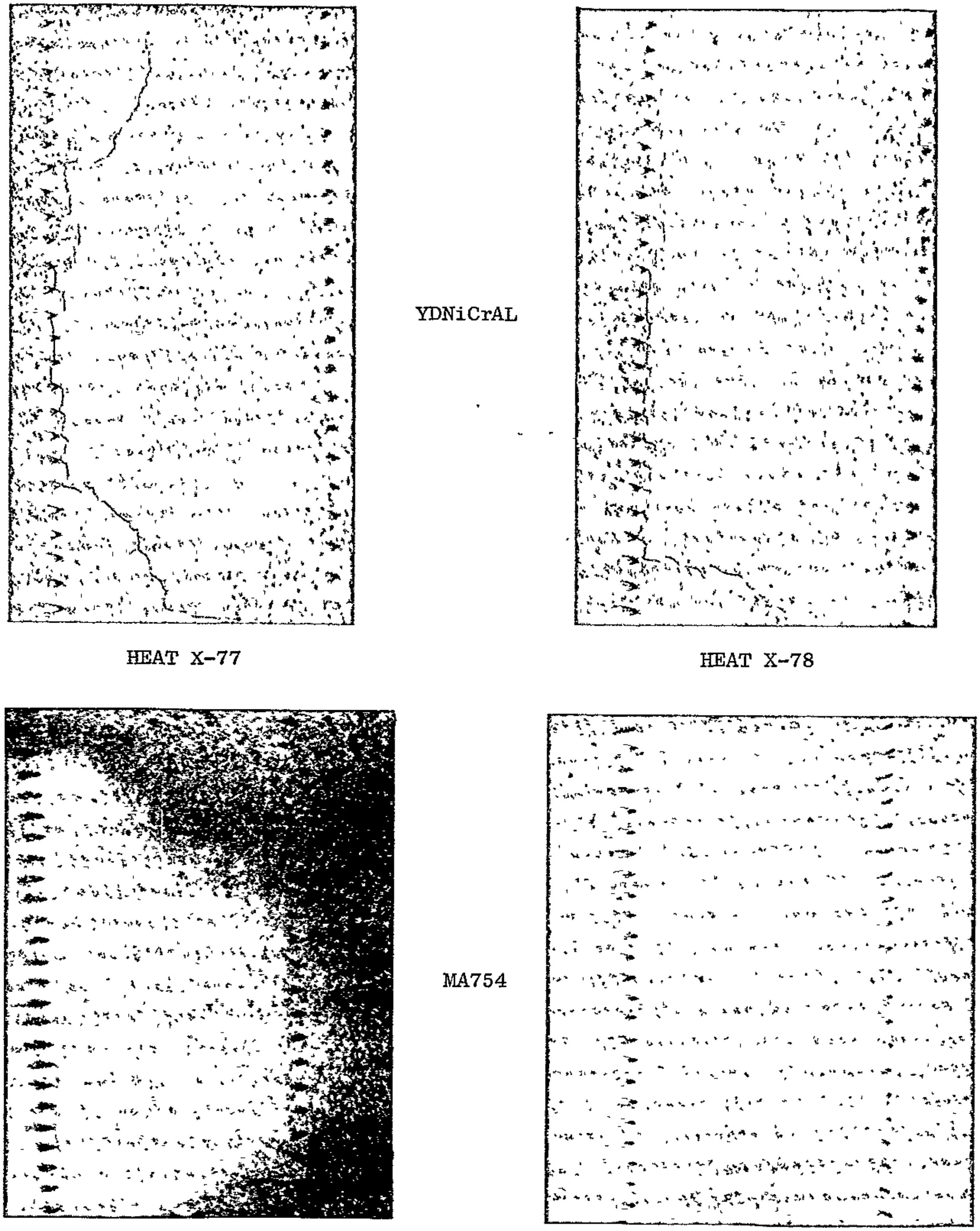

Figure 73 YDNiCrAl & MA754 Vane Closeups, F101 Test

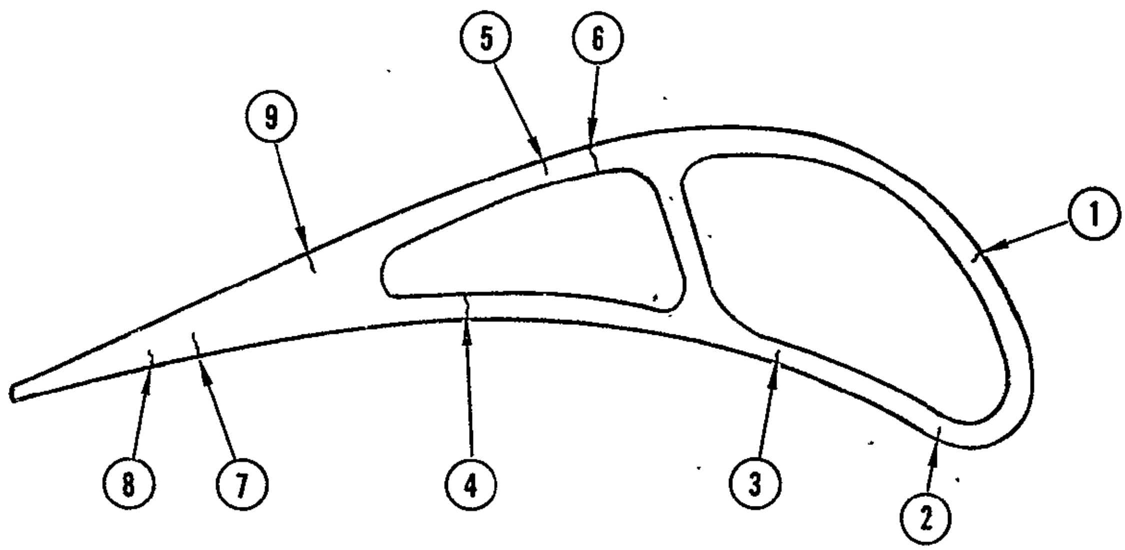

MICROSECTIONS SHOWN IN FIGURES 75, 76 AND 77

Figure 74 YD NiCrAl Vane Crack Locations F101 HPT Test

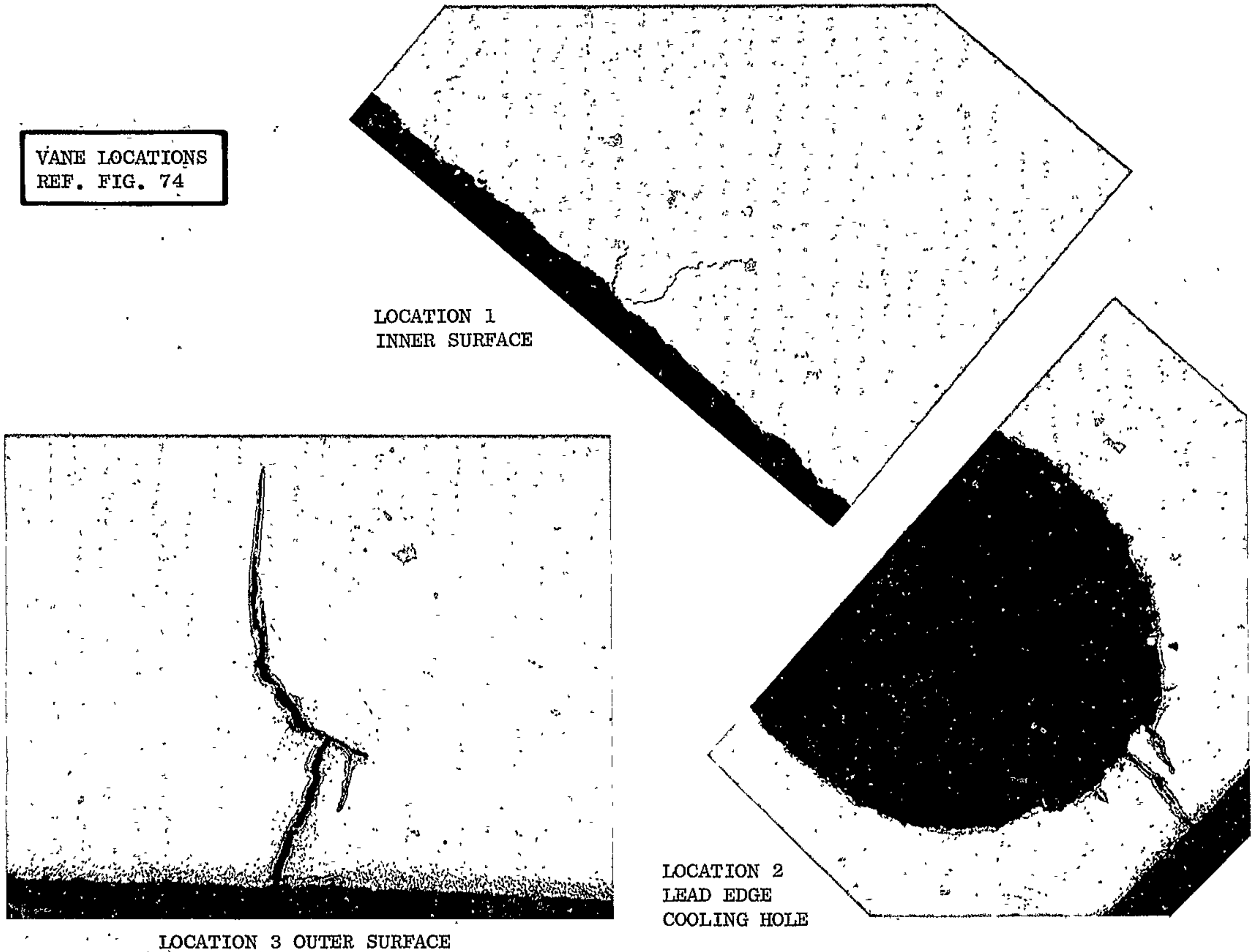

Figure 75 YD NiCrAl Lead Cavity Microstructures F101 HPT Test

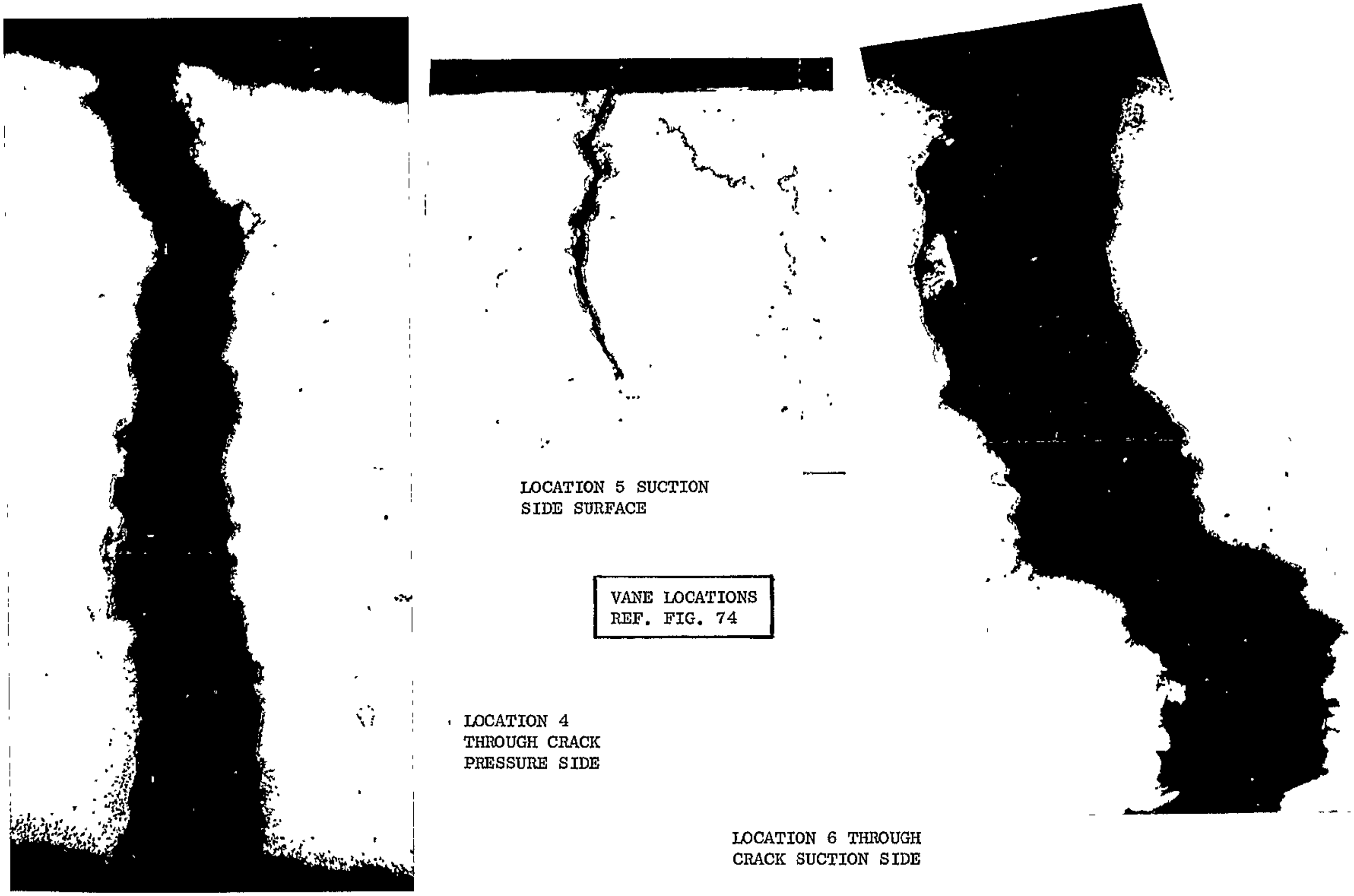

Figure 76 YD NiCrAl Aft Cavity Microstructures F101 HPT Test

VANE LOCATIONS
REF. FIG. 74

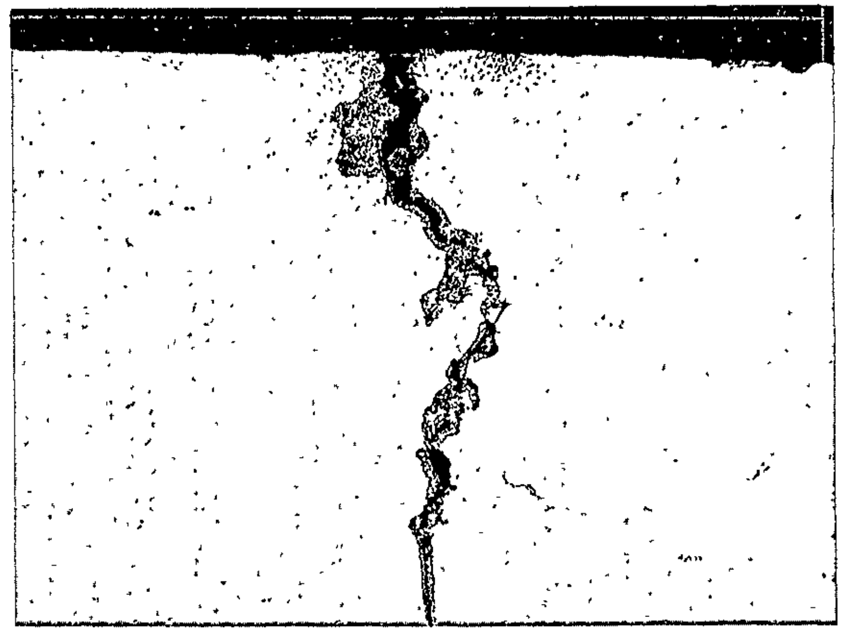

LOCATION 9 SUCTION SIDE SURFACE 100X

LOCATION 8 PRESSURE SIDE SURFACE 100X

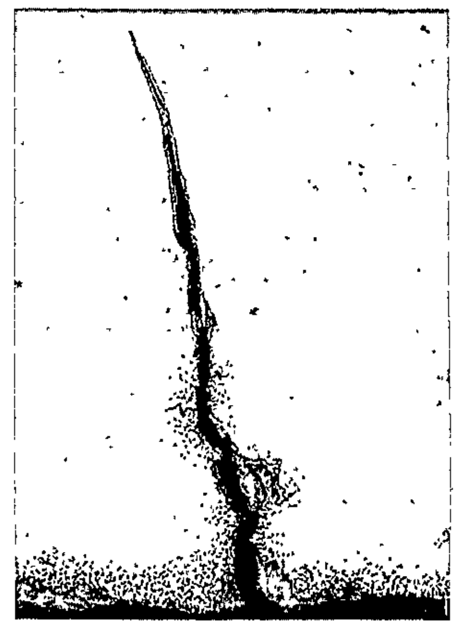

LOCATION 7 PRESSURE SIDE SURFACE 100X

Figure 77 YD NiCrAl Trailing Edge Microstructures F101 HPT Test

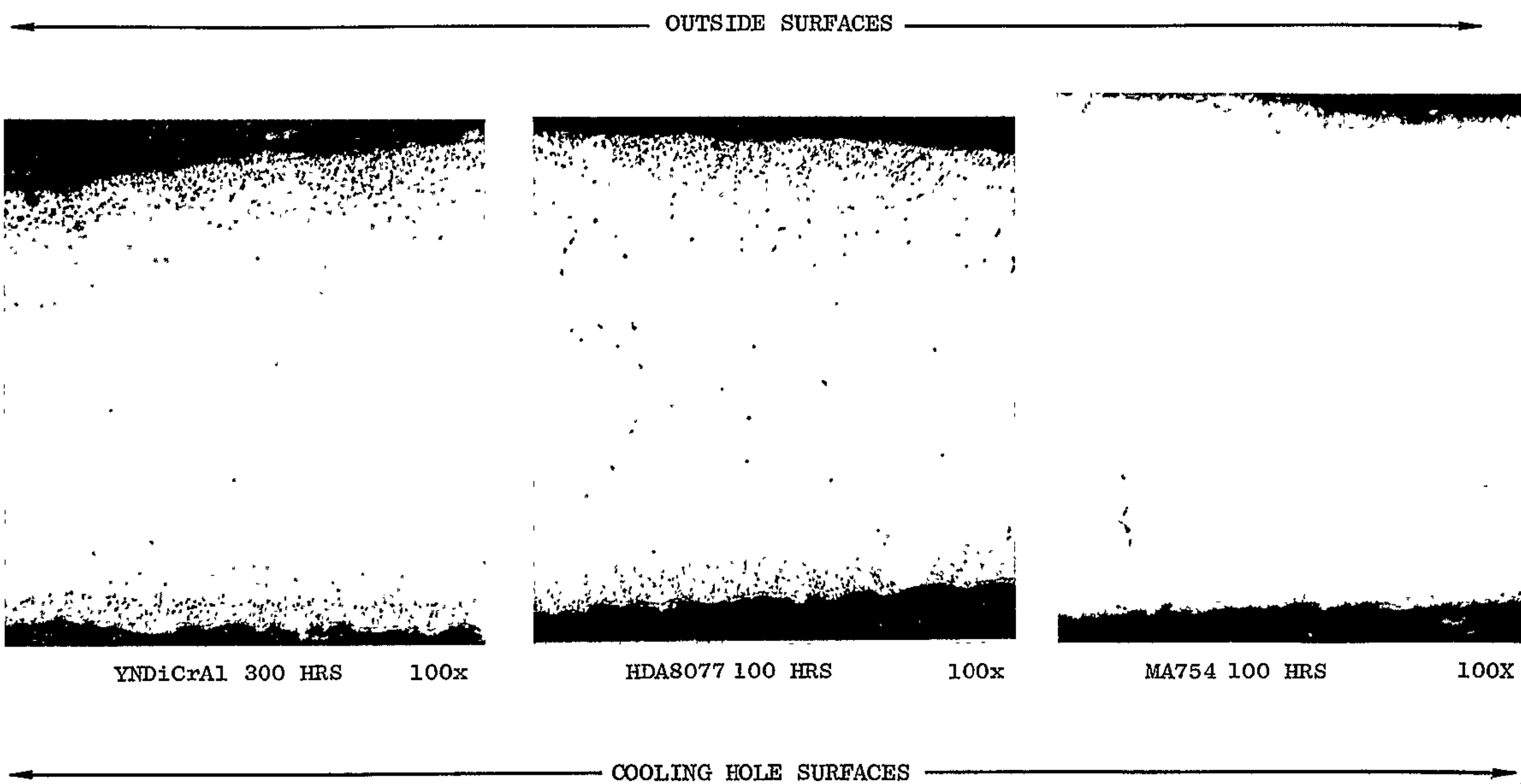

FIGURE 78 Trailing Edge Surface Microstructures F101 HPT Vanes

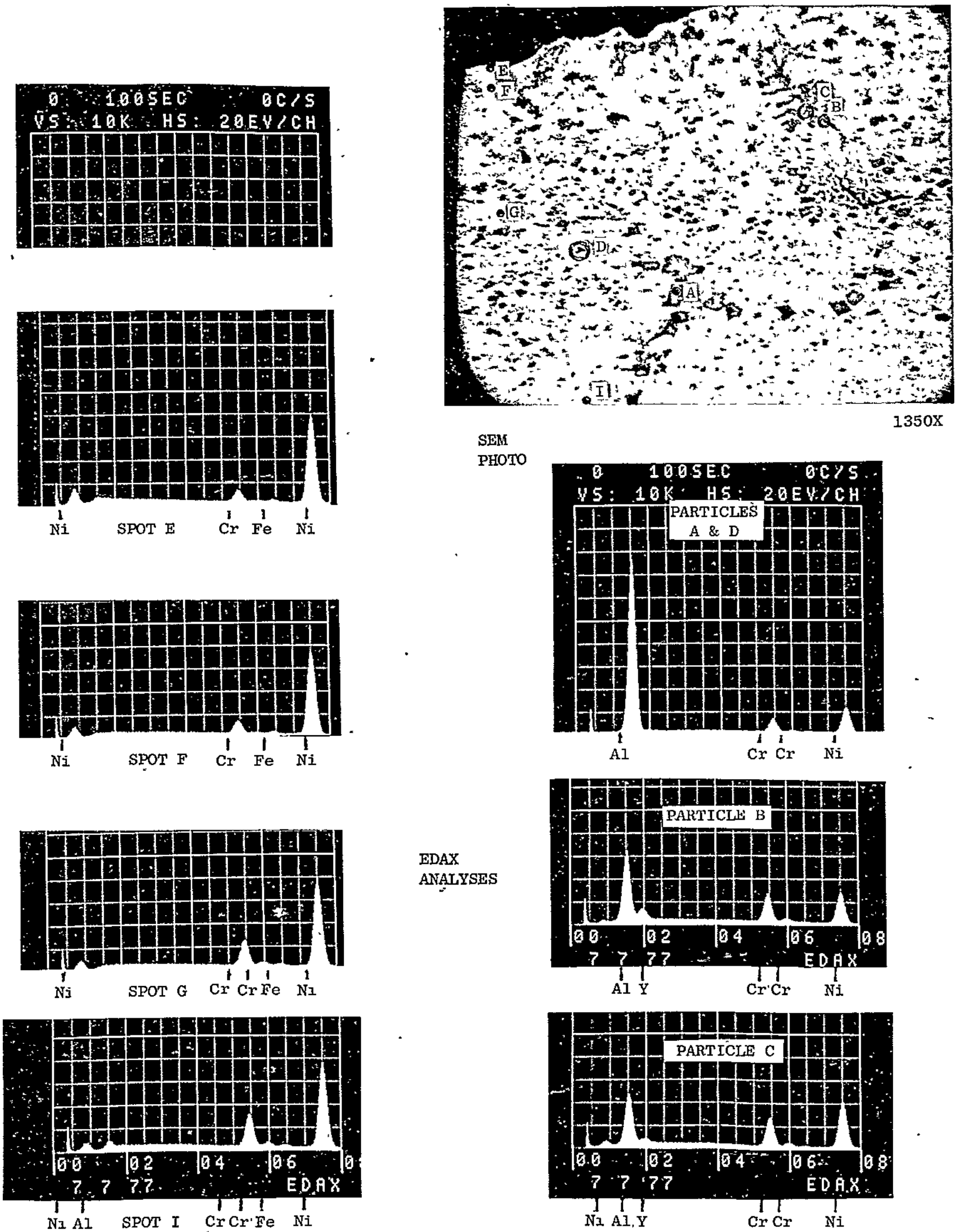

Figure 79 HDA8077 Oxidation-SEM and EDAX Analysis

In another instance of aggravated oxidation, this time observed on a YD NiCrAl vane, iron was identified. It is speculated that, in this case, iron oxide (present in the test cell air environment) caused a destruction of the protective Al_2O_3 on the vane. Figure 80 depicts the phenomenon in light microscopy, SEM, and EDAX.

In summary, HDA 8077 and YD NiCrAl displayed deficiencies in the F101 HPT vane engine test in both mechanical properties and environmental resistance, relative to MA 754.

3.3.3 CF6-50 Engine Test

The engine test that will be described herein was initiated because of the demonstrated excellent oxidation resistance of HDA 8077 and YD NiCrAl in Task I of this program. General Electric felt that the CF6-50 engine test, in combination with the F101 tests, would provide a more complete assessment of the capabilities of these alloys than could the F101 tests alone.

The CF6-50 HPT nozzle in its current production configuration is composed of integrally case X-40 vane and band segments. For the engine test, X-40 vanes were removed from existing segments by Electro Discharge Machining (EDM) and the ODS vanes brazed into their places (Figure 81). The vanes consisted of seven bare HDA 8077, seven bare YD NiCrAl, and eight MA 754 vanes coated with a Ni-Cr-Al-Y composition by a physical vapor deposition (PVD) process.

The engine test used the "C" cycles pictured in Figure 82. This cycle simulates a commercial flight mission but compresses it into 15 minutes by deleting the cruise portion.

The maximum vane metal temperatures are calculated to be just a few degrees above 1204° C (2000° F) on the pressure (concave) side of the vane leading edge under maximum hot-streak conditions.

At the 52-hour, 207-cycle point, the test was shut down for examination of a section of the engine other than the high pressure turbine. Fortunately for the evaluation of the ODS alloys, the early cycles of the planned 1000 cycles were run at maximum design operating conditions. Less severe cycles had been planned for the continuing cycles.

Because visible cracks were seen in some of the ODS vanes, it was decided to remove them for examination. Representative closup views of the ODS vanes are displayed in Figures 83 through 85. A number of vanes were cut up for metallographic examination. These results are catalogued in Table 16. In general, the ODS vanes exhibited more cracking than the X-40 vanes. Among the ODS vanes, the HDA 8077 vanes cracked more severely than those made from MA 754 and YD NiCrAl. Crack locations are mapped for sections of the ODS vanes (Figures 86 through 88). In most cases, the pitch section (midway between bands) exhibited the most damage. Typical microsections of the three ODS alloy vanes are shown in Figures 89 through 91. In some cases, this

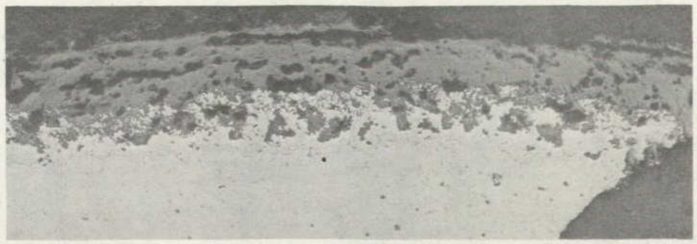

LIGHT MICROSCOPY 100X

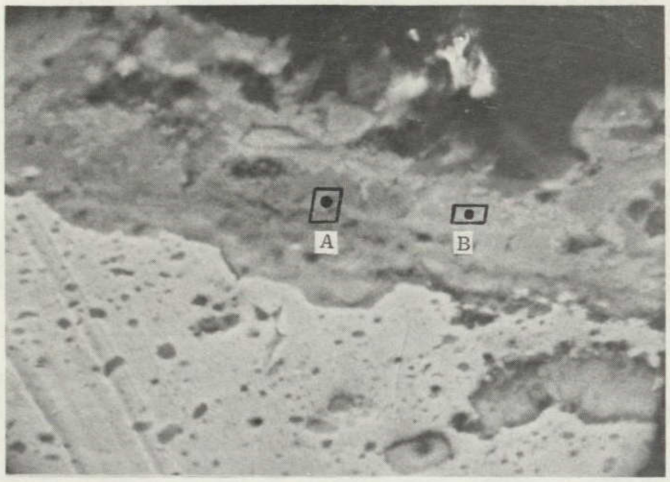

SEM VIEW 2900X

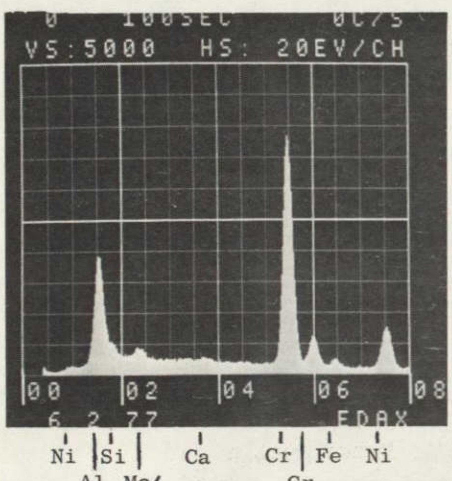

AREA A EDAX

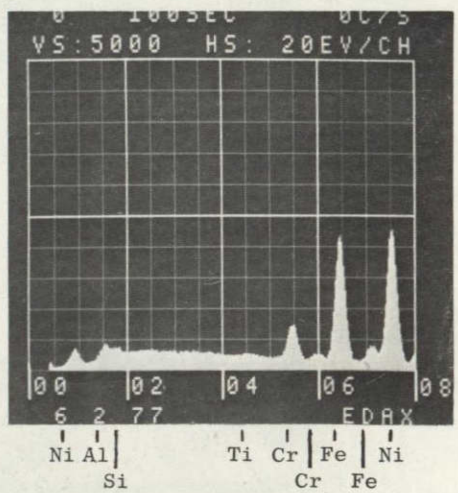

AREA B EDAX

Figure 80 YDNiCrAl Aggravated Oxidation F101 Test

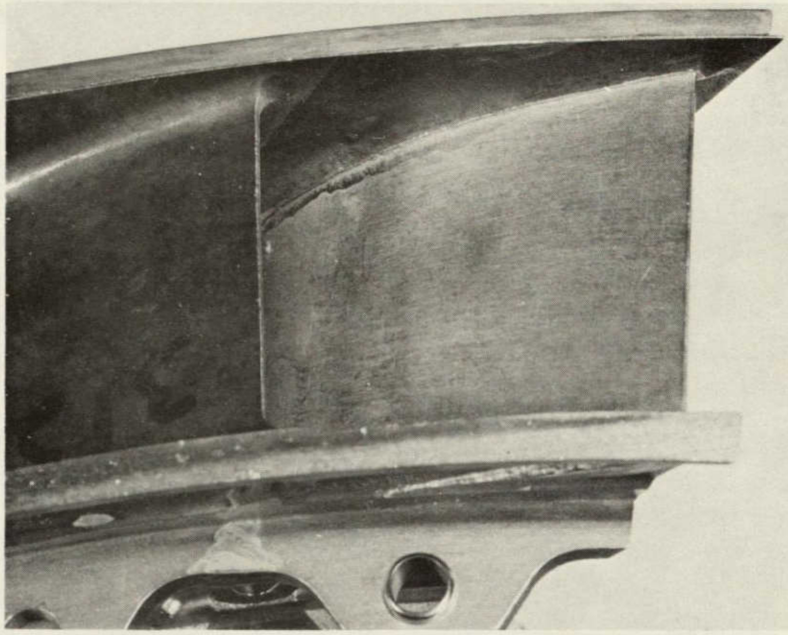

SUCTION SIDE

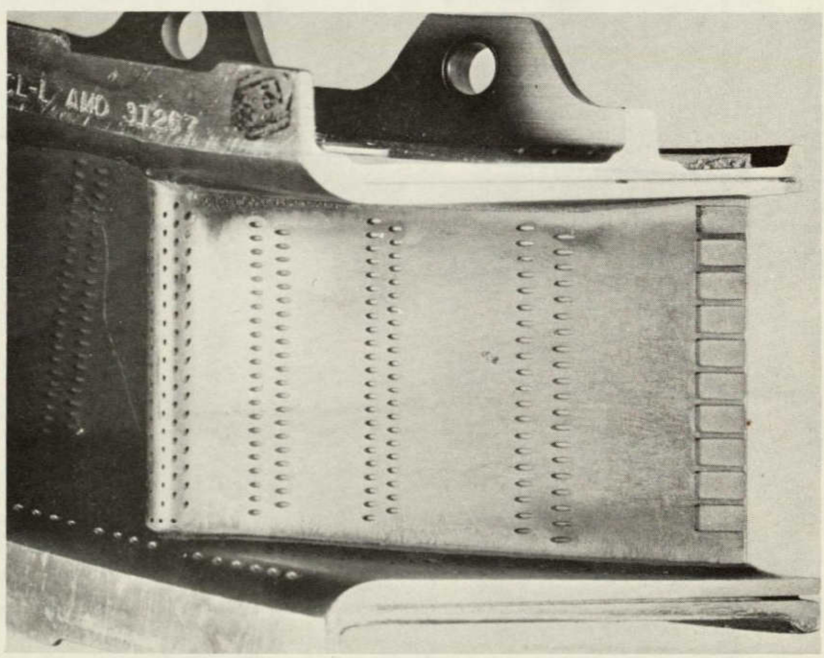

PRESSURE SIDE

Figure 81 YD NiCrAl CF6-50 HPT Vane

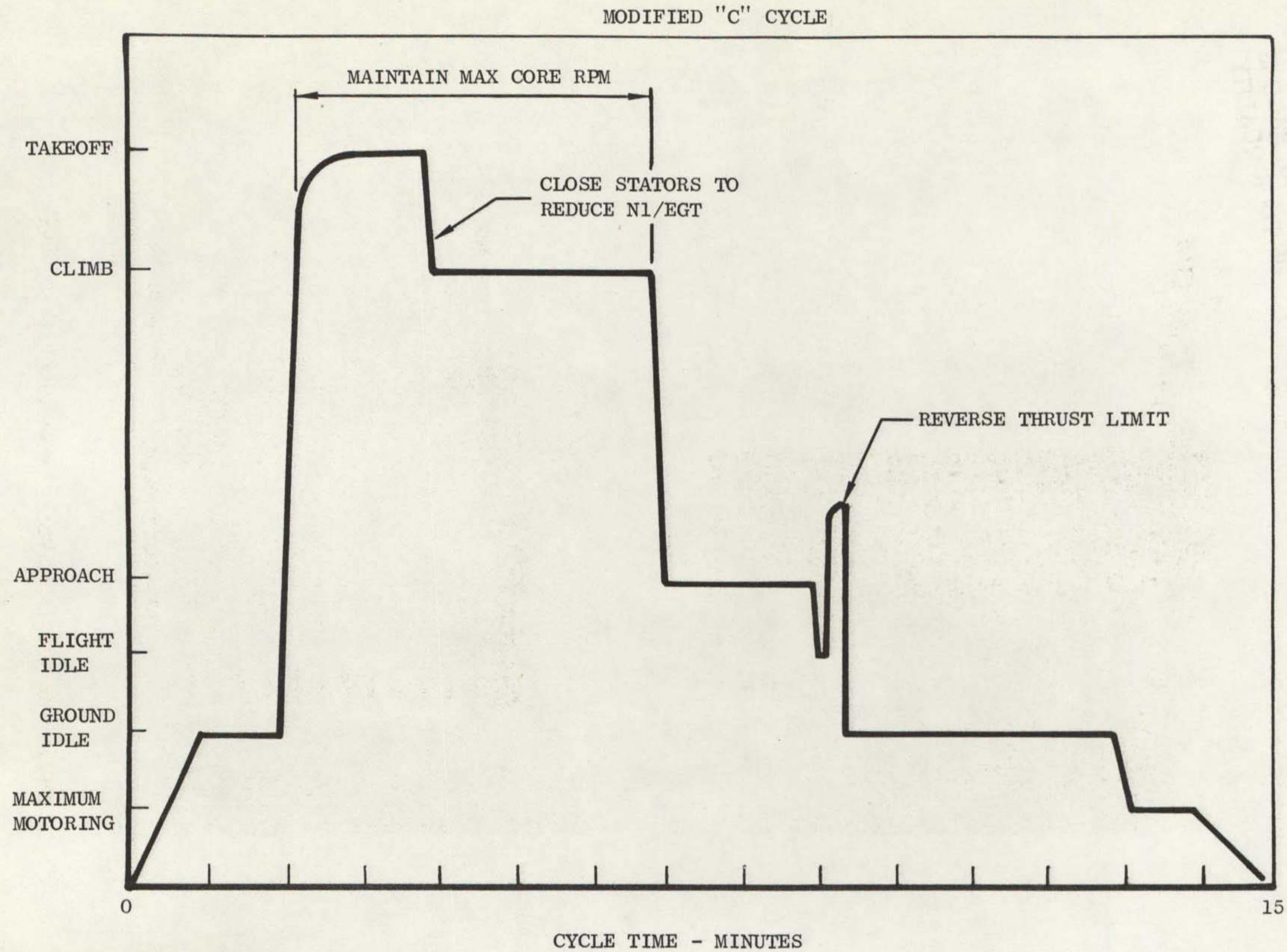

Figure 82 CF6-50 HPT Engine Test Cycle

LEADING EDGE

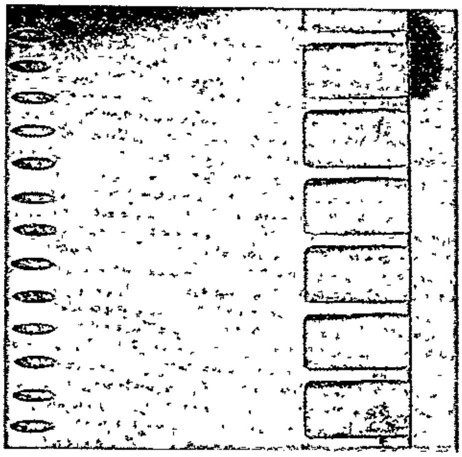

TRAILING EDGE

Figure 83 HDA 8077 Engine Run Vane CF6-50 Test

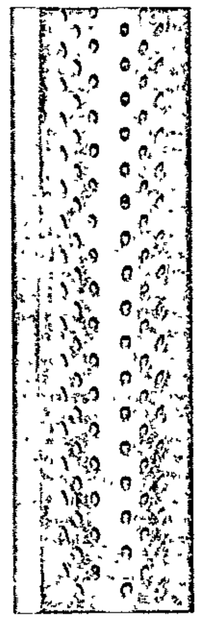

LEADING EDGE

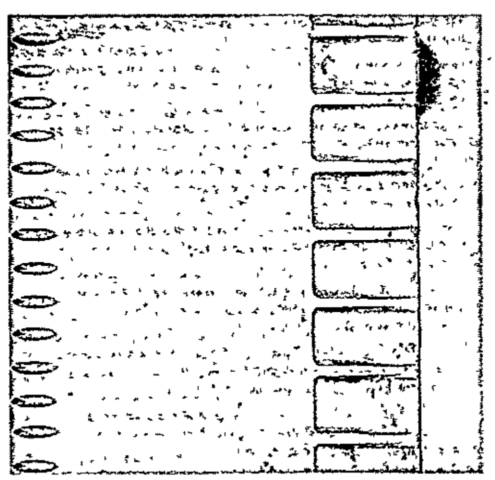

TRAILING EDGE.

Figure 84. YD NiCrAl Engine Run Vane CF6-50 Test

LEADING EDGE

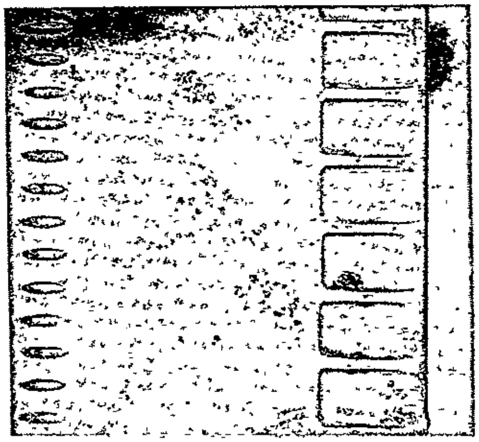

TRAILING EDGE

Figure 85 MA 754 Engine Run Vane CF6-50 Test

Table 16. CF6-50 - Engine Test Vane Crack Ratings.

Airfoil Type	Airfoils Evaluated	Leading Edge Cracks	Pressure Side Radial Cracks	T/E Slot Axials	T/E Slot Radial Rib Cracks
MA 754 (Coated)	5	1	3	5	2
HDA 8077 (Bare)	5	4	5	1	1
YD NiCrAl (Bare)	4	3	4	3	3
X-40 (Coating A)	5	2	3	1	0
X-40 (Coating B)	9	3	3	2	0

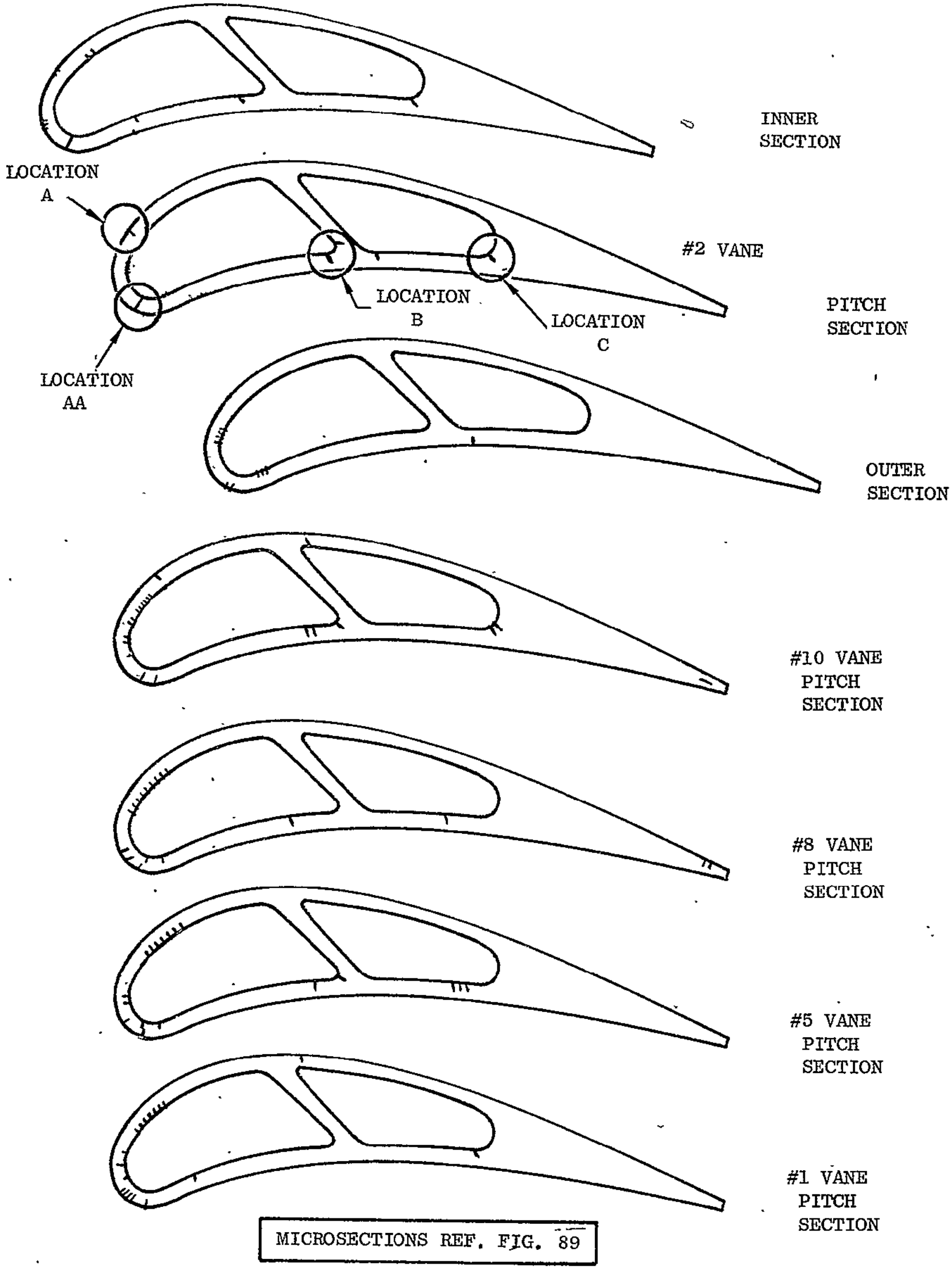

Figure 86 HDA8077 Vane Crack Locations CF6-50 Test

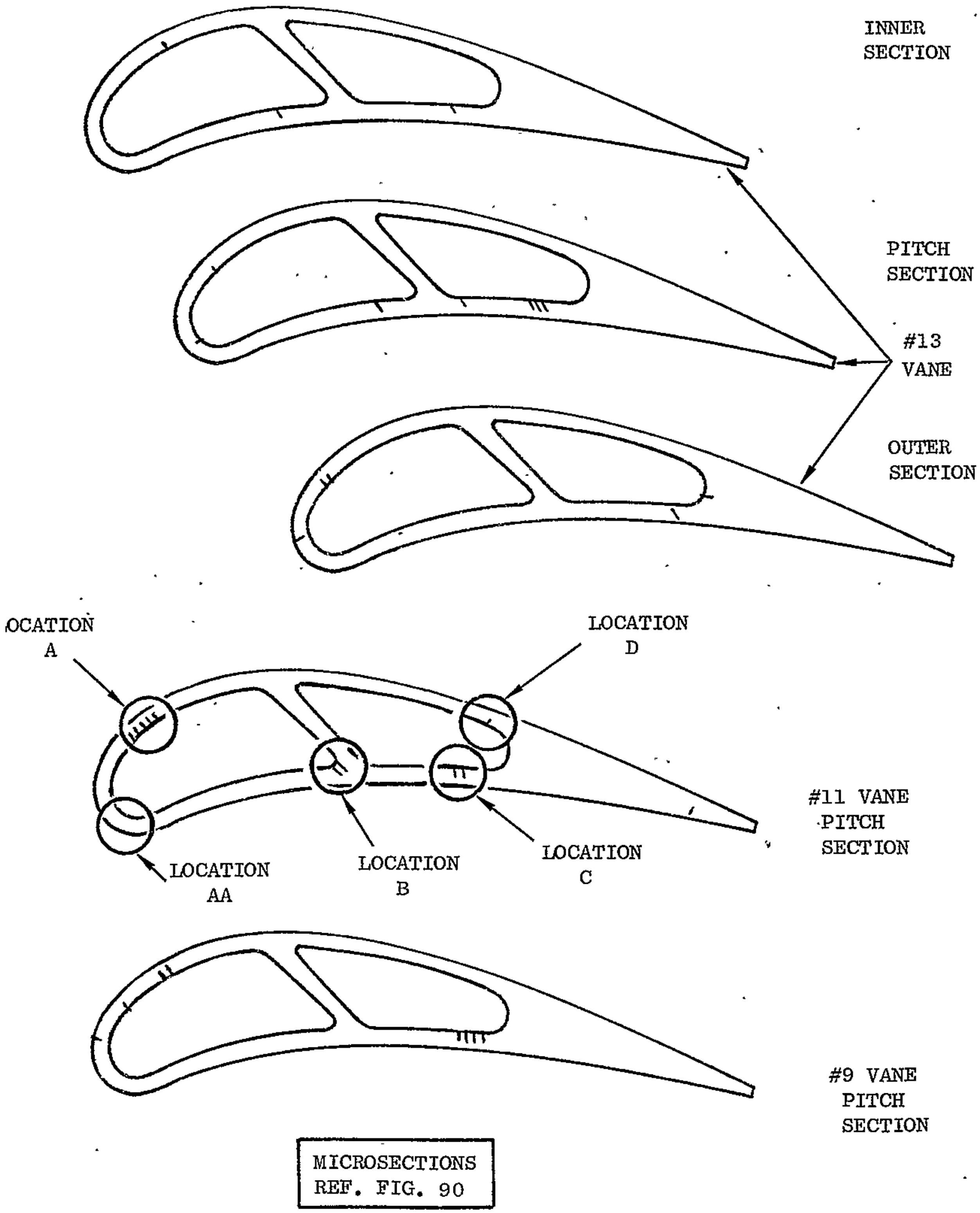

Figure 87 YDNiCrAl Vane Crack Locations CF6-50 Test

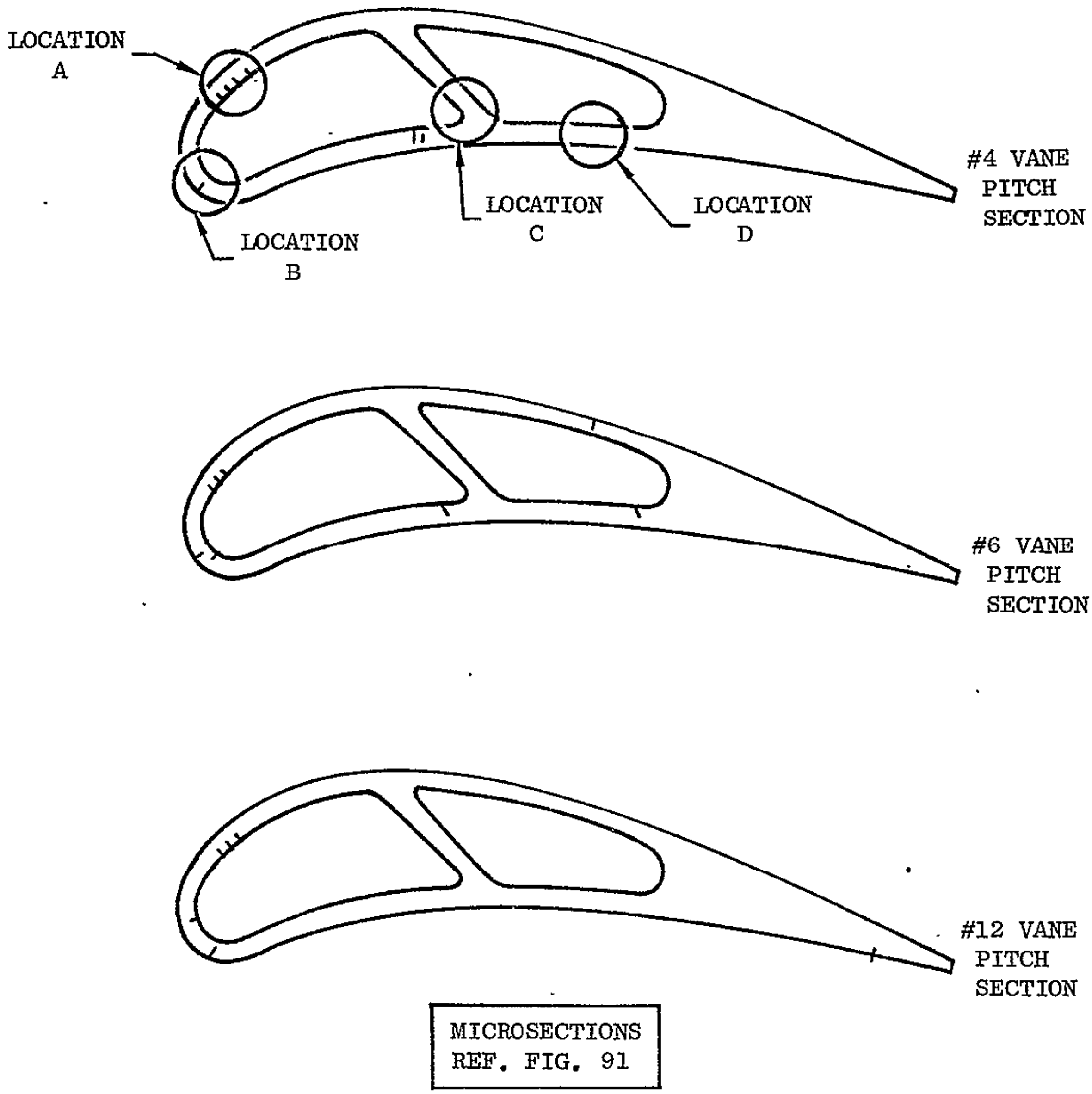

Figure 88 MA754 Vane Crack Locations CF6-50 TEST

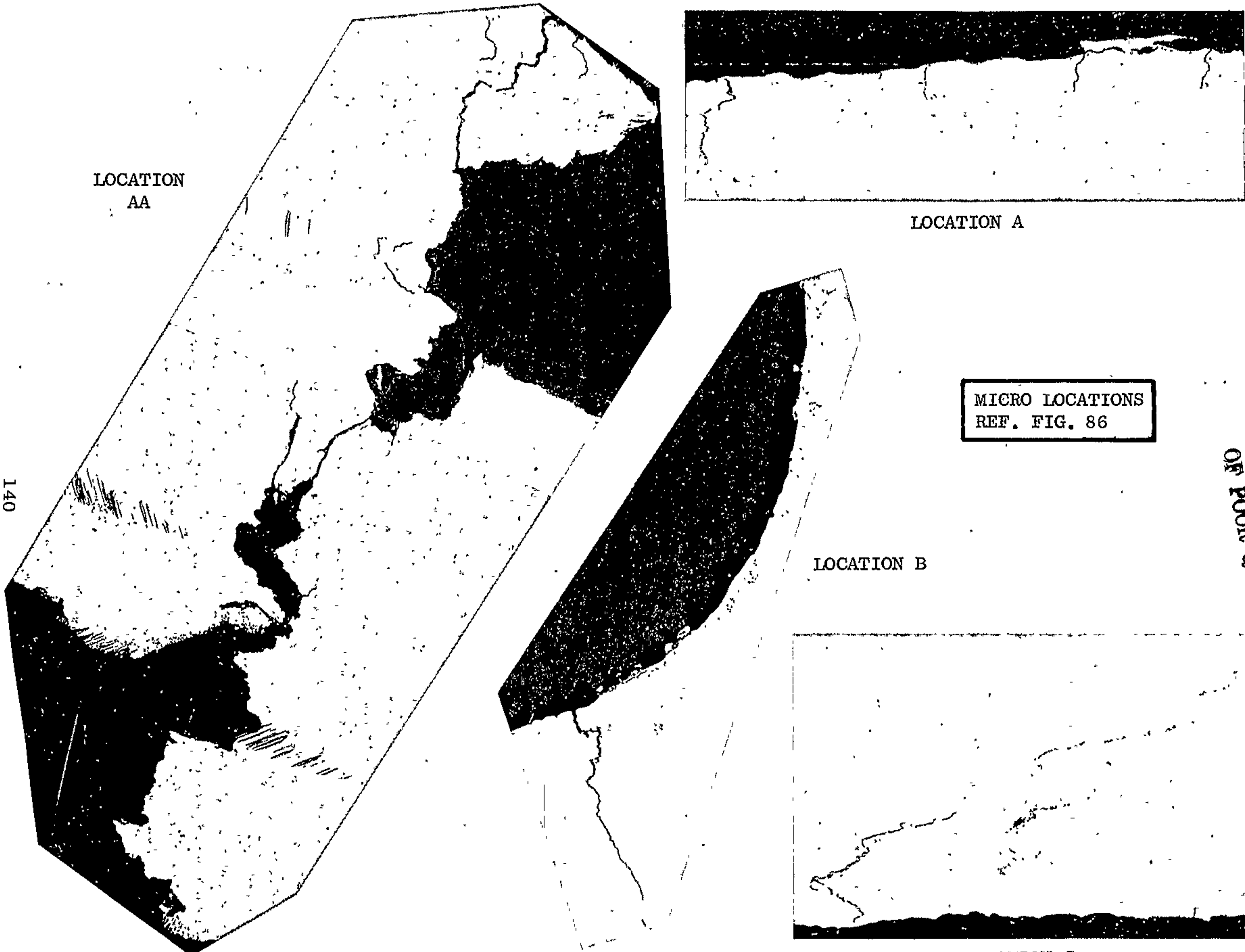

Figure 89 HDA Vane No.2 Microsections CF6-50 Test

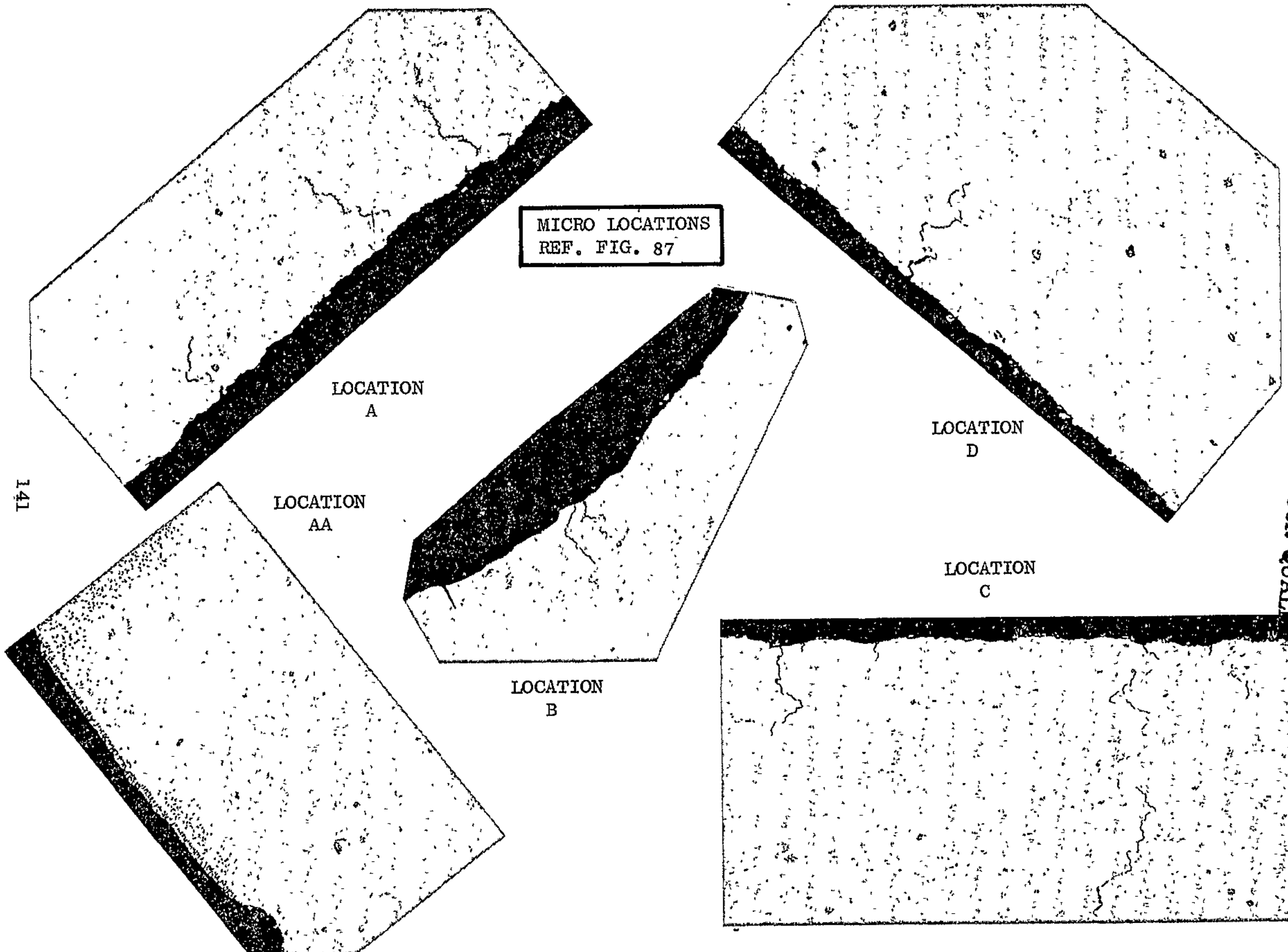

Figure 90 YD NiCrAl Vane No. 11 Microsections CF6-50 Test

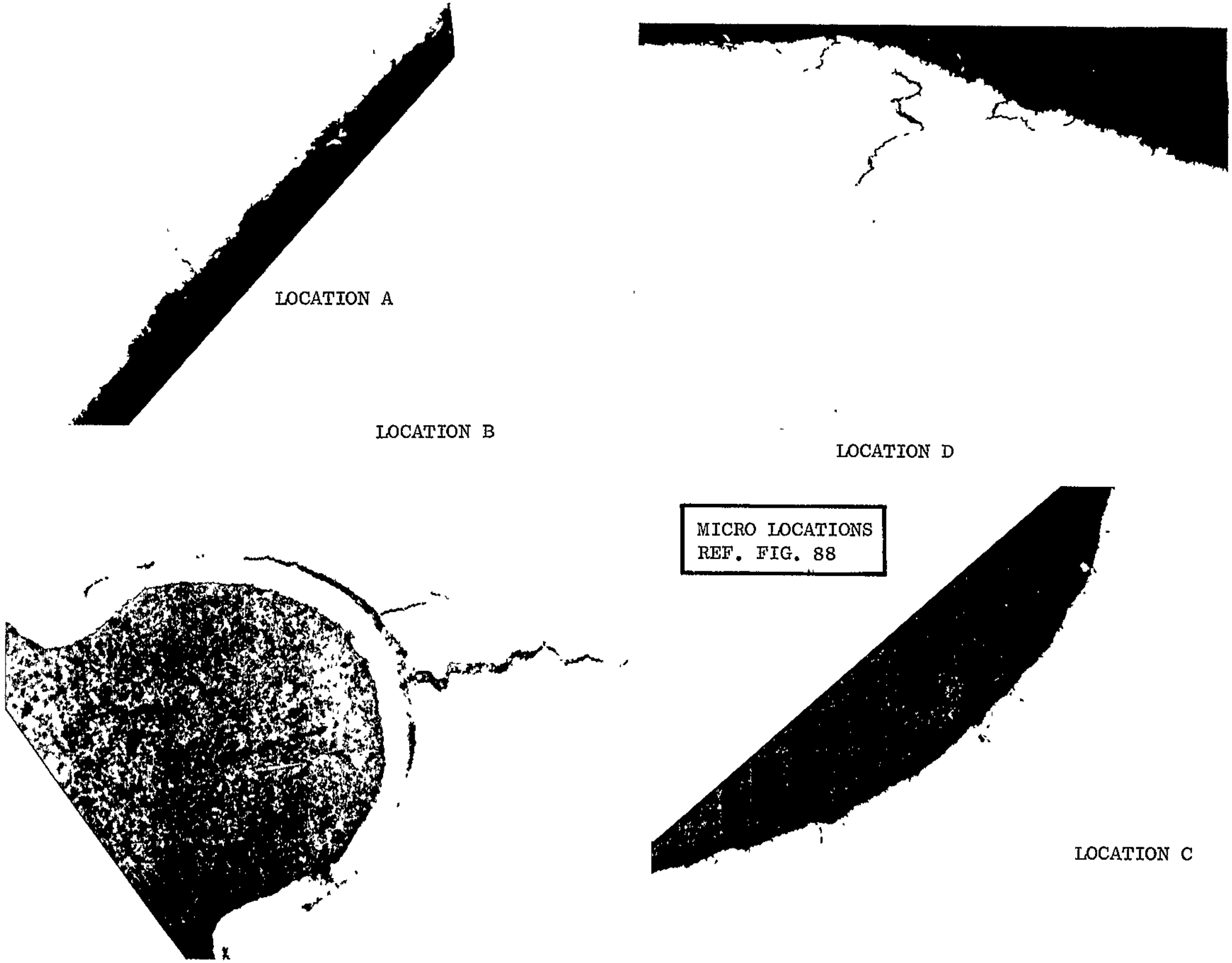

Figure 91 MA 754 Vane No. 4 Microsections CF6-50 Test

damage was manifested in through-the-wall cracking. In others it showed up simply as a greater quantity of cracks. Nearly all the cracking in all three ODS alloys was attributed by microevaluation to thermal gradients, causing stress rupture failure at grain boundaries. Gas pressure loads calculated are not large enough to cause the cracks. Very few fatigue-type cracks (transgranular) were observed in this engine test. Evidence of ODS alloy creep resistance is indicated in Figure 92. None of the ODS vanes showed any trailing edge bowing while several of the X-40 vanes did. This evidence is somewhat circumstantial, since it is possible that compressive stresses could have been more severe in the trailing vane (X-40) than in the leading vane locations of the ODS vanes.

3.3.4 Additional Evaluation

Subsequent to the engine test evaluations, further study was undertaken to determine why the HDA 8077 performed so poorly in engine testing compared with MA 754. Though HDA 8077 is somewhat lower in stress rupture strength in the longitudinal direction, transverse rupture properties are similar and both are made by International Nickel's mechanical alloying process. Referring to thermal and low cycle fatigue deficiencies with HDA 8077, it was postulated that there might be grain boundary differences between the two alloys. Grain boundaries are the primary high temperature fracture locations in ODS alloys.

Examination by replica electron microscopy did reveal a nearly continuous grain boundary phase in HDA 8077 that does not appear to be present in the other ODS-NiCrAl, YD NiCrAl and MA 757. Micrographs in Figures 93 and 94 show this and a similar, but much less, continuous phase in MA 754. Not much has been learned about this phase except that it appears to be rich in Chromium, as the SEM-EDAX analysis in Figure 95 indicates. Other analyses, however, show grain boundary phase compositions not substantially different from the matrix. Thus, circumstantial evidence appears to indicate that the presence of a grain boundary phase degrades the properties of HDA 8077 though the composition and source of the phase is unclear.

The first study of the Ni-16Cr-4Al matrix composition for ODS alloys was by NASA in a program at Fansteel to develop ODS alloys for the Space Shuttle (Reference 4). The composition was selected on the basis of oxidation resistance. Alloying content (CR + Al) was kept at a 20% level to maximize strength, preferred orientation, and melting point. Even at this alloying level, strength and orientation were more difficult to achieve than in TD NiCr (Ni-20Cr). In addition, aluminum contents were kept below 5% to minimize γ' formation, which could interfere with processing and grain stability.

The engine testing which showed reduced resistance to vane wall cracking and trailing edge bowing with YD NiCrAl and especially HDA 8077 is difficult to explain fully, even considering the HDA 8077 grain boundary phase. We don't really have a good explanation of why the ODS-NiCrAls are inferior in

ORIGINAL PAGE IS
OF POOR QUALITY

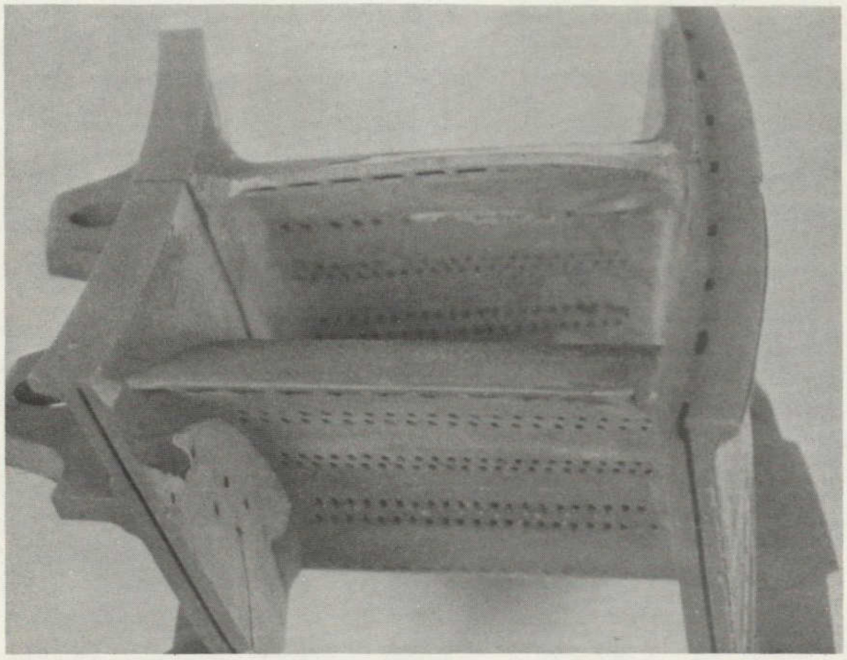

X-40 VANE

MA754 VANE

Figure 92 Bowing Resistance of ODS Vanes in CF6-50 Test

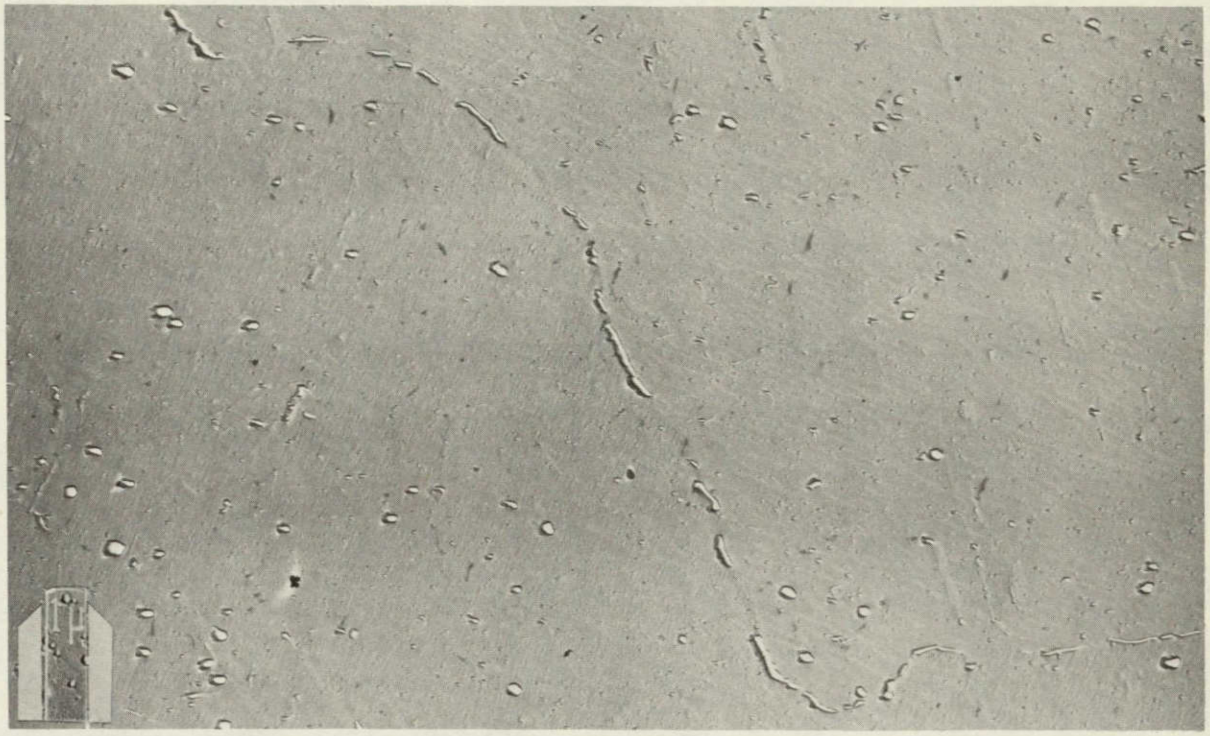

HDA8077 5000X

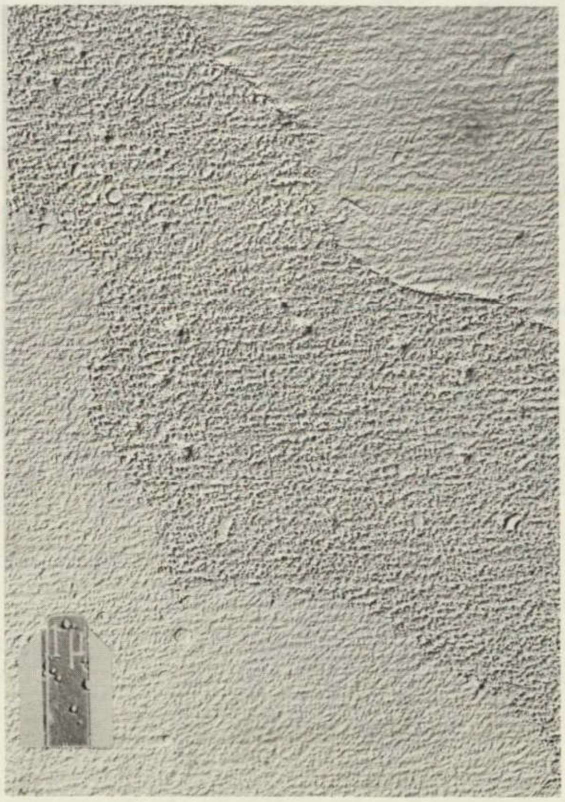

5000X

5000X

YDNiCrAl

REPLICA ELECTRON MICROGRAPHS
ETCHANT - SWABBED 3 GLYCERIN, 2 HCL, 1 HNO_3

Figure 93 HDA 8077 & TD NiCrAl Grain Boundaries

MA754 5000X

MA757 5000X

REPLICA ELECTRON MICROGRAPHS
ETCHANT - SWABBED 3 GLYCERINE, 2 HCl, 1 HNO_3

Figure 94 MA 754 & MA 757 Grain Boundaries

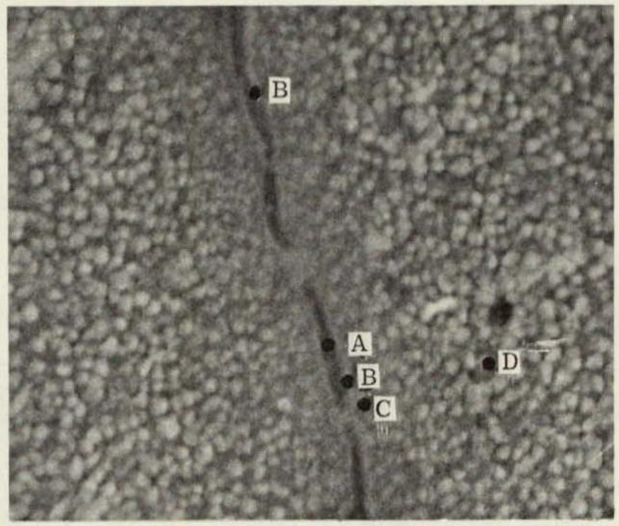

SEM VIEW 7000X

SEM-EDAX of Area A
ALPHA-Cr

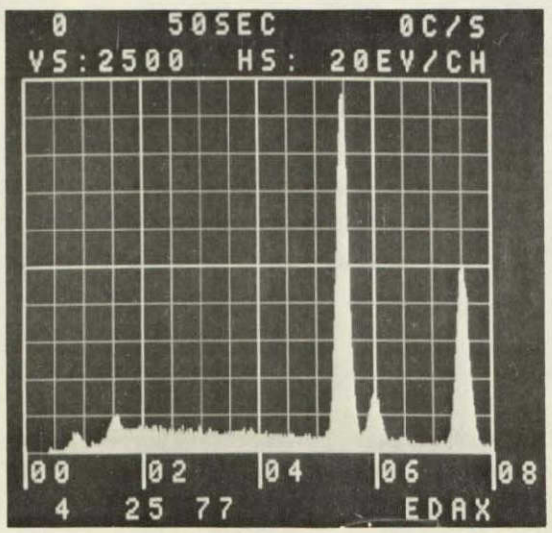

Ni Al Cr Ni

SEM-EDAX OF AREA B

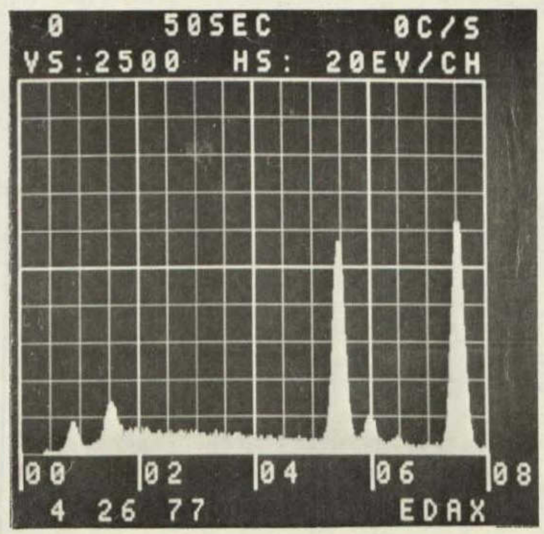

Ni Al Cr Ni

SEM-EDAX OF AREAS C
AND D

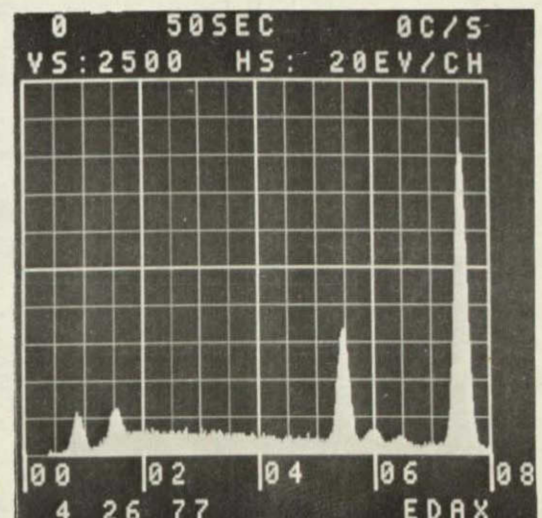

Ni Al Cr Ni

Figure 95 SEM-EDAX Analysis of HDA 8077 Grain Boundary Phase strength to the ODS-NiCrs. One can speculate that the aluminum addition causes deleterious γ' interactions with the matrix or directly affects grain or grain boundary strength; but, we have no hard facts. Historically, however, ODS-NiCrAl alloys have always been weaker than their ODS-NiCr counterparts:

ODS-NiCrAl	ODS-NiCr	Producer
TD NiCrAl	TD NiCr	Fansteel
DS NiCrAl	DS NiCr	Sherritt-Gordon
YD NiCrAl	---	Special Metals
Ma 757	MA 754	Huntington Alloys

Summarizing, in comparison to ODS-Ni20Cr, the ODS-Ni-16Cr-4Al alloys are slightly weaker, and poorer in any environmental resistance except the high velocity rig, probably because of the lean Cr and Al. The only conflicting results are the NASA hot corrosion tests which showed all ODS alloys superior to conventional superalloys. These inferior ODS-NiCrAl characteristics are manifested during engine testing as premature cracking, vane bowing, and accelerated surface attack. Methods of correcting these deficiencies are not apparent, because increasing the Cr and Al, though expected to improve environmental resistance, would be at the expense of strength and texture.

4.0 CONCLUSIONS

The following is a summary of conclusions reached as a result of this program:

- The ODS-NiCrAl alloys have a lower maximum attainable level of mechanical properties than their equivalently alloyed (Cr + Al = 20%) NiCr counterparts, though the alloys selected in this program for engine testing (HDA 8077 and YD NiCrAl) met established program goals of melting point, oxidation resistance, low cycle fatigue, and stress rupture.

- The ODS-NiCrAl alloys proved to be easily fabricable by machining and brazing processes established for MA 754.

- In engine tests, the ODS-NiCrAl alloys are less resistant to vane bowing and thermal cracking than ODS-NiCr (MA 754).

- Grain boundary phases are possible causes of reduced thermal cracking resistance in HDA 8077.

- The coarser (than MA 754) and unevenly distributed dispersoid in YD NiCrAl may have contributed to its inadequate resistance to trailing edge vane bowing.

- Though hot corrosion testing in this program, and outside of it, produced conflicting results, the environmental resistance of the ODS-NiCrAl alloys is judged to be inferior to the ODS-NiCr alloys in other than simple oxidizing situations.

5.0 REFERENCES

1. Bailey, P.G. and Kutchera, R.E., "Manufacturing Methods for Directional Recrystallization Process," AFML TR 73-294, December 1973.

2. Perkins, R.J. and Bailey, P.G., "Low Cost Processes for Manufacturing of ODS Turbine Nozzle Components," AFML Interim Report No. 4, July 1977.

3. Perkins, R.J. and Bailey, P.G., "Low Cost Fabrication of ODS Alloy Vanes," (to be issued) December 1977.

4. Klinger, L.J., W.R. Weinberger, P.G. Bailey, S. Baranow, "Development of Dispersion-Strengthened Nickel-Chromium Alloy ($NiCrThO_2$) Sheet for Space Shuttle Vehicles," Part II, NASA CR-121164, December 1972.

5. Karstrom, D.L. and R. Grierson, "Optimization of an oxide-Dispersion-Strengthened NiCrAl Alloy for Gas Turbine Engine Vanes," NASA CR-134901, October 1975.

6. Benjamin, J.S., "Composite Metal Powder," U.S. Patent 3,591,362, July 1971.

7. Bailey, P.G. and H.J. Bauer, Jr., "Strengthening of FeCrAl Oxidation Resistant Alloys," Final Report for Naval Air Development Center, March 1975.

8. Deadmore D.L., Lowell, C.E., and Santoro G.J., "High Gas Velocity Oxidation and Hot Corrosion Testing of ODS Nickel-Base Alloys," NASA TMX-71835, November 1975.

9. Lowell, C.E. and Deadmore, D.L., "High Velocity Oxidation and Hot Corrosion of Some ODS Alloys," NASA TMX-73656, April 1977.

DISTRIBUTION LIST

One copy unless otherwise specified.

NASA-Headquarters
600 Independence Avenue, S.W.
Washington, DC 20546
Attn: RWM/J. Gangler
RLC/D. Miller
RTG/R. Winblade
RT/W.S. Aiken
RL/H.W. Johnson

NASA-Lewis Research Center
21000 Brookpark Road
Cleveland, Ohio 44135
Attn: R.L. Dreshfield, MS 105-1
C.P. Blankenship, MS 105-1 — 10 copies
N.T. Saunders, MS 501-2
R.L. Davies MS 106-1
C.M. Scheuermann MS 49-3
H.B. Probst, MS 49-3
S.J. Grisaffe, MS 49-3
T. Glasgow, MS 49-3
H.R. Gray, MS 49-3
D. Whittenberger MS 105-1
M & S Div. File MS 49-1
C.E. Lowell, MS 49-3
M.H. Hirschberg MS 49-1
R.A. Signorelli MS 106-1
J.W. Weeton MS 106-1
R.A. Rudey, MS 60-4
R.W. Schroeder, MS 501-5
Contracts Sections B, MS 500-313

Technology Utilization, MS 3-19
Library, MS 60-3 — 2 copies
AFSC Liason Office, MS 501-3
AAMRDL, MS 77-5
Report Control Office MS 5-5

NASA-Ames Research Center
Moffett Field
CA 94035
Attn: M. Waters 237-9
Library

NASA-Langley Research Center
Langley Field, VA 23365
Attn: W.A. Brooks, Jr.
Library

NASA-Dryden Flight Research Center
P.O. Box 273
Edwards, CA 93523
Attn: Library

NASA-Marshall Space Flight Center
Huntsville
AL 35812
Attn: R. Schwinghammer
Library

U.S. Air Force
Wright-Patterson AFB, OH 45433
Attn: AFML/LLM N. Geyer
AFAPL/TBP T.J. Norbut
AFML/LTM H. Johnson
AFAPL/TBP L.J. Obery
AFML/LL L.Hjelm
AFML/LTM J.K. Elbaum
AFML/LAM Technical Library

NASA-Scientific and Technical Information Facility 10 copies
Attn: Accessioning Department
P.O. Box 8757
Baltimore/Washington International Airport
Maryland 21240

Eustis Directorate
U.S. Army Air Mobility
R & D Laboratory
Fort Eustis
VA 23604
Attn: J. Lane SAVDL-EU-TAPP

Army Materials &
Mechanical Research Center
Watertown, MA 02172
Attn: S. Isserow DRXMR-KA
Library

Navy Department
Naval Air Systems Command
Washington, D.C. 20361
Attn: I. Machlin Air-52031B

Naval Air Development Center
Warminster, PA 18974
Attn: F.R. Johns (301)

Defense Documentation Ctr.
Cameron Station
5010 Duke St.
Alexandria, VA 22314

Research & Technology Div.
NAPTC
Trenton, NJ 08628
Attn: J. Glatz

National Science Foundation
Washington, DC 20550
Attn: B.A. Wilcox

Navy Department
Naval Ship R&D Center
Annapolis, MD 21402
Attn: G.A. Wacker code 2812

ERDA
Washington, D.C. 20545
Attn: S. Freedman
J. Neal

FAA Headquarters
800 Independence Ave., SW
Washington, D.C. 25091
Attn: A. Broderick (AEQ 10)
D. Winer (AEQ-110)

AiResearch Manufacturing Company
P.O. Box 5217
Phenix, AZ 85010
Attn: C. Corrigan, Dept. 93-12
R. Kirby

AVCO-Lycoming Div.
550 S. Main St.
Stratford, CT 06497
Attn: L.J. Fiedler

Detroit Diesel Allison
P.O. Box 894
Indianapolis, Ind., 46206
Attn: M. Herman

General Electric Co.
Gas Turbine Prod. Div.
Schenectady, NY 12345
Attn: C. Sims

General Electric Co.
Corporate R&D Center
P.O. Box 8
Schenectady, NY 12301
Attn: Library

Pratt and Whitney Aircraft
United Tech. Corp
400 Main St.
East Hardford, CT 06108
Attn: R.A. Sprague
M.L. Gell

Pratt and Whitney Aircraft
Box 2691
West Palm Beach
FL 33402
Attn: J. Moore

Solar
Div of Int. Harvester
P.O. Box 80966
San Diego, CA 92138
Attn: A. Stetson
A. Metcalfe

TeleDyne CAE
Mat. Dev. and Manuf. Engr.
P.O. Box 6971
Toledo, OH 43612
Attn: R. Beck

Williams Research
2280 W. Maple
Walled Lake, MI 48081
Attn: Wm. P. Schimmel

Battelle Memorial Inst
505 King Ave.
Columbus, Ohio 43210
Attn: A.H. Clauer
Technical Library

Cameron Iron Works
P.O. Box 1212
Houston, Tx 77001
Attn: N. Wilkinson

Cannon-Muskegon Corp.
P.O. Box 506
Muskegon, MI 49443
Attn: R. Schwer

Cartech Inc.
P.O. Box 662
Reading, PA 19603
Attn: D. Muzyka

Case Western Reserve University
Met. & Mat'l Sciences Dep't
Cleveland, OH 44106
Attn: L.J. Ebert

Certified Alloys Products Inc.
3245 Cherry Ave.
Long Beach, CA 90807
Attn: M. Woulds

Chrysler Corp.
P.O. Box 1118
Detroit, MI 48231
Attn: J. Witherow

Climax Molybdenum Co.
P.O. Box 1568
Ann Arbor, MI 48106
Attn: C. Clark

Colt Industries
Crucible Inc., Materials Research Center
P.O. Box 88
Pittsburgh, PA 15230
Attn: E. Dulis

Cummins Engine Techn. Ctr.
500 S. Poplar St.
Columbus, IN 47201
Attn: J.R. Drake

Ford Motor Company
Metallurgical Dept.
P.O. Box 2053
Dearborn, MI 48121
Attn: C. Feltner

General Motors Corp.
Technical Center
Warren, MI 48090
Attn: E. Reynolds

Gould Inc.
450 E. 105th St.
Cleveland, OH 44180
Attn: E. Thellman

Grumman Aerospace Corp.
Bethpage, NY 11714
Attn: M.H. Siegel

Howmet Corporation
Technical Center
699 Benston Rd.
Whitehall, MI 49461
Attn: W. Freeman

Howmet Corporation
Austenal Division
Dover, NJ 07801
Attn: F. Jaeger

Howmet Corporation
Turbine Components Division
Dover, NJ 07801
Attn: E. Corozza

Huntington Alloys Div.
International Nickel Co.
Huntington, WV 25720
Attn: F. Perry

Industrial Materials Technology, Inc.
19 Wheeling Avenue
Woburn, MA 01801
Attn: R. Widmer

IIT Research Institute
10 West 35th Street
Chicago, IL 60616
Attn: K. Kulkarni

International Nickel Corp.
Sterling Forest
Suffern, NY 10901
Attn: J. Benjamin
Library

Kelsey Hayes
7250 Whitmore Lake Road
Brighton, MI 48116
Attn: T. Miles

Ladish Company
Cudahy, WI 53110
Attn. R. Daykin

Lockheed-California Co.
P.O. Box 551
Burbank, CA 91503
Attn: T. Sedjwick

M.I.T.
Dept of Metallurgy
Cambridge, MA 02139
Attn. N.J. Grant

MCIC
Battelle Memorial Institute
505 King Ave.
Columbus, OH 43201

Nuclear Metals, Inc.
229 Main St.
Concord, MA 01742
Attn: G. Friedman

RSC Materials Technology Assocs.
P.O. Box 312
Clinton, N.Y. 13323
Attn: R. Cremisio

Rocketdyne Division
Rockwell International
6633 Canoga Ave.
Canoga Park, CA 91304
Attn: T.G. McNamara

Rockwell International
Science Center
Thousand Oaks, Calif. 91360
Attn: N. Paton

Special Metals, INc.
New Hartford
New York 13413
Attn: S. Reichman
S. Baronow

Special Metals, Inc.
Utica Power Division
2310 S. Industrial Highway
Ann Arbor, MI 48104
Attn: W. Castledyne

Stanford University
Dept. of Mat'l Science
Palo Alto, CA 94305
Attn: O. Sherby

Stellite Division
Cabot Corporation
1020 West Park Ave.
Kokomo, ID 46901
Attn: S.T. Wlodek
R. Grierson

TRW, Inc.
23555 Euclid Ave.
Cleveland, OH 44117
Attn: J. Alexander
I. Toth
J. McCarthy

TRW, Inc.
Metals Division
Minerva, OH 44567
Attn: E.A. Steigerwald

Turbodyne Corp.
711 Anderson Ave. N
St. Cloud MN 56301
Attn: L. Engel

United Technologies Research Center
East Hatford, CT 06108
Attn: Library

Universal Cyclops
650 Washington Rd.
Pittsburgh, PA 15228
Attn: L. Lherbier

Vought Corp.
P.O. Box 5907
Dallas TX 75222
Attn: W.R. Boruff
Library

Westinghouse Electric Co.
P.O. Box 10864
Pittsburg, PA 15236
Attn: D. Thomas
D. Moon
D. Goldberg

Westinghouse Electric Co.
P.o. Box 9175
Lester, PA 19113
Attn: F. Wall

Wyman-Gordon Company
N. Grafton, MA 01536
Attn: J. Coyne